STUDY OF PARTICLES AT FLUID-FLUID INTERFACES

by

Prachi Thareja

B. Tech., Harcourt Butler Technological Institute (HBTI) Kanpur, India, 2003

M.S., University of Pittsburgh, 2006

Submitted to the Graduate Faculty of

Swanson School of Engineering in partial fulfillment

of the requirements for the degree of

Doctor of Philosophy

University of Pittsburgh

2008

UNIVERSITY OF PITTSBURGH

SWANSON SCHOOL OF ENGINEERING

This dissertation was presented

by

Prachi Thareja

It was defended on

June 17, 2008

and approved by

Robert M. Enick, Ph.D., Professor, Department of Chemical and Petroleum Engineering

Joseph J. McCarthy, Ph.D., Associate Professor, Department of Chemical and Petroleum Engineering

Anne M. Robertson, Ph.D., Associate Professor, Department of Mechanical Engineering and Materials Science

Dissertation Director: Sachin S. Velankar, Ph.D., Assistant Professor, Department of Chemical and Petroleum Engineering

STUDY OF PARTICLES AT FLUID-FLUID INTERFACES

Prachi Thareja, PhD

University of Pittsburgh, 2008

Particles are known to adsorb at fluid-fluid interfaces in small molecule systems such as oil/water emulsions. These particle stabilized emulsions are called *Pickering* emulsions. This thesis aims to extend the phenomenon of particle adsorption as observed in *Pickering* emulsions to polymer blends. Polymer blends are high viscosity analogs of emulsions. They present an economical way of obtaining a material with desired properties by blending two immiscible polymers. The goal of this work is to examine the effects of interfacial adsorption of particles in polymer blends.

We examine the effect of the simultaneous adsorption of silica particles at two polymer-polymer interfaces in polyisobutylene/polydimethylsiloxane (PIB/PDMS) and polyethyleneoxide/polyisobutylene (PEO/PIB) blends, leading to the *bridging* of drops. Microscopically and rheologically, the particle mediated drop bridging is shown to result in the formation of clusters and networks of drops. This is reported to impart weak gel-like characteristics to the blend.

A variety of commercially available particles viz. polytetrafluoroethylene (PTFE), iron (Fe), iron oxyhydroxide (FeOOH) and titanium dioxide (TiO_2) are shown to be interfacially active at chemically different polyisoprene/polydimethylsiloxane (PI/PDMS) and not so different polyisoprene/polyisobutylene (PI/PIB) interfaces. This has led to the possibility of exploiting the phenomenon of interfacial adsorption of particles, as particulate compatibilizers, to suppress the drop coalescence in PI/PDMS blends. Rheology is presented as a microstructural tool to

qualitatively probe the effect of interfacial activity of particles on the drop size. Our rheology and microscopy results with 0.5vol% of particles show that none of the particle types suppress coalescence of drops in the blends. Instead, PTFE and Fe particles *promote* coalescence of the drops in PI/PDMS blends.

We also examine the stabilization of polymer foams, specifically polystyrene (PS) and polyisobutylene (PIB) by PTFE particles. Our experimental results show that PTFE particles can significantly enhance the stabilization of PS and PIB foams, making them stable for extended periods of time. We believe that this approach of using PTFE particles to stabilize PS and PIB foams may prove useful in a variety of other polymers as well, and may extend the range of polymers and processing conditions under which foaming can be conducted.

TABLE OF CONTENTS

LIST OF TABLES

LIST OF FIGURES

ACKNOWLEDGEMENTS

My words are not enough to express my gratitude to my advisor Dr. Sachin Velankar, for his guidance, support and continued patience. Working under his supervision has definitely been a learning experience, and I am very thankful to him for the knowledge he has imparted to me. I also thank my committee members, Dr. Enick, Dr. McCarthy and Dr. Robertson for their guidance and valuable suggestions.

I would also like to extend "thank you" to my past and present colleagues Dr. Jeff Martin, Candice, Linda, Melissa, Sam and Kevin who have made my stay in the lab very memorable. My special thanks to Bob Barr and Scott Macpherson (machine shop), for their wonderful guidance and help in designing apparatus components. I also thank Bob Maniet and Ron Bartlet for always giving advice if I had any experimental problems. I would also like to thank Rob Toplak and other department staff for their guidance on administrative issues. I also thank the members of Center of Biological Imaging (CBI) for their help and training in optical microscopy, and allowing us to access their state of the art microscopy facilities.

I believe I would have never accomplished all this without the support and love of my husband Sharad. I am thankful to my parents-in-law (Mr. Susheel Kumar Gupta and Mrs. Om Lata Gupta), my borther-in-law Sourabh for their love and support.

I am extremely thankful to my father (Dr. Raj Kumar Thareja), my mother (Dr. Sukarma Thareja), my brother Aditya, who have not only shared but have also stood by me during the dullest periods of my doctoral studies. I am forever thankful to them for their unconditional love

and encouragement. I thank my friends (in department and elsewhere) and my room mates for very beautiful and cherishable moments I have spent with them. Finally, this thesis is dedicated to my husband Sharad and my mother Dr. Sukarma Thareja whose love, patience and continuous support during all these years have enabled me to complete my doctoral studies.

I thank the University of Pittsburgh and National Science Foundation (NSF) for financial support for this research.

1.0 INTRODUCTION

Particles have been known to adsorb at the planar air/water and oil/water interface for more than a century, since 1903 when Ramsden[1] first reported that particle covered air bubbles and drops were irregular in shape and gave the appearance of large globules. Over the last two decades there has been a renewed interest in this area. Numerous studies published on the behavior of particles at planar air/water and oil/water interfaces[2, 3] have given a deeper insight into interparticle interactions and aggregation mechanisms of the particles at the fluid-fluid interfaces. There has also been much interest in particles adsorbed at curved fluid-fluid interfaces e.g. emulsions and foams.

Emulsions consisting of a liquid as a droplet phase dispersed in another liquid as a continuous phase are commonly studied dispersion systems. Since emulsions are thermodynamically unstable, a third component known as surfactant is required to stabilize and render them practically useful. Surfactants are amphiphilic in chemical nature and stabilize the emulsions by adsorbing at the interface of the two liquids. An interesting alternative to molecular surfactants is to employ solid, non amphiphilic, colloidal particles. Such colloid-stabilized emulsions known as *Pickering emulsions*[4] are now key ingredients in many commercially available food and cosmetic formulations.

In *Pickering emulsions*, particles that are partially wetted by two fluids (oil or water) adsorb at the fluid-fluid (oil/water) interface and suppress the coalescence of emulsion drops that

leads to the stabilization of emulsion. Particles of various degrees of complexity such as non spherical particles,[5-9] paramagnetic particles[10,11] and naturally occurring particles[12, 13] have been reported as stabilizers.

This phenomenon of particles stabilizing small molecule emulsions, e.g. oil/water, may also be extended to macromolecular systems such as immiscible polymer blends. Conventionally, interfacial compatibilizers which are macromolecular surfactants are used as stabilizers in polymer blends. Compatibilizers adsorb at the polymer-polymer interface due to their amphiphilic chemical nature. If the non amphiphilic particles can be made to adsorb at the polymer-polymer interface, then they may be able to play the same role as conventional interfacial compatibilizers. A potential advantage of particles over compatibilizers is their non specificity: the same particles may be interfacially active in a variety of blends.

The goal of this thesis is to examine the consequences of interfacial adsorption of particles in polymeric systems. This thesis is organized as follows:

- **Chapter 2:** Background

  Review of the adsorption of particles at both planar and curved oil-water interfaces (*Pickering* emulsions) is given in sections 2.2 and 2.3. The concept of particles bridging of two fluid interfaces is discussed in section 2.4. Section 2.5 deals with the study of particle stabilized aqueous foams. The interfacial adsorption of particles (specifically organoclays and carbon black) in polymer blends is presented in section 2.6. Section 2.7 reviews the dynamics of immiscible blends and in particular the use of rheology as a tool for probing the microstructure of polymer blends.

- **Chapter 3:** Particle induced bridging in immiscible polyisobutylene /polydimethylsiloxane (PIB/PDMS) blends.

Sometimes, a single particle can *bridge* across a thin film between two fluid-fluid interfaces. Such bridging particles can glue together drops of an emulsion. This chapter discusses the consequences of bridging of polyisobutylene drops via fumed silica particles in polyisobutylene/polydimethylsiloxane (PIB/PDMS) blends. This phenomenon is demonstrated to have significant structural consequences which are probed by measuring the rheology of the particle laden PIB/PDMS blend.

- **Chapter 4:** Rheology of polyethyleneoxide/polyisobutylene (PEO/PIB) blends with particle induced drop clusters.

In contrast to the fumed silica particles which form large aggregates among themselves, the spherical silica particles are used in PEO/PIB blends. Thus demonstrating that the rheology of particle laden PEO/PIB blends is attributed solely to the structure resulting from the particles bridging the drops. The ability to visualize the particles due to their bigger size than fumed silica particles is used to relate the blend microstructure to rheological properties.

- **Chapter 5:** Interfacial activity of particles at PI/PDMS and PI/PIB interfaces: Analysis based on Girifalco-Good theory.

Particle adsorption at chemically similar polymer-polymer interfaces is expected to be difficult. In this chapter we discuss the adsorption of various commercially available particles at polyisoprene/polydimethylsiloxane (PI/PDMS) and chemically similar

polyisoprene/polyisobutylene (PI/PIB) interface. This surprising observation of interfacial activity of a variety of particles is explained in terms of Girifalco Good theory.

- **Chapter 6:** Effect of particles on the rheology and morphology of polyisoprene/polydimethylsiloxane (PI/PDMS) blends.

While Chapter 5 shows the interfacial adsorption of particles in polymer blends, no practical use was demonstrated. This chapter discusses the possibility of using interfacial particles as compatibilizers in PI/PDMS blends. The consequence of particle adsorption at PI/PDMS interface is probed via studying the droplet size evolution in the blend by dynamic oscillatory rheology experiments.

- **Chapter 7:** Polymer foams stabilized by particles adsorbed at the air/polymer interface.

The concept of interfacial adsorption of particle in stabilizing polymeric foams is demonstrated in chapter 7. In addition to the high viscosity of the polymer fluid, the interfacial adsorption of particles at the gas-polymer interface may provide an extra stability to polymer foams, thus making them ultra stable at room temperature.

- **Chapter 8:** Future directions.

This chapter discusses the possible research directions for the future.

2.0 BACKGROUND

In small-molecule systems, especially oil/water, interfacial adsorption of non-amphiphilic particles has been attributed to the partial wettability of the particle surfaces. This section discusses the basic physical picture and the energetics of particle adsorption at oil/water interface. Sections 2.2 and 2.3 review the adsorption of particles at planar oil/water interface and curved oil/water interfaces respectively. Section 2.4 reviews the complex phenomenon of bridging via a single particle simultaneously adsorbing at two oil/water interfaces. The concept of interfacial adsorption of particles at oil/water interfaces can be extended to adsorption at air/water interfaces and consequently to stabilization of aqueous foams. The relevant studies are reviewed in section 2.5. Section 2.6 discusses the interfacial activity of particles at polymer-polymer interfaces in polymer blends.

2.1 ADSORPTION OF PARTICLES AT FLUID-FLUID INTERFACE

As shown in Figure 1a, an oil/water interface makes an equilibrium contact angle θ with a flat solid surface. The contact angle θ (measured through water) can be related to the interfacial energies as per Young's equation:

$$\cos\theta = \frac{\alpha_{os} - \alpha_{ws}}{\alpha_{ow}} \qquad [1]$$

where α_{ws}, α_{os} and α_{ow} are the interfacial energies (also called interfacial tensions) of the water/solid, oil/solid, and oil/water interfaces respectively. Such a surface is partially wettable. If this same surface is a spherical particle (Figure 1b), then θ will decide the preferential wettability of the particle towards oil and water i.e. if $0° < \theta < 180°$, the solid surface is partially-wetted by both the liquid phases, and particle adsorption at the interface is expected. On the other hand, if the particle is fully-wetted by either phase, it will not be interfacially active. A relatively hydrophilic particle will have a greater wettability in water, $\theta < 90°$ (Figure 1c) than a relatively hydrophobic particle $\theta > 90°$ (Figure 1d). When many particles are adsorbed, the resulting structure is called a monolayer. Figure 1e shows a monolayer of particles adsorbed at the oil/water interface.

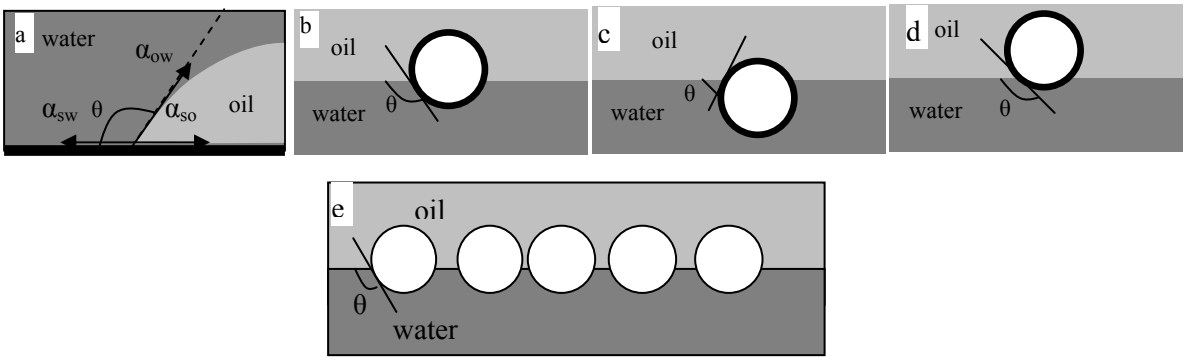

Figure 1. (a) Schematic of a flat solid surface making equilibrium contact angle θ at oil/water interface. (b) A spherical solid particle with the same interfacial characteristics adsorbs at the oil/water interface. (c) Relatively hydrophilic particle preferentially wetting towards water phase. (d) Relatively hydrophobic particle preferentially wetting towards oil phase. (e) A particle monolayer adsorbed at oil/water interface.

The energy of the detachment E of the particle from the oil/water interface into one of the bulk phases is dependent on radius R and interfacial tension α_{ow}. E is given by the equation[3]:

$$E = \pi R^2 \alpha_{ow} (1 \pm \cos\theta)^2 \qquad [2]$$

where θ is measured through the water phase. The negative sign in Equation 2 is for displacing particle into the water phase, whereas the positive sign is for the oil phase. For a particle of radius R = 10^{-8} m, α_{ow} = 0.036 Nm^{-1} for a typical case such as toluene/water, θ = 90º then E is 2750kT^3. As θ moves away from 90°, E decreases but still remains above 100kT for 25° ≤ θ ≤ 155°. Thus for a wide range of contact angles, once the particle is at its desired contact angle, the energy of detachment of particle from the interface is several orders of magnitude higher than thermal energy kT. E is less than 10kT for θ ≤ 20° and θ ≥ 160° thus indicating that only for particles that are highly hydrophilic or highly hydrophobic, the particle will be easily desorbed from the interface by thermal fluctuations.

2.2 PARTICLE MONOLAYERS AND INTERPARTICLE INTERACTIONS AT PLANAR OIL/WATER INTERFACES: SURFACE PRESSURE

The previous section discussed the adsorption of a single particle at oil/water interface. We now describe the adsorption of a particle monolayer at oil/water interface. In the sections below (2.2, 2.3 and 2.4), we have restricted the discussion of interfacial particles at both planar and curved fluid-fluid interfaces to monodisperse spherical particles only (specifically silica and polystyrene). Particles being spherical have well defined shape and contact angle θ at the oil/water interface.

Depending on the wettabilty and interparticle interactions, the monolayers can have different arrangement of particles at the interface. These may range from highly ordered closed packed monolayers to completely disordered monolayers. In some cases fractal like arrangement of particles is also observed.

Horozov et al.[14] studied the behavior of monolayers containing silica particle of different wettabilities at the horizontal oil/water interface. In the case of monolayers of the most hydrophobic silica particles, the authors observed particles forming a hexagonal lattice at the interface. The less hydrophobic particles formed disordered aggregates. Moreover, a transition from disordered to ordered monolayer was observed with increasing hydrophobicity as shown in Figure 2.[14]

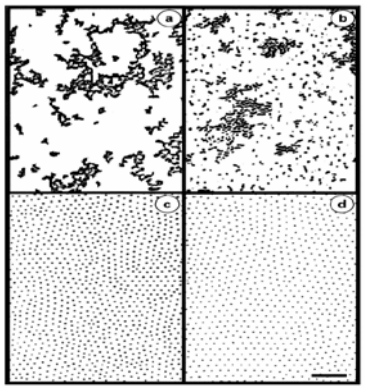

Figure 2. Disorder-order transition of silica particles at the oil/water interface. The particle hydrophobicity increases from a-d. Reprinted with permission from (Ref 14). Copyright (2003) American Chemical Society.

Before *Horozov et al.,* Pieranski[15] had reported the formation of an ordered monolayer of charged polystyrene particles at the air/water and oil/water interface. He reasoned this ordering as the result of the strong dipole-dipole repulsion between the particles. The asymmetric distribution of charge was reported to lead to a dipole which was perpendicular to the interface as

shown in Figure 3a. From theoretical calculations, *Horozov et al.* established the origin of ordered structure as the Coulombic repulsion between residual charges at the particle-oil interface through the oil phase as shown in Figure 3b and disregarded the earlier proposed notion of dipole-dipole repulsion by Pieranski.[15] According to the authors this dipole-dipole repulsion between the particles was too weak to cause ordering of the monolayer.

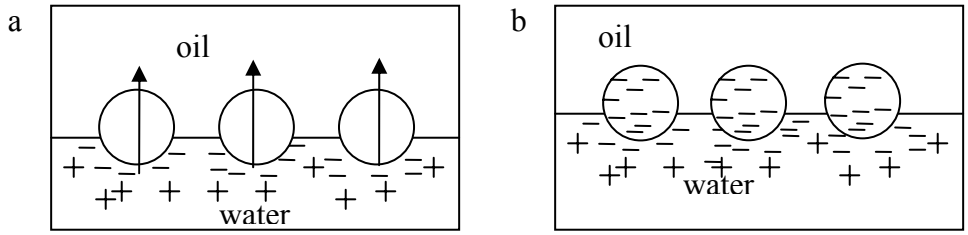

Figure 3. (a) Pieranski's picture of particles behaving as dipoles due to the uneven distribution of charges. (b) Residual charges at the particle-oil interface causing repulsion between them.

Horozov et al.[16] also studied the silica particles of varying hydrophobicity at vertical oil/water interface. The hydrophilic silica particles formed aggregates at the vertical oil/water interface and deposited at the bottom, in contrast to hydrophobic silica particles which formed ordered monolayer and did not sediment. Thus the interparticle repulsion was strong enough to prevent sedimentation due to gravity.

Particles are also known to aggregate indicating interparticle attraction forces. At least three mechanisms are available to explain attraction. The first mechanism proposes the short range attraction between the particles arising from van der Waals forces between particles. Another mechanism is the presence of undulations at the contact line of the particles and the liquid interface due to surface roughness of the particle.[17] Even nanometer size undulations can lead to a large attractive interaction potential. Finally, *Nikolaides et al.*[18] proposed that distortion

of the interface due to electrostatic stresses could also cause a capillary attraction. These stresses are due to the large difference in the dielectric constant of oil and water leading to an asymmetric distribution of charges at the interface.

Another way to study the interparticle interactions is to study the monolayer in a *Langmuir* trough. It consists of a trough with movable barriers to compress/expand the monolayer and measure the surface pressure (π) with respect to area (A) of the monolayer. π is the decrease in the interfacial tension due the presence of particles. *Aveyard et al.*[19] published the compression of hexagonally ordered PS latex monolayer at oil/water interface in the *Langmuir* trough and quantified it in terms of π-A isotherms as shown in Figure 4.

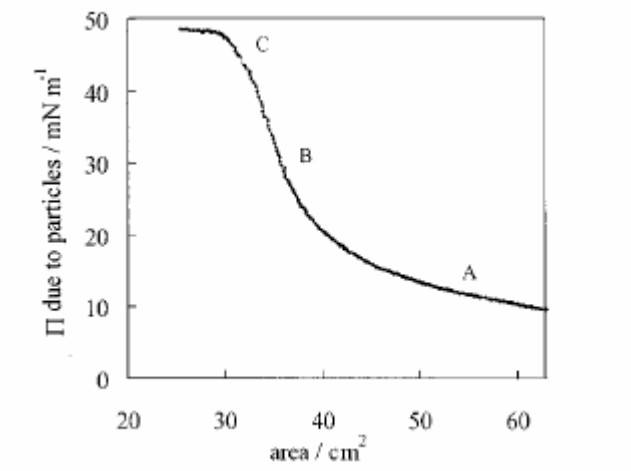

Figure 4. π-A isotherm of PS latex monolayer at oil/water interface. Reprinted with permission from (Ref 20). Copyright (2000). American Chemical Society

The authors found that π increased rapidly with initial compression (region A–B) indicating increased repulsion between the particles due to the decrease in interparticle distance. This was followed by the sudden slow down (region B-C). This was where the monolayer could not be compressed further without developing wrinkles suggesting that it was practically

incompressible. Beyond point C was referred to as collapse pressure π_c, where the particle monolayer buckled or formed ridges. π_c was found to be equal to the bare interface surface tension and was independent of particle wettability.

An interesting study of π-A isotherms of different size particles ranging from 100 nm to 9 μm anionic PS latex was published by *Fuller et al.*[20] The authors also studied the very interesting scenario when the monolayer consisted of bidisperse particles. The shape of the isotherm remained similar to Figure 4 and was unchanged for all the particle sizes considered. The interesting point of their study was that even for different size and ratios of bidisperse particles in the monolayer, the shape of the isotherm and the surface pressure on monolayer collapse remained unchanged. This was true regardless of the degree of order or disorder of the particles and only depended on the kind of interparticle interactions.

An idea of the interparticle forces can also be obtained from the behavior of particle monolayers under flow. *Stancik et al.*[21] used this concept and subjected the monolayer of polystyrene latex particle at oil/water interface to shear flow. The shear rate applied and the concentration of the particles influenced the particle dynamics at the interface. When the shear rate or the particle concentration was low, the particles which were originally arranged in a hexagonal lattice due to the dipole-dipole electrostatic repulsions aligned in the direction of the flow forming string like structures which could slip past one another. In contrast, at a high shear rate or high concentration of particles, the electrostatic forces dominated and did not let the individual particles leave their lattices. The particles moved in domains under flow and maintained their relative positions.

2.3 PARTICLES AT OIL/WATER INTERFACES: PICKERING EMULSIONS

Emulsions consist of one fluid dispersed as droplets into another fluid, thereby creating a curved fluid-fluid interface between the drops and the matrix. Three factors are important in the case of *Pickering* emulsions: size, wettability and concentration of the particles.

In *Pickering* emulsions, the wettability of the particle dictates the kind of emulsion formed and follows an analog of *Bancroft rule* which says that the phase to which particles are less wetting forms the dispersed phase. Thus metal oxides which are relatively hydrophilic stabilize oil in water (o/w) emulsions whereas relatively hydrophobic carbon black particles form water in oil (w/o) emulsions.[22] Recent studies on *Pickering* emulsions use silica particles due to the ease of manipulating their wettability by hydrophobic modification, thus allowing a careful study of wettability with no change in particle size or polydispersity.

Particle wettability not only correlates the kind of emulsions formed but also influences their stability. Binks and Lumsdon[23] showed the effect of particle wettability of silica particles on the stability of the water in oil (w/o) emulsions. The stabilization by the particles of intermediate hydrobhobicity (67% SiOH groups) was reported to result from their strong adsorption at the oil/water interface forming an envelope around the dispersed drops. This provides a steric hindrance to droplet coalescence as shown in Figure 5.

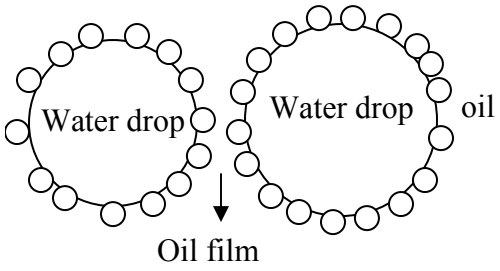

Figure 5. Hydrophobic particles suppress coalescence of drops in w/o emulsions.

Binks and Whitby[24, 25] published a detailed study on the effect of concentration of partially hydrophobic silica particle on stability of o/w emulsions. The authors concluded that increasing the concentration of particles led to smaller emulsion drops and an increase in emulsion stability. However, beyond some high particle concentration, addition of particles did not increase the stability any further. This was explained by considering the ratio of number of total particle to the number of particles available for maximum surface coverage of the drops. This ratio increased with the particle concentration, and became constant above a certain particle loading. The complete coverage is assumed to be achieved when a hexagonal close-packed monolayer is formed at the interface. Once the maximum coverage of drops was reached, the stability did not change.

The stability of *Pickering* emulsions is also influenced by the size of particles as it controls the coverage of interfacial area. It has been reported earlier by *Bechhold et al.*[26] that the stability of emulsions increases as the size of the particles is decreased until a critical size is reached. Once the particle size is less than the critical particle size, the Brownian effects are significant to effect the partitioning of particles at the oil/water interface. Experimentally, it was reported by *Tambe et al.*[2] who compared alumina particles of 4 μm with 37 μm and showed that the emulsion volume was greater for 4 μm particles, indicating the formation of smaller and

stable drops. For spherical particles, *Binks et al.*[27] reported the size dependence of hydrophobic PS latex particles on the stability of water/cyclohexane emulsions. The authors reported that as the size of particles increased from 0.21 μm to 2.7 μm the fraction of phase resolved due to the sedimentation of emulsified water drops also increased. This indicates that with 2.7 μm particles, the emulsion had larger water drops which sedimented at the bottom than with 0.21 μm particles which led to the formation of smaller stable drops.

Emulsion stability can also be affected by the change in the pH of aqueous phase in w/o emulsions. Binks and Lumsdon[28] studied the effect of change in pH of the aqueous phase in w/o emulsions stabilized by partially hydrophobic silica particles. They found that the increase in pH led to the destabilization of the w/o emulsions. At high pH the silanol groups on the silica particles lost their protons and acquired negative charge thus becoming more hydrophilic and hence desorbing into water. This pH dependent phase separation has industrial application in destabilization of water/crude emulsions.

2.4 COALESCENCE SUPPRESSION THROUGH BRIDGING

As mentioned in section 2.3, the steric hindrance mechanism of stabilization of *Pickering* emulsions is possible only when a dense particle layer is formed around the emulsion drops. But if the drops are not fully covered, a more complex stabilization mechanism is possible where the emulsion drops are "bridged" via particles that prevent drop coalescence.

The particles are able to bridge two fluid-fluid interfaces together as shown in Figure 6. Here, the particles satisfy the same contact angle θ at two oil/water interfaces leading to their *bridging*.

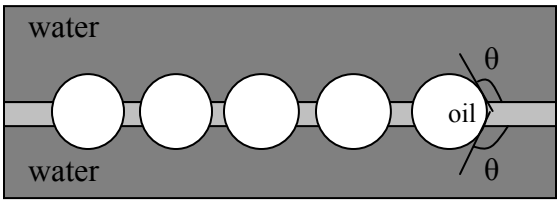

Figure 6. Particles bridging two oil/water interfaces.

Stancik et al.[29] demonstrated the bridging of two oil/water interfaces by colloidal hydrophobic polystyrene latex particles. In their experimental set up, the authors brought a water drop covered with hydrophobic particles dispersed in oil to the flat particle laden oil/water interface as shown in Figure 7a. The particles were observed to satisfy the same contact angle at both the interfaces, resulting in equal portion of them in the water phase. The authors reported the formation of a dense ordered disk of particles which bridged the two interfaces together. The two bridged oil/water interfaces are shown in Figure 7b.[29] The dense bridging disk was reported to be formed as there was no dipole-dipole repulsion between the particles from uneven distribution of charge, since equal portion of particles resided in water phase at both interfaces (refer to Figure 3a). Also the Coulombic repulsion between the particles was reduced due to the thin oil film between the two interfaces. This oil film was reported to be extremely stable against film thinning or thickening.

As the authors tried to pull the bridged interfaces apart, the strong force of adhesion between the drop and the interface led to the distortion of the interface as shown in Figure 7c.[29] The authors also calculated the maximum adhesive force exerted by the particles which depended on the number of particles at the periphery of the aggregated structure, its radius and the three phase contact angle.[30]

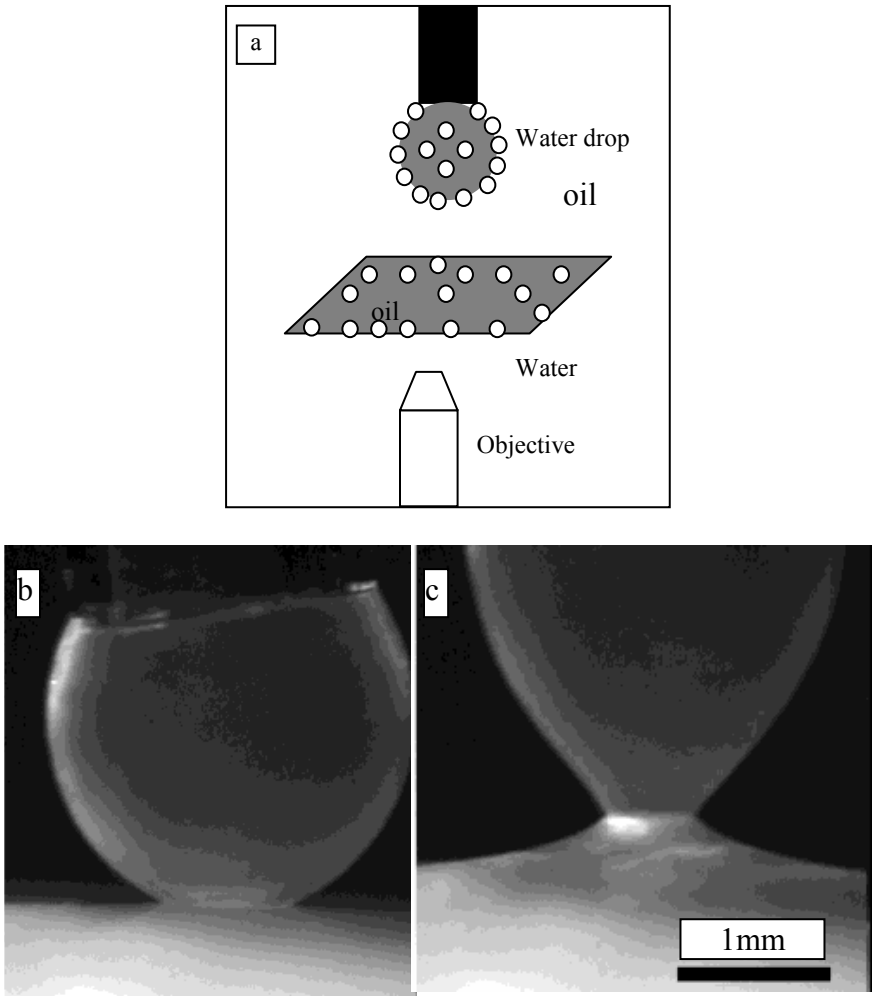

Figure 7. (a) Experimental set up of *Stancik et al.*: a particle laden water drop in oil is brought close to a particle laden flat oil/water interface. (b) Particles bridging the two oil/water interfaces. (c) Deformation of the interface as the water drop is pulled to detach the two interfaces. Reprinted with permission from (Ref. 29). Copyright (2004) American Chemical Society.

Similarly, *Ashby et al.*[31] showed the bridging of two oil/water interfaces by polystyrene latex particles. The authors also calculated the contact angle for bridging by image analysis of the pendant drop meniscus and showed that it was greater than 90°, consistent with the fact that bridging occurred across an oil film.

The bridging (in this case dubbed as "zipping") of two vertical oil/water interfaces by hydrophobic and hydrophilic silica particle monolayers was studied by *Horozov el al.*[32] They directly varied the thickness of the film by pushing fluid into and out of it. As the authors made the film thinner by pulling fluid out (Figure 8a) the particles in both the monolayers formed triangular lattices randomly oriented to each other as shown in the micrograph of Figure 9a. On further thinning (Figure 8b), the particles in opposite monolayer register with each other i.e particles in one monolayer sat below the interstitial spaces of another and formed square lattices (Figure 9b). As the film was made thinner (Figure 8c), the particle again rearranged themselves into triangular lattice with a smaller lattice constant (Figure 9c and d). It was at this point the particles on one interface in the thinnest region of the film started touching the other interface. In an attempt to satisfy the same contact angle at both the interfaces, hence bridging the interfaces, the particles were found to deform the interfaces (Figure 8d). The deformation of interfaces caused an attractive capillary force between the particles which pulled the bridging particles towards each other (Figure 8e), forming a bridging disk (Figure 9e). As the particles came closer to each other, the influence of attractive force increased further causing a rapid growth in the size of the bridging disk (Figure 9f). As with *Stancik et al.*[29] and *Ashby et al.*[31], this dense disk was found to *zip* two oil/water interfaces together with an extremely stable oil film in between. These hydrophobic particles were not observed to sediment at bottom due to the long range Coulombic repulsions among them.

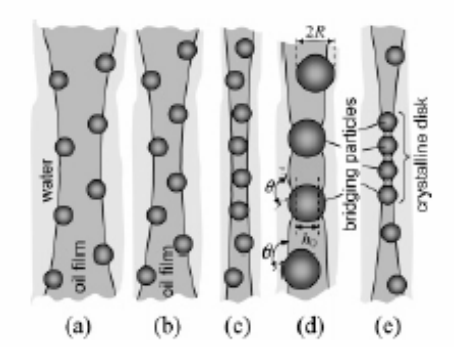

Figure 8. The progressive thinning of a vertical oil film between two oil/water interfaces. Particles bridge the interfaces as the oil film is thinned by sucking fluid out of it (a-e). Reprinted with permission from (Ref. 32). Copyright (2005) American Chemical Society.

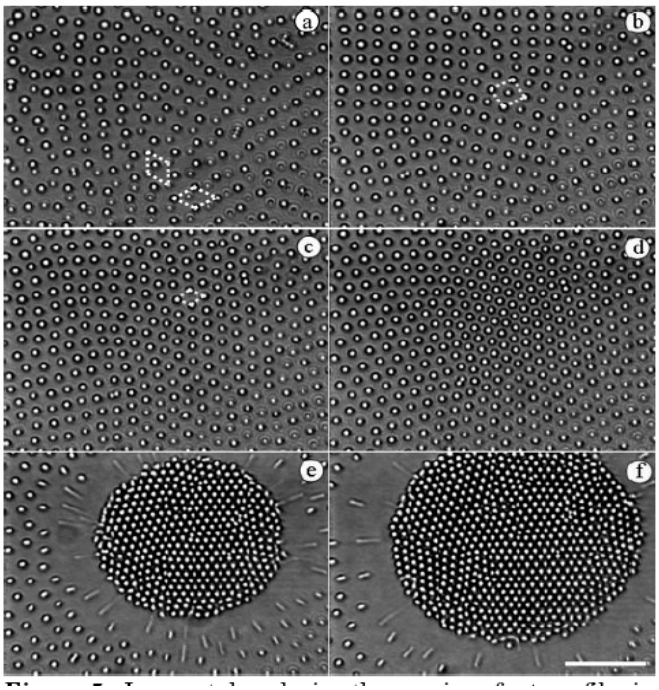

Figure 9. The micrographs of particles forming a bridging disc as the film is thinned (a-f). Reprinted with permission from (Ref. 32). Copyright (2005) American Chemical Society.

While the above mentioned particle bridging studies involve planar oil/water interfaces, the same principles can be applied to curved oil/water interfaces in emulsions. *Vignati et al.*[33] proposed that bridging can be the main mechanism of stabilization through coalescence suppression of the drops, when the particle concentration is much less than what was required for a complete particle shell formation on the surface of the drop. The microscopic results of authors showed that the particles redistribute themselves by diffusion to form a dense monolayer of particles at the contact region, thereby bridging the droplets.

The experimental evidence for drops bridged via particles as a possible mechanism for emulsion stabilization was presented by *Horozov et al.*[34] These authors used relatively hydrophobic ($\theta = 152°$) silica particles to stabilize water in oil (w/o) emulsions. Similar to the particles bridging a planar film between two oil/water interfaces, the microscopic observations by the authors showed the presence of a dense bridging disc of particles between two emulsion water droplets. The micrograph published by the authors (Figure 10a) showed water drops sticking to each other. The oil film between two water drops (region F in Figure 10a) was stabilized by dense monolayer of particles (Figure 10b). This directly proves that bridging can be the stabilization mechanism in emulsions, even when the drop surface is not fully covered by a dense monolayer of particles.

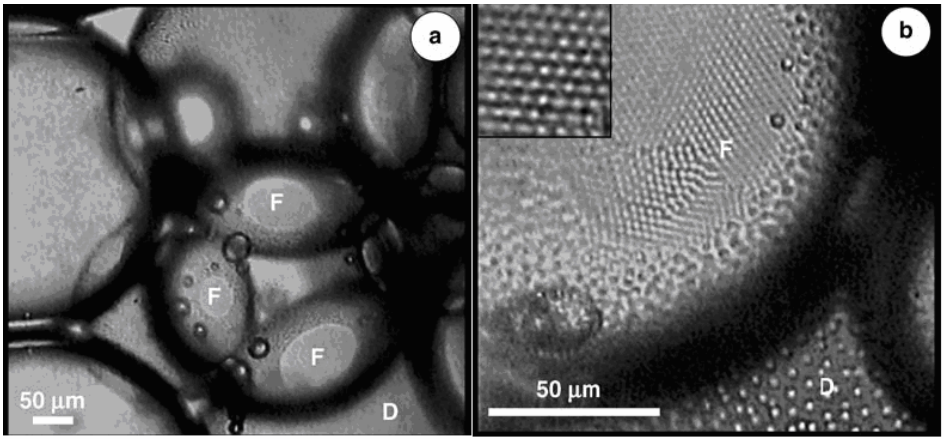

Figure 10. (a) Water in oil (w/o) emulsions stabilized by relatively hydrophobic particles.[34] (b) Micrograph of particles bridging the water drops with the oil film in between. Horozov T.S., Binks B.P. : Particle-stabilized emulsions: A bilayer or a bridging monolayer?. Angewandte Chemie- International Edition. 2006. 45. 773-776. Copyright Wiley-VCH Verlag Gmbh & Co. KGaA. Reproduced with permission.

Recently, *Xu et al.*[20] have shown that the registry of particles at the two fluid interfaces is not the necessary condition for bridging. In most of the experiments registry was not observed at all since the bridging of the two interfaces by the particles is independent of the size of particles and depends only on the contact angle. The authors also used binary mixture of particles to study the bridging phenomenon. In the case of two kinds of particles differing in sizes, small bridging discs of smaller particles were observed inside the bridging discs of bigger particles, effectively phase separating the two kinds of particles.

2.5 PARTICLES STABILIZED AQUEOUS FOAMS

So far, the adsorption of preferentially wetting particles at oil/water interfaces was being discussed. We now focus our attention on particle adsorption at the air/water interface. This

section deals with the stabilization of aqueous foams using particles. Similar to the interfacial adsorption of particles at the fluid-fluid interface which leads to *Pickering* emulsions, the adsorption of particles at the air/water interface can be exploited to form particle stabilized foams as shown in Figure 11.

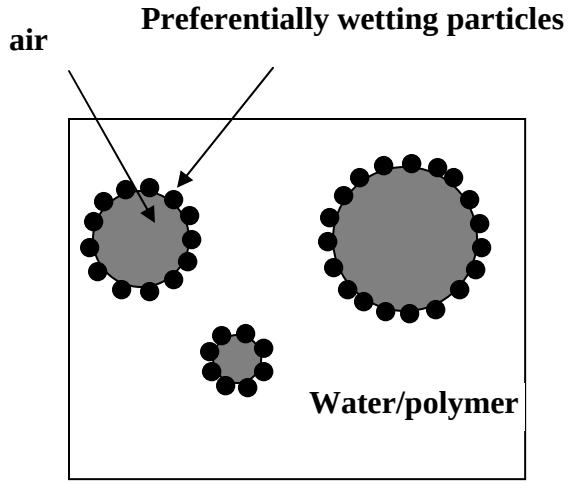

Figure 11. Particle stabilized aqueous foam.

The most common method to prepare aqueous foam is to generate air bubbles by directly bubbling air/gas in the liquid or by a sudden reduction in pressure to cause bubble nucleation. Foams are non equilibrium systems, and can be unstable due to the drainage of liquid film between the bubbles under gravity, bubble coalescence and disproportionation.[35] Surfactants have been conventionally used to stabilize the foams. The two mechanisms of stabilization by surfactants are a) Marangoni stress b) steric hindrance by surfactants. The Marangoni stress mechanism implies that as the two air bubbles approach each other, the drainage flow causes the surfactant to squeeze out of the region between the air bubbles. This creates a surfactant concentration gradient hence an interfacial tension gradient. To counteract this concentration

gradient, Marangoni stress acts tangentially along the interface in the opposite direction of the drainage flow. This retards both the drainage flow and surface flow, thereby suppressing the coalescence of air bubbles. The steric hindrance mechanism comes into play when the fluid film between the two bubbles is very thin. In this case the surfactants inhibit the coalescence of air bubbles by forming an elastic interfacial layer, which inhibits the coalescence of two approaching air bubbles.

Studies have been done on the stabilization of aqueous foams using proteins which adsorb at the air/water interface and form an elastic layer thereby preventing bubble coalescence and film drainage. However, they are not able to completely stop the bubble shrinkage due to the dissolution of the gas in aqueous phase.

Instead of using amphiphilic proteins and surfactants, a novel way of stabilizing foam can be to use solid particles as they have a very high free energy of adsorption. Similar to the interfacial adsorption of particles at the fluid-fluid interface which leads to *Pickering* emulsions, the adsorption of particles at the air-water interface can be exploited to form particle stabilized foams as shown in Figure 11.

Usually surfactants or an additive to the continuous phase is used to achieve desired stability of foam. For example, in the industrial process of froth flotation which is used in mineral recovery, the mineral particles are first rendered hydrophobic by the adsorption of a surfactant. Air is then bubbled through the slurry, which causes the hydrophobic mineral particles to be carried with the air bubbles to the top and separated from the undesirable residue. However, aqueous foams can be stabilized by particles even without surfactants.

Fujii et al.[36] used micron size polystyrene latex particles to stabilize the foams. The structure of the stable aqueous foam was studied by drying the foam. The authors dried the

polystyrene latex stabilized aqueous foams at 100 °C which led to the evaporation of water and the sintering of latex particles. They reported crystallized bilayer of particles separating bubbles.

The ultra stability of macroscopic aqueous foams using inorganic colloidal particles like alumina, ZrO_2, SiO_2 and $Ca_3(PO4)_2$ was demonstrated by *Gonzenbach et al.*[37] These particles, which were originally hydrophilic, were made partially hydrophobic by lyophobization. Lyophobization refers to the attachment of short amphiphilic molecules to the particle surface by either strong electrostatic interactions or ligand exchange reactions such that the hydrophobic tail of the molecule is exposed to the aqueous phase. The ultra stability of the foam was attributed to a strong network formed between the particles at the interface and throughout the foam lamella. The authors speculated that the strong attachment of particles at the air-water interface could lead to the formation of hollow "colloidosomes".

An interesting consequence of ZrO_2 and PS latex particle adsorption at air water interface was demonstrated by *Subramaniam et al.*[38] The authors studied the interfacial jamming of the particles where the interface is so packed with particles that it has solid like properties and can support non spherical bubble shapes. The authors called these particles jammed non spherical air bubbles as "armored bubbles". The interfacial jamming of particles resulted in what are called "interfacial composite materials" (ICM) where the jammed interface had both the properties of a fluid-fluid interface and a rigidity of solid particles. This was reported to have the potential to prevent disproportionation of bubbles.

Formation and stabilization of surfactant free and particle containing aqueous foam was demonstrated by Binks and Horozov.[39] The authors used hydrophobic nano silica particles and reported that fumed silica particles containing 32% SiOH groups were most effective in stabilizing the foams. The micrographs of the particle stabilized foam showed non spherical air

bubbles with rough surface as the interface got jammed with particles. Addition of NaCl was reported to increase the stability of the foam.

The shape of particles can greatly affect the foamability and stability. This was demonstrated by *Alargova et al.*[40] who used polymer micro rods to make extremely stable foams. The authors explained the super stabilization of the foams due to the entanglement to micro rods which lead to the formation of a solid shell around the bubbles. This provided a steric hindrance for bubble coalescence and did not allow the bubbles to shrink or expand thus making the foam stable.

Along with the interfacial stabilization of aqueous foams, the particles can also form networks in the bulk which can get attached to the interface. The combination of these two effects can give enhanced stability to the foam. This was shown by *Dickinson et al.*[41] who generated the air bubbles by applying a pressure drop to an aqueous suspension of partially hydrophobic fumed silica particles. The authors showed that the increase in the particle concentration increased the stability of the foam. This was because at high concentration of fumed silica particles, the particle network in the bulk got attached to the interfacial particle layer, thereby rendering stability to the foam. This was also confirmed by the confocal scanning laser microscopy of the foam sample.

2.6 PARTICLES AT POLYMER-POLYMER INTERFACES

We now focus our attention to high viscosity and macromolecular analogs of oil/water emulsions i.e. polymer blends. Polymer blends are of great technological importance as they may give materials with properties far superior to those of individual constituents. Also, blending provides

an economic alternative for better materials rather than investing in cost intensive chemical synthesis. To improve the blending of two immiscible polymers, compatibilizers are often added. Compatibilizers are graft, block and star copolymers which due to their amphiphilic chemical nature adsorb at the interface of two polymers.

In contrast to compatibilizers, the particles being non amphiphilic i.e. having a uniform surface characteristic can still adsorb at the interface due to their partial wetting towards both the phases. Therefore, interfacially adsorbed particles may present a convenient alternative to compatibilizers as they are not specific to a particular polymer blend. Thus if the particles are able to adsorb at the polymer-polymer interface, they may find use as a compatibilizer in immiscible polymer blends.

As mentioned in section 2.2, 2.3 and 2.4, particles adsorb at the oil/water interfaces. The energetics of particle adsorption is governed by the oil/water interfacial tension, wettability, radius of particles and pH. In case of oil/water interfaces where the polarity difference between oil and water phases is large, finding a particle type which is partially wetting towards both phases is usually not a difficult task. But in the case of polymer-polymer interfaces, where the polarity difference of the phases is much smaller, finding an interfacially active particle might not be straight forward. Yet there has been some research on particle adsorption at polymer-polymer interfaces. The most extensively studied particle containing polymer blends are that of organoclays and carbon black. The section below specifically reviews the polymer blends containing these particles.

2.6.1 Organoclays

Organoclay nanocomposites have gathered enormous attention ever since Toyota researchers incorporated organomontmorillonite clay in nylon to improve mechanical and thermal properties.[42] A clay platelet consists of layers and these layers stack upon one another with a van der Waals gap between them called interlayer or a gallery. These layered silicates when dispersed in a polymer matrix, form two types of structures a) intercalated b) exfoliated. The intercalated structure is formed when the polymer matrix goes into the interlayer space in a regular polymer/layer arrangement as shown in Figure 12. Exfoliated structure is formed when clay layers are well separated from each in polymer matrix, there is no regular arrangement of layer and polymer.[42]

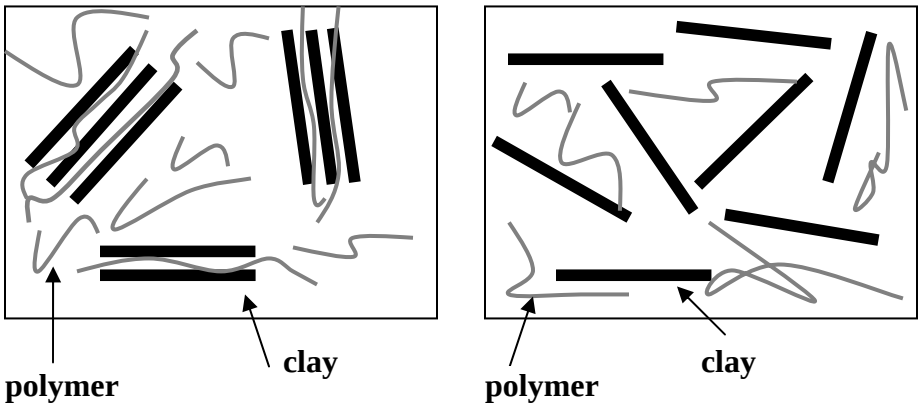

Figure 12. (a) Intercalated and (b) exfoliated structure of clay platelets in polymer matrix.

Ray et al.[43] have demonstrated the use of organically modified layered silicate structure as an interfacial modifier in polystyrene (PS)/polypropylylene (PP) blends and the PS/PP-g-MA (polypropylene grafted with maleic anhydride). The organically modified layered silicate acted

as an interfacial modifier in the case of PS/PP blends as both kinds of polymer chains went into the silicate layers forming an intercalated structure. Since the intercalated structure was shared by both the polymers, the layered silicate was found to be at the interface of PS and PP. The interfacial action of layered silicate was also confirmed by the decrease in interfacial tension by the drop deformation method.[44] In the case of PS and PP-g-MA, the layered silicate was exfoliated in the PP-g-MA. Thus along with the presence of layered silicate at the interface, it was also dispersed in PP-g-MA matrix. Both the interfacial action of layered silicate and the higher viscosity of the matrix due to their presence led to the suppression of coalescence of PS domains.

The role of organically modified layered silicate in the breakup and coalescence of droplets in immiscible polybutylene terephthalate/polyethylene (PBT/PE) blend has been shown by *Hong et al.*[45] The authors showed that if small amount of organoclay was added, the clay was found to be at the interface. As they increased the amount of organoclay, the remaining clay was found to go into the phase with which it had a higher affinity. In the case of PBT/PE, the organoclay was observed to have more affinity for the PBT phase. Thus when the drop phase was PBT, the domain size of PBT was found to increase with increase in the concentration of organoclay. According to the authors, this was because the clay in the drop phase made the drop less deformable and thus less breakable. In contrast when they had PBT as the matrix, the presence of clay in PBT changed the rheology of the clay/PBT and the authors reasoned that this exerted a hydrodynamic stress on the drop phase which could suppress coalescence. To confirm that the interfacial activity of organocaly was also responsible for suppressing coalescence, the authors compared the interfacial tension of clay laden blends with blends containing no clay. The interfacial tension was measured by fitting the dynamic oscillatory rheological data to Palierne

model.[46] The authors showed a decrease in interfacial tension of the clay containing blends, this was attributed to the presence of organoclays at the interface.

In a later publication,[47] the authors correlated the decrease in interfacial tension due to the adsorption of organoclays to the rheological properties of the particle laden blends. The authors used extensional force measurements to measure the interfacial tension. They argued that the force measured on the blend is the sum of the forces on the individual components of the blend and the force on the interface, which comes from the interfacial tension. By comparing the organoclay free and organoclay laden blends, the authors were able to conclude that the interfacial tension was reduced because of the adsorption of organoclays at the interface. The consequence was that the coalescence was suppressed and the drops had a higher tendency to break, therefore the particle laden blend showed smaller droplet size.

The compatibilizing effect of organoclays was demonstrated by *Si et al.*[48] in polycarbonate (PC)/styrene acrylonitrile (SAN) where SAN was the minority phase. The authors showed that with the increase in organoclay concentration, the SAN domain size progressively decreased. Beyond 3% of organoclay loading, the domain size became not only small but also irregular due to the crowding of the interface by organoclays. The presence of organoclay at the interface is shown in the TEM micrograph below in Figure 13.

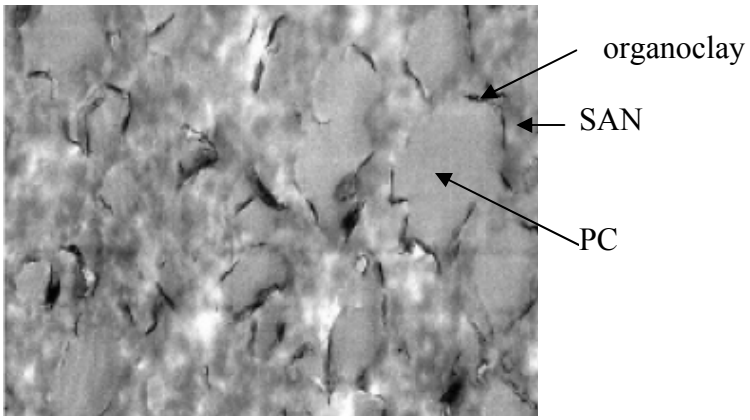

Figure 13. TEM micrograph showing organoclays at the interface of PC/SAN. SAN domains have irregular shape due to the crowding of interface with organoclays. Reprinted with permission from (Ref. 48). Copyright (2006) American Chemical Society.

2.6.2 Carbon black

Carbon black is another filler that has been studied extensively. It is used not only as reinforcement but also as conductive filler. However to provide a conductive pathway through the blend, carbon black has to be percolated throughout the blend.[49] The minimum concentration of carbon black required (i.e. percolation threshold) for a conductive pathway in a polymer, such as polyethylene (PE), is 5 wt% which might not be economical always.[50] To reduce the percolation threshold *Gubbels et al.*[50,51] presented the polyethylene (PE)/polystyrene (PS) blends with the carbon black particles at the interface. The important point highlighted by the authors was that the carbon black has weak interactions with both the polymers resulting in the location of carbon black at the interface. The authors reported a PE:PS ratio of 45:55 at which the maximum reduction in percolation threshold from 5 wt% to 0.4 wt% was observed. At this composition the blend had cocontinuous morphology, and the localization of carbon black at the

interface caused the formation of a 2D chain like structure, spanning throughout the blend. In a separate study, the authors also reported the localization of carbon black at the interface of polystyrene (PS) and polyisoprene (PI) blend.[52] A percolation threshold of 0.2 vol% of carbon black was reported at a ratio of 45:55 for PS/PI cocontinuous blend. The micrograph showing the presence of carbon black at the interface is given below in Figure 14.

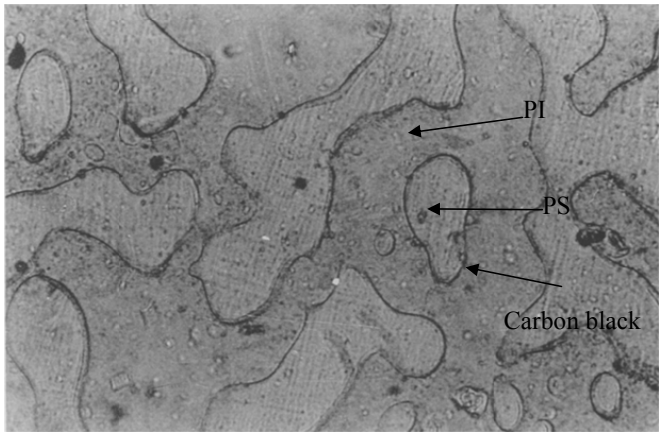

Figure 14. Optical micrograph of carbon black particles at the interface of cocontinuous polystyrene/polyisoprene blend. With kind permission from Springer Science + Business Media: Polymer Bulletin, Electrical Conductivity in carbon black-loaded polystyrene-polyisoprene blends. Selective localization of carbon black at the interface, 35, **1995**, 223-228, Soares, B. G.; Gubbels, F.; Jerome, R.; Teyssie, P.; Vanlathem, E.; Deltour, R., Figure 4.

Calberg et al.[53] studied carbon black filled polystyrene in cocontinuous polystyrene (PS)/polymethylene methacrylate (PMMA) blends. The authors showed the stabilization of these blends against coalescence as the CB localized at the interface. Since the blend morphology could be stabilized by CB, the composition range in which these blends were cocontinuous could be manipulated easily as well.

Apart from organoclay and carbon black, we are aware of only one publication where alumina (Al_2O_3) nanoparticles have been reported to adsorb at the polymer-polymer interface in polypropylene (PP)/nylon (Ny) blends.[54]

Although both organoclays and carbon black have been reported to adsorb at polymer-polymer interface, these particle containing blends show complex behavior because of the small particle size and their tendency to form aggregates. Thus, further research is needed to shed light on the role of particles in polymer blends.

2.7 MORPHOLOGY AND RHEOLOGY OF PARTICLE FREE IMMISCIBLE POLYMER BLENDS

As mentioned before, the goal of this thesis is to examine the effect of particles at polymer-polymer interfaces in polymer blends. Similar to particle free polymer blends, we expect that the properties of the particle laden blends will be dependent on its microstructure. A convenient way to study the microstructure of particle laden blends is to trace their morphological evolution with the applied flow field. Rheology provides a vital tool for studying the microstructure of the blends in terms of rheological properties such as viscosity and modulus. The response of the blend is studied under a given flow field, which is related to the structure. Various rheological experiments have been performed with model immiscible blends with droplet-matrix morphology to study the morphological evolution with the flow.[55] The studies show that blends have higher elasticity due to the deformation and relaxation of the interface of the drop and the matrix. Thus an understanding of the droplet deformation and relaxation provides the basis for predicting the overall morphology of the blend. The blends discussed in the sections below are

the blends of two immiscible Newtonian fluids. Newtonian fluids are not viscoelastic, therefore the viscoelasticity of blends is attributed only to the deformation of interface and not to the bulk phases. Since polymers have high viscosity, the gravitational and inertial effects are neglected in these systems.

2.7.1 Single drop deformation and breakup

When a single drop is subjected to shear flow, it will deform, orient itself to the flow and possibly breakup. The only two forces acting on an isolated drop are the applied viscous force that tends to deform the drop and interfacial tension which tends to keep the drops spherical. The drop deforms under the applied shear stress and after cessation of flow the drops retract back due to the interfacial tension.

The ratio of viscous stress to the interfacial stress is a dimensionless number called the capillary number Ca, defined as:[56]

$$Ca = \frac{\sigma}{\alpha / R} \qquad [3]$$

where σ is the applied shear stress, R is the radius of drop and α the interfacial tension between the two phases. If the applied stress is high enough, it can overcome the interfacial tension ultimately leading to the breaking of drop. Thus a critical capillary number (Ca_{cr}) is defined above which the droplets break.

2.7.2 Coalescence and Dynamic Equilibrium between breakup and coalescence

When the blend is sheared and $Ca < Ca_{cr}$, drops coalesce and result in an increase in R. For the drops to coalesce, they must first collide with each other. When the drops collide, the drop interface becomes flat with a layer of fluid in between. It is the drainage of this fluid film which leads to the coalescence of drops. The thickness of the fluid film has to be small enough so that the short range van der Waals forces between the droplets can cause film rupture leading to the coalescence of drops.

The coalescence of drops continues until $Ca > Ca_{cr}$ after which the drops break. As the drops decrease in R due to breakup, Ca becomes less than Ca_{cr} and the coalescence dominates. This interplay of coalescence and breakup of drops continues till the drop size reaches a steady state, although sometimes the approach to steady state can take a long time. Therefore at steady state there is a dynamic equilibrium between the drop coalescence and breakup. However, before the dynamic equilibrium is established, the morphology of the blend or the size of the droplets is strongly dependent on the applied shear history.

2.7.3 Rheology

The changes in morphology caused by breakup and coalescence are reflected in rheological properties. The sections below discuss three rheological properties which are used to interpret the morphology of the blends: viscosity, strain recovery and dynamic modulus.

2.7.3.1 Viscosity

The viscosity of the blend is dependent on the volume fraction φ of the dispersed phase. The simplest case corresponds to a dilute suspension of solid particles in a matrix. The viscosity of the suspension is given by Einstein's equation:

$$\frac{\eta}{\eta_m} = (1 + 2.5\phi) \qquad [4]$$

where η_m is the viscosity of the matrix phase. Extending the theory to emulsions/blends where the solid particles are replaced by drops which deform and break, Taylor[57] included the internal circulation in the droplet phase. The factor 2.5 in Einstein equation is replaced by $K = \frac{5}{2}\frac{p+0.4}{p+1}$, in Taylor's expression for emulsion viscosity as given in Equation [5].

$$\frac{\eta}{\eta_m} = 1 + \frac{1 + 2.5p}{1 + p}\phi \qquad [5]$$

where p is the ratio of viscosities of drop phase to the matrix phase ($p = \frac{\eta_d}{\eta_m}$).

Einstein's equation assumes a dilute suspension and Taylor's equation is good for emulsions but both ignore hydrodynamic interactions between the drops. As the volume fraction of drops is increased, the hydrodynamic interactions start playing a vital role. To include the hydrodynamic interactions, Choi and Schowalter[58] proposed the following equation for viscosity:

$$\frac{\eta}{\eta_m} = 1 + \phi\frac{(5p+2)}{2(p+1)}.\left(1 + \phi\frac{5(5p+2)}{4(p+1)}\right) \qquad [6]$$

Here, the viscosity is the function of viscosity ratio p and volume faction φ, but does not have any morphological dependence. Therefore, the viscosity does not give any information about the morphology of the blend. The morphological information about the blend is deduced from the strain recovery and dynamic oscillatory properties of blend.

2.7.3.2 Strain recovery of Blends

After the cessation of the flow, the drops retract back to their spherical shape due to the interfacial tension between the droplet and matrix. If drop retraction occurs without any applied stress it causes elastic recovery, also called "recoil" of the blend. This recoil of the blend after the cessation of steady state shearing can give vital information about the morphology of the blend. Since pure Newtonian bulk phases, by definition, show no recoil behavior, the recoil of the blend can be attributed solely to the action of the interface. [59,60]

The kinetics of strain recovery for a blend of monodisperse drops is given by *Vinckier et al.*[59] as shown below:

$$\gamma_r = \gamma_\infty[1 - \exp(-t/\tau_2)] \qquad [7]$$

where τ_2 is defined as the characteristic retardation time of the drops to retract back to the spherical shape after the cessation of flow and γ_∞ is the ultimate recoil. From dimensional analysis $\tau_2 \propto \frac{R\eta_m}{\alpha}$; where R is the radius of the drop, η_m is the viscosity of the matrix and α is the interfacial tension between the two phases.

Using τ_2 from Graebling model,[61] the ultimate recoil after steady shear flow is given by Equation [8].

$$\gamma_\infty = f(Ca, p, \phi) \qquad [8]$$

Here p the viscosity ratio and φ is the volume fraction of the dispersed phase. Also Taylor's theory[57] predicts that for small Ca, the deformation (D_{Taylor}) is given by Equation [9].

$$D_{Taylor} = Ca\frac{19p + 16}{16(p + 1)} \qquad [9]$$

Thus both τ_2 and γ_∞ are a strong function of Ca and hence the deformation (D). It should be noted that both τ_2 and γ_∞ depend on the morphology of the blend, thus measuring these rheological properties can give an insight about the blend microstructure.

2.7.3.3 Dynamic Oscillatory behavior

The small amplitude oscillatory frequency sweep experiment is used for probing the morphology of the blend as the applied strain is small enough to keep the morphology intact. The sinusoidal strain for a specific frequency ω is given by:[62]

$$\gamma = \gamma_0 \sin \omega t \qquad [10]$$

The stress response of the sample is also sinusoidal and is out of phase by an angle δ:

$$\tau = \tau_0 \sin(\omega t + \delta) = (\tau_0 \cos\delta)\sin\omega t + (\tau_0 \sin\delta)\cos\omega t \qquad [11]$$

$$= \gamma_0 G' \sin\omega t + \gamma_0 G'' \cos\omega t \qquad [12]$$

The oscillatory experiment is usually repeated at several frequencies: the frequency spectrum thus generated provides a way of probing the morphology without disturbing it and gives the dynamic moduli G' and G". The storage modulus G' is indicative of solid like behavior, whereas the loss modulus G" is indicative of the liquid like nature of the material. In blends, the variation of G' and G" with the oscillatory frequency ω is directly related to the morphology. At high frequency of oscillation the drops deform with the applied oscillatory flow with no significant relaxation. However at lower frequencies, the drops deform during the applied flow and relax back under the influence of interfacial tension. This causes the appearance of a characteristic shoulder in the logG' vs logω curves as shown in Figure 15a. The presence of the shoulder is manifested as the interfacial relaxation, provided that the relaxation time of the

matrix and droplet fluids is much smaller than the interface relaxation. Another rheological property which is also deduced from the frequency spectrum is complex viscosity η*.

The magnitude of complex viscosity $|\eta^*|$ is defined as:

$$|\eta^*| = \lim \omega \to 0 \frac{|G^*(\omega)|}{\omega} \quad [13]$$

where the complex modulus G* is defined as:

$$G^* = G' + iG'' \quad [14]$$

$$|G^*| = \sqrt{G'^2 + G''^2} \quad [15]$$

There is extensive literature available on model immiscible blends[46,61,63,64] showing that the additional relaxation process causing the shoulder in |η*| (Figure 15b) and G' corresponds to deformation and relaxation of the drops in the blends. Dimensional analysis suggests, and detailed theory confirms,[61] that the characteristic frequency of this process must scale as $\alpha/\eta_m R$, where R is the mean drop size, and η_m is the viscosity of the matrix phase. Therefore a shift of shoulder to lower or a higher frequency can track changes in drop size.

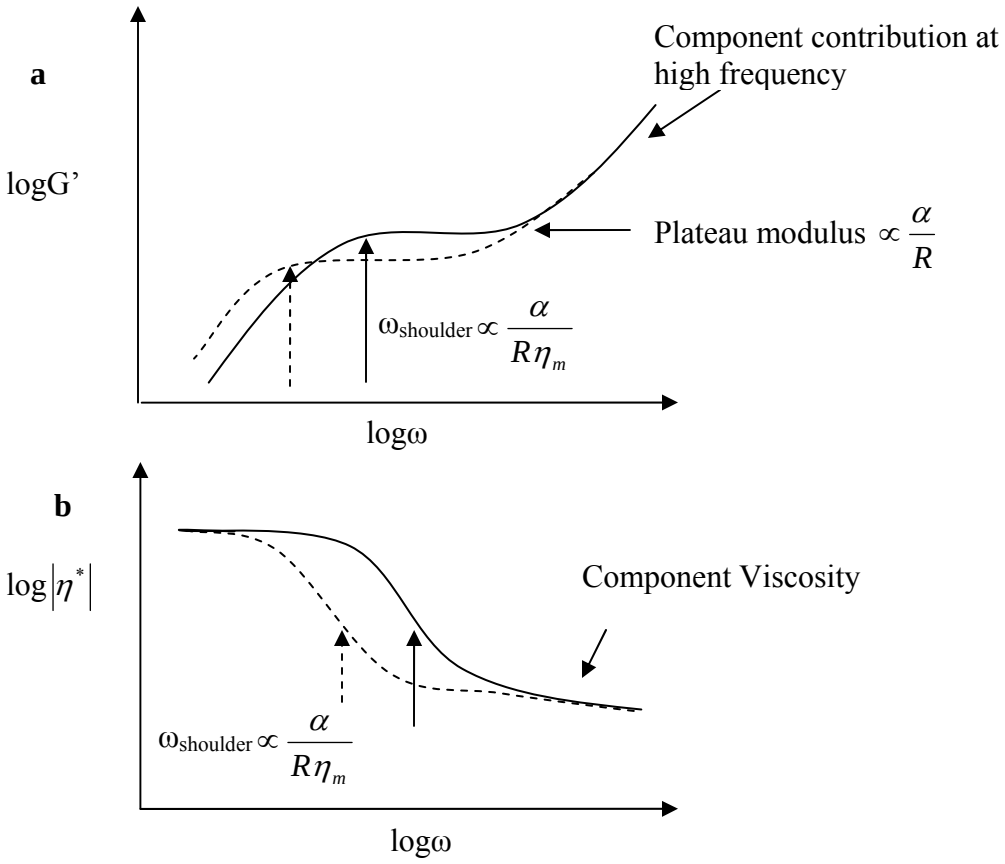

Figure 15. (a) log G' versus logω; (b) log |η*| versus logω for particle free blend. The presence of a shoulder is attributable to deformation and relaxation of drops.

In summary, strain recovery and oscillatory experiments can give microstructural information about the blends in terms of their rheological properties. The recoverable strain and the kinetics of recovery can be related to the morphological evolution under a flow field. The dynamic oscillatory frequency sweeps from the drop deformation and relaxation provide a valuable tool for probing the morphology and giving information about the droplet size.

In the forthcoming chapters, rheology is used as a tool for studying the microstructure of particle laden polymer blends in conjunction with the optical microscopy studies. We will

interpret the change in rheological properties in terms of changes caused by the particle adsorption at the polymer-polymer interface in polymer blends.

3.0 PARTICLE INDUCED BRIDGING IN IMMISCIBLE POLYISOBUTYLENE/POLYDIMETHYLSILOXANE (PIB/PDMS) BLENDS[65]

This chapter focuses on the consequences of bridging of two drop interfaces by the particles in polymer blends. We hypothesize that such bridging interactions should have a significant effect when particles are added to droplet-matrix blends of immiscible homopolymers. In particular, if the particles are wetted preferentially by the continuous phase, the dispersed phase droplets should be able to stick together without coalescing, giving rise to drop clusters. Such clustering is likely to have rheological consequences, especially if the clusters are large or form an extended network.

In a recent paper, *Vermant et al.*[66] studied the effect of adding fumed silica particles to droplet-matrix blends of PIB and PDMS. Cryo-SEM images showed that the silica particles were adsorbed at the interface between PIB and PDMS. Furthermore, rheological investigations revealed that the particles could prevent coalescence in blends with droplet-matrix morphologies provided that PIB formed the drop phase, and the PDMS formed the matrix phase. In the reverse morphology (PDMS drops in a PIB matrix), coalescence was not suppressed. This asymmetry of coalescence led *Vermant et al.* to suggest that the particles were preferentially-wetted by the PDMS phase in PIB-in-PDMS blends. These particles would then protrude well outside the drops and suppress coalescence, whereas in PDMS-in-PIB blends, coalescence would not be suppressed. Based on the discussion above, we hypothesize that in PIB-in-PDMS blends, fumed

silica particles will be able to glue together PIB drops, and the resulting drop clusters will significantly affect the rheological properties of the blend.

The first goal of this chapter is to test this hypothesis by optical and rheological methods. If the hypothesis is validated, i.e. bridging is indeed evident, the PIB/PDMS/fumed silica system may be a convenient model system to further study the effects of particle bridging. The second goal of this chapter is to critically evaluate the suitability of this system as a model system for studying particle-bridging effects in polymer blends.

3.1 EXPERIMENTAL

Experiments were conducted on blends of PIB (Soltex, viscosity 69 Pa.s) and PDMS (Rhodia, viscosity 95 Pa.s). Both homopolymers are nearly Newtonian fluids under experimental conditions. Hydrophobic fumed silica particles (Degussa, Aerosil Rhodorsil R 972) were used up to 1% by weight. These are the same particles used by *Vermant et al.* They have a primary particle diameter of 16 nm, and the manufacturer coats them with dichlorodimethylsilane (DCDMS) to render them hydrophobic. Samples were blended by two methods, either by hand-blending with a spatula (following *Vermant et al.*) or by a "Minimax" mechanical mixer[67] as described later in the text. Samples are designated Bx-y, where x is the weight percent of PIB in the blends (either 10 or 30%), and y is the weight percent of the fumed silica particles (either 0 or 1%).

The rheological measurements were carried out in a stress controlled rheometer (AR 2000) using a stainless steel cone and plate geometry (cone angle of 1° and a diameter of 40 mm). Sample temperature was maintained at 23 °C with a Peltier plate device. The blends were

presheared at 400 Pa for 2000 s. Shearing was then stopped and the dynamic moduli were measured at 25% strain in the frequency range 100 – 0.02 rad/s. The oscillatory measurements were repeated three times, with the sample remaining under quiescent conditions for two hours between successive frequency sweeps.

3.2 RESULTS

3.2.1 Optical Microscopy of hand-mixed samples

The hypothesis is that the drops of particle-containing blend are able to glue together and form clusters. Thus, the first goal is to validate such cluster formation by direct visualization. The cluster formation requires that drops come sufficiently close to each other so that the particles can glue them together. We considered two different ways of doing so: inducing collisions by shear flow, and inducing collisions under quiescent conditions due to van der Waals forces or buoyancy forces.

The first method, shear-induced coalescence, used a home-built parallel plate apparatus, which consists of two glass plates that can be mounted on an ARES rheometer in a parallel plate geometry. The sample is loaded between the plates at the desired gap and subjected to the desired shear history. The plates can then be removed from the rheometer without disturbing the sample between them (i.e. maintaining the gap) and examined under a standard microscope.

A B10-1 blend was loaded in this apparatus at a gap of 0.127 mm, sheared at 0.1 s^{-1} for 2.5 hours to induce collisions between drops, and then examined under microscope. Some ill-defined drop clusters were evident to the eye, but the image quality at this gap of 0.127 mm was

poor due to intense scattering. The plates were therefore gently squeezed together over several hours so as to reduce the gap, and improve the image quality. When the gap is sufficiently small, droplet clustering becomes more clearly evident (Figure 16).

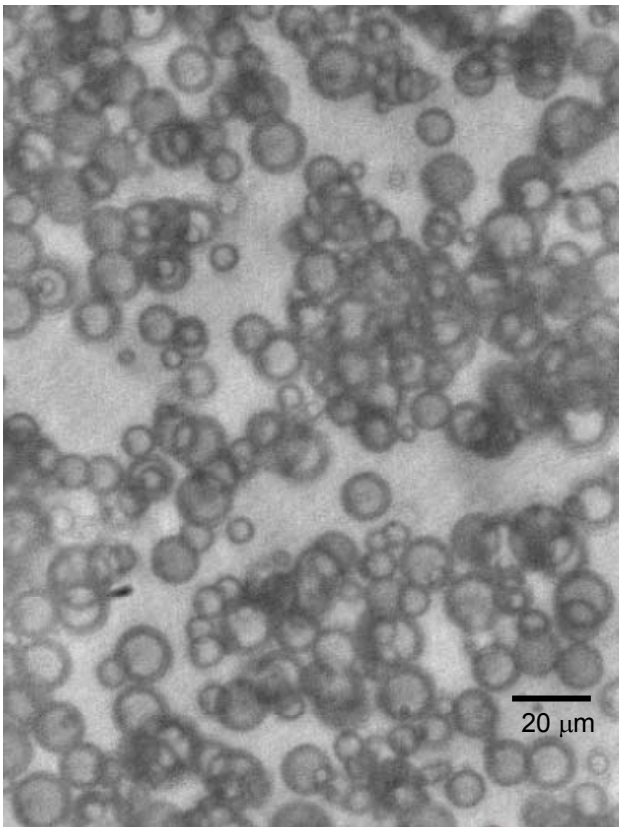

Figure 16. B10-1 following the shear history described in the text.

The second method, quiescent coalescence, was conducted by storing a B10-1 sample in a petridish under quiescent conditions for several weeks, and then examining it under microscope. Once again, ill-defined drop clusters were evident to the eye, but due to the small drop size (see Figure 18b to be discussed later), image quality was very poor. Therefore, a small sample of this blend was placed in a petridish, and 2-3 ml of low viscosity (0.1 Pa.s) silicone oil (PDMS) was added to this petridish. This silicone oil is fully miscible with the PDMS used as

the matrix of the blend, and hence acts as a solvent or diluent for the matrix phase. The petridish was then tilted back and forth gently several times to force the low viscosity PDMS to wash over the blend and gently disperse it throughout the petridish. The petridish was examined frequently under microscope during this process. The rationale behind this procedure was that if the drops of B10-1 were indeed glued together into large clusters at the very low stresses involved in the gentle flow, at least some drop clusters should survive. Indeed we found large clusters breaking off the periphery of the B10-1 sample and dispersing. Figure 17 shows some examples of such clusters. We were also able to image some of these clusters during gentle flow in the petridish and observe their undulating motions, as well as tumbling about the vorticity direction under shear. Finally, upon swirling the petridish violently, the clusters broke apart into small clusters or individual drops.

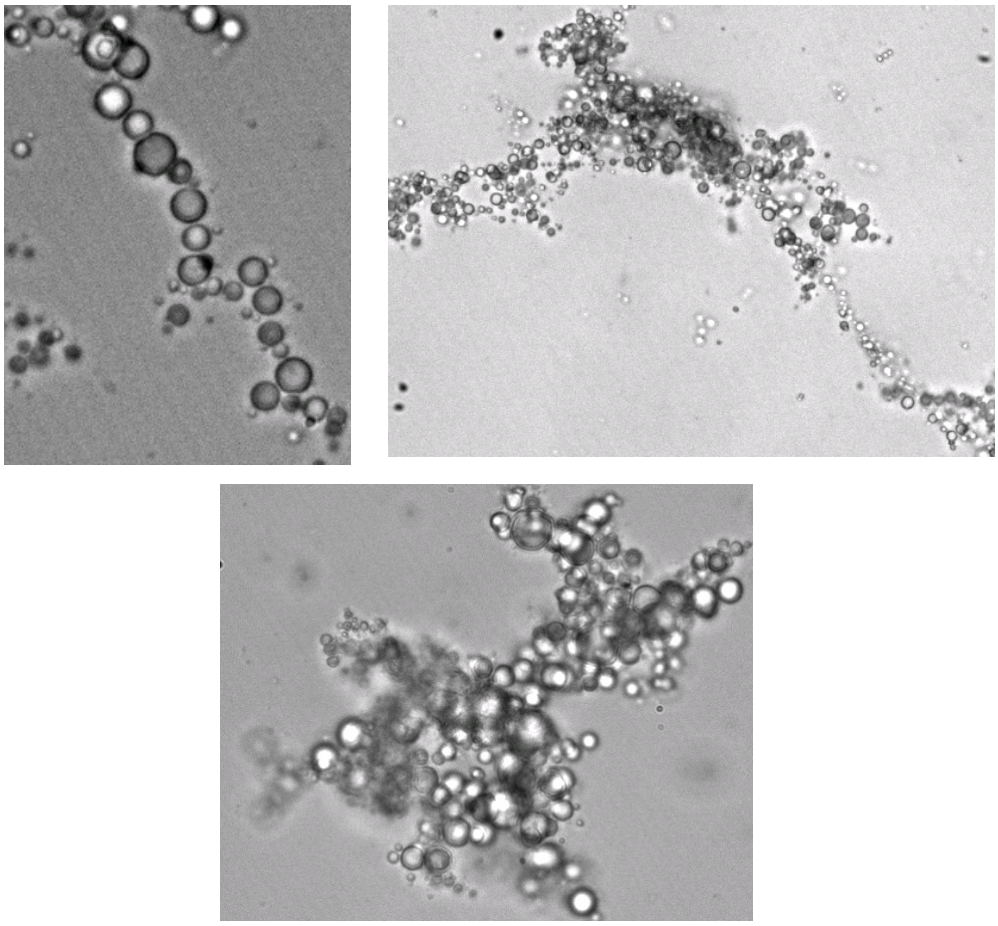

Figure 17. Drop clusters of B10-1 imaged as described in the text.

In summary, Figure 16 and Figure 17 are evidences that cluster formation is possible in PIB/PDMS/fumed silica blends. In the remainder of this chapter, we will consider the rheological consequences of such clustering.

3.2.2 Rheology of hand-mixed samples

Before proceeding with well-controlled rheological experiments, it is interesting to note a large qualitative change in the rheology of the above B10-1 sample left in the petridish for several weeks. This sample had been mixed by a spatula and hence it had – naturally – been unevenly

distributed in the petridish with a few – bare – patches. After several weeks, it was evident even to the naked eye that the sample had *not* spread out evenly in the petridish. Some portions of the petridish had a much thicker layer of sample than others, and some portions remained bare without any blend (Figure 18a). In these bare patches, the bottom of the petridish had a wetting layer of PDMS, but had no PIB drops. This uneven thickness of the sample layer in the petridish is perhaps the best indication that this sample has converted into a gel with some finite yield stress. Observation of the edge of the bare patch reveals tightly packed drops forming a barrier (Figure 18b), and preventing the patch from being filled in by the blend.

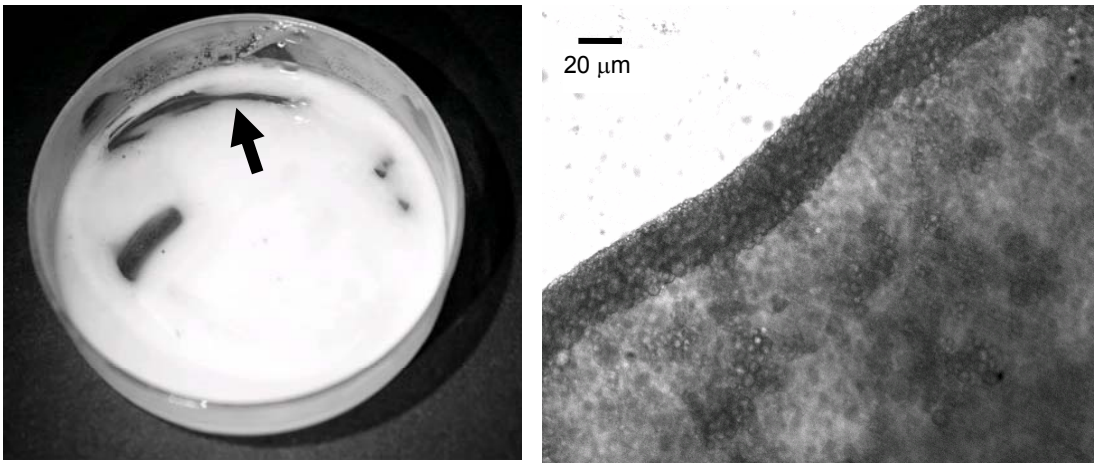

Figure 18. (a) Bare patches in a petridish containing B10-1 after several weeks. (b) Image of the sample at the location approximately denoted by the arrow in (a).

In the rest of this chapter, only the simplest shear history is considered: quiescent annealing with the protocol mentioned in the Experimental section (preshear at 400 Pa for 2000 s followed by frequency sweeps at two hour intervals). Figure 19 shows the storage modulus G′ and the magnitude of the complex viscosity |η*| of various blends of the particles, PIB, and

PDMS. We first focus on the samples without particles. Comparing the particle-free blend B30-0 (circles) with the matrix PDMS (solid line), B30-0 shows enhanced G′ and |η*| at low frequency, indicative of an additional relaxation process in the blend. Furthermore, after 6 hours of quiescent annealing, there is a slight shift in the relaxation process to lower frequency (open vs solid circles); this may be noted by the slight increase in G′ at low frequency, and in the shift of the shoulder in |η*| towards lower frequency. From extensive past literature on such blends, it is well-known that the additional relaxation process causing the shoulder in |η*| and G′ corresponds to deformation and relaxation of the drops in the blends.[61, 63, 64, 68] Dimensional analysis suggests, and detailed theory[63, 68] confirms, that the characteristic frequency of this process must scale as $\sigma/\eta_m R$, where R is the mean drop size, and η_m is the viscosity of the matrix phase. Thus, the slight shift to lower frequency is indicative of a corresponding increase in mean drop size by quiescent coalescence.

Next we consider the effect of particles. Figure 19 shows that addition of particles to the PDMS homopolymer increases the G′ and |η*| only slightly (solid vs dashed lines). However, in the B30-1 blend, there is a very large increase in these quantities at low frequency. After 6 hours of annealing, the G′ shows a low-frequency plateau, and the |η*| shows a significant upturn at low frequency with no sign of a leveling off at a limiting value. Both of these features are indicative of gel-like behavior in the sample. Such behavior may be attributable to the particles gluing the drops together into large clusters. A more critical evaluation may be performed by comparing blends with different volume fractions of drops: certainly any gel-like behavior induced by drops sticking to each other should become far weaker upon reducing the volume fraction of the drops.

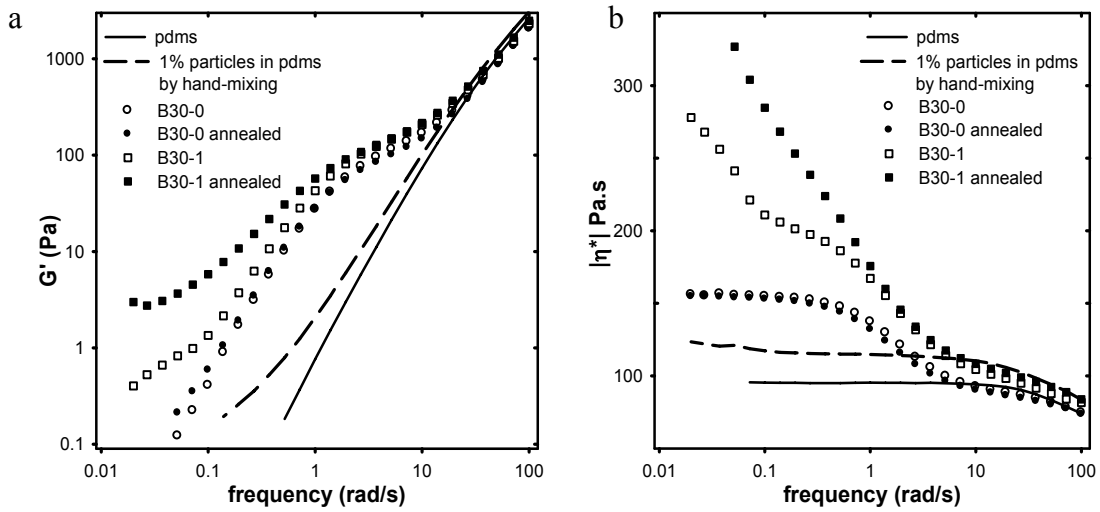

Figure 19. Effect of 1% fumed silica particles on the linear viscoelastic properties of PDMS homopolymer, and of PIB/PDMS blends with 30% PIB: (a) G′ and (b) |η*|. All blends were mixed by hand; see text for shear history.

Accordingly, Figure 20 compares blends containing 10% drops vs. 30% drops. Indeed, B10-1 shows only a modest rise in |η*| at low frequency, as compared to B30-1. The results for G′ (not shown) are similar: the plateau in G′ is considerably weaker in B10-1 as compared to B30-1. These observations lend support to the idea that particles cause the drops to stick together, and the resulting drop clusters are responsible for the plateau in G′ and the upturn in |η*| at low frequency.

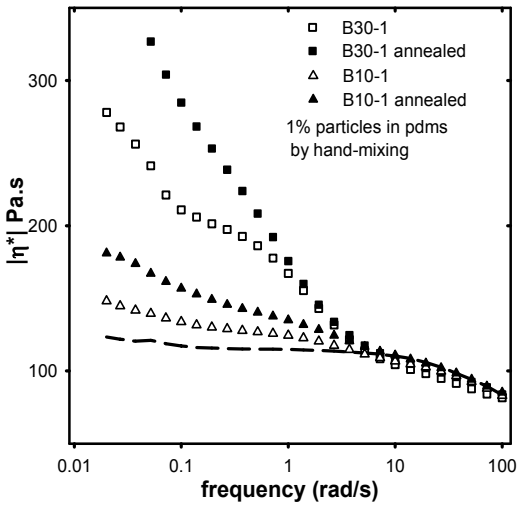

Figure 20. Effect of droplet volume fraction on the magnitude of the complex viscosity of PIB/PDMS blends with 1% fumed silica. All blends were mixed by hand; see text for shear history.

3.2.3 Rheology of machine-mixed samples

During our studies of these blends we noted that the rheological results on particle-containing blends were not highly reproducible. For example, several samples of B30-1 were mixed independently on different days, and subjected to the same shear history as described above (400 Pa preshear followed by quiescent annealing). While the results were always qualitatively similar to the squares shown in Figure 19, there were nevertheless substantial differences in the plateau in G′ and the rise in |η*| at low frequency. These differences were attributed to inconsistent hand-mixing. Preshearing is known to erase inconsistencies of hand-mixing in particle-free blends,[69] but that may not be true in the present samples. Therefore, we sought to develop a blending procedure that could be applied consistently. A small batch mixer, similar to the "Minimax" mixer,[67] was used for this purpose. This mixer resembles a parallel-plate geometry

with the sample being sheared by rotating the top plate with respect to the bottom; however three balls are added to the sample to induce chaotic streamlines, leading to efficient blending.[67] We used a mixer of diameter ~ 30 mm, with a gap (= ball diameter) of ~ 9.5 mm. Samples were mixed by rotating at 100 rpm for 10 minutes.

Figure 21 compares the |η*| of the B30-1 blend prepared in the Minimax mixer with B30-1 blend prepared by hand-mixing. Both sets of data were measured immediately after the preshearing step (400 Pa for 2000 s). The mixing has a large effect on the rheological properties, and the gel-like behavior is substantially stronger in the B30-1 prepared in the Minimax mixer.

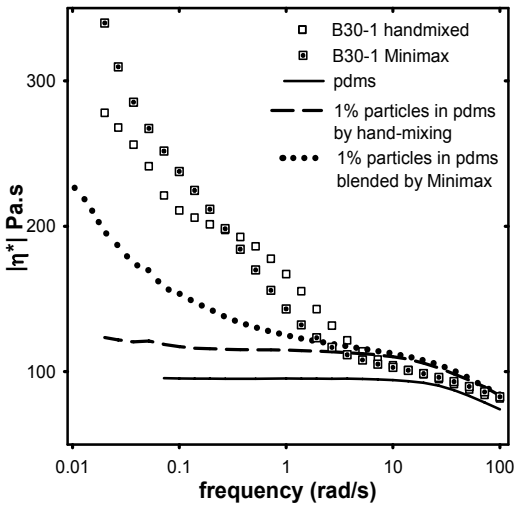

Figure 21. Effect of blending method on the magnitude of the complex viscosity of blends with 30% PIB with 1% fumed silica and of PDMS homopolymer with 1% fumed silica. Samples were all presheared at 400 Pa immediately before measurement.

The mixer was also used to make a suspension of 1% fumed silica particles in PDMS (without any drop phase at all). Figure 21 shows that in contrast to the hand-mixed suspension (dashed lines, same as in Figure 19), this Minimax-mixed suspension has a significant upturn in

|η*| at low frequency. The results for G′ (not shown) also show gel-like behavior: the low-frequency G′ is far higher in the Minimax-mixed samples than in the hand-mixed samples. These observations on the fumed silica-in-PDMS suspensions indicate that the particles can form a gel *by themselves*, even in the absence of any drops. Such gelation in suspensions of fumed silica is well-known, and is the basis of the commercial use of fumed silica as a rheology modifier.

3.3 DISCUSSION

This research started with the hypothesis that bridging particles can cause drops to cluster together, and that such clustering will be evident rheologically. Section 3.2.1 has demonstrated conclusively that it is indeed possible for particles to glue drops together and form clusters. Rheological studies indicate that particles cause gel-like behavior in blends, however, the interpretation of this result is complicated by the observation that particles/PDMS suspensions also show gel-like behavior. Thus, we first consider a very limited question: can *at least some* of the gel-like behavior of particle-containing blends be attributed to clustering of drops? The best evidence comes from Figure 20 which shows that the effect of added particles on |η*| at low frequency increases in the sequence: (PDMS + 1% particles) < B10-1 < B30-1. This trend of increasing gel-like behavior with drop content shows that particle-induced droplet-droplet interactions are at least partially responsible for the gel-like behavior. Yet, this still does not conclusively prove that drop clustering is responsible: hydrodynamic interactions between the drops, combined with the weak gel-like behavior of the matrix, may be responsible for the upturn in |η*|. To test this, we performed model calculations using the Palierne model which can predict the linear viscoelastic properties of droplet-matrix blends composed of linear viscoelastic phases.

For these calculations, the immiscible phases were given gel-like properties that roughly matched those of the B0-1 suspension of Figure 19. We found that while hydrodynamic interactions can account for a part of the upturn in $|\eta^*|$ at low frequency, the observed magnitude of the upturn is substantially larger than that predicted by Palierne model. Therefore we tentatively conclude that the clustering is responsible for a part of the gel-like behavior of the blends. In summary, the gel-like behavior has three causes: particle-particle interactions in the bulk, hydrodynamic interactions between drops (given that the matrix is a weak gel), and drop clustering. This chapter is most interested about the last one, but there seems to be no simple way to subtract out the first two effects and isolate the drop clustering.

Next, we note two differences with the research by *Vermant et al.*[66] on blends composed of very similar PIB and PDMS, and the same grade of fumed silicas (R972 from Degussa). (1) We found gel-like behavior at low frequency for all particle-containing blends. This includes hand-blended samples measured immediately following preshearing, a shear history for which *Vermant et al.* found only liquid-like behavior. (2) We found that the rheological properties were sensitive to blending procedures, whereas *Vermant et al.* tested various hand-blending procedures and found that the rheological properties were insensitive to the blending procedure. We are unable to cite a reason for these differences. Moldenaers[70] suggested that the gel-like behavior of our samples may be due to a higher moisture content in our silica particles. Therefore we repeated experiments on a dried B30-1 sample prepared as follows: weighed particles were dried for several hours at 75 °C in vacuum, then immediately added to a petridish already containing appropriate quantities of dried PIB and PDMS, and hand-blended. This allows no opportunity for atmospheric moisture to readsorb onto the particles. The blends were degassed and loaded promptly into the rheometer. Yet, the gel-like behavior was nearly

unaffected. Thus the cause for the discrepancy between our results and those of *Vermant et al*. remains unclear.

Finally, we turn to the question of whether PIB/PDMS/fumed silica would be a good model system to study particle-bridging effects between drops in polymer blends. The results above point to at least two undesirable aspects of this system: that the results are highly sensitive to mixing procedures, and that the fumed silica particles tend to form a gel in the bulk phases, making it difficult to isolate the effects of drops sticking together. Furthermore, there are at least two more disadvantages: that the particles are too small to be resolved optically (hence bridging cannot be observed directly), and that fumed silicas are known to be fractal-like aggregates, making them more difficult to model than spherical particles.

We instead propose that colloidal silica particles provide a model system that may address all the deficiencies of the fumed silica particles. Monodisperse spherical silicas can be purchased in a wide variety of sizes, their surface-wetting properties can be tuned by surface-grafting,[71, 72] and they can be synthesized with fluorescent cores to enable fluorescent or confocal microscopy.[73] We have followed this route: monodisperse silicas of 2.7 μm diameter were purchased from Tokuyama Industries, and their surfaces were coated with dichlorodimethylsilane (DCDMS) in cyclohexane solution using the procedure described in the literature.[72] DCDMS in slight excess of that required to fully coat the particle surfaces was used in the reaction. After the surface-coating reaction was complete, the particles were then washed thoroughly with cyclohexane and chloroform, dried, and blended with PIB and PDMS. Figure 22 shows that the particles do indeed adsorb at the PIB/PDMS interface, and that drops of PIB can indeed be glued together by the particles. An obvious advantage of the large particle size used here is that the particle-bridging is unambiguous and the contact angles can be measured directly,

thus facilitating modeling efforts. However, with such large particles, a relatively large volume fraction is needed to cover a given interfacial area. Hence, for studying issues such as effects of particles on coalescence, smaller particles may be more desirable. A detailed study of polymer blends containing such monodisperse spherical silica particles is discussed in the next chapter.

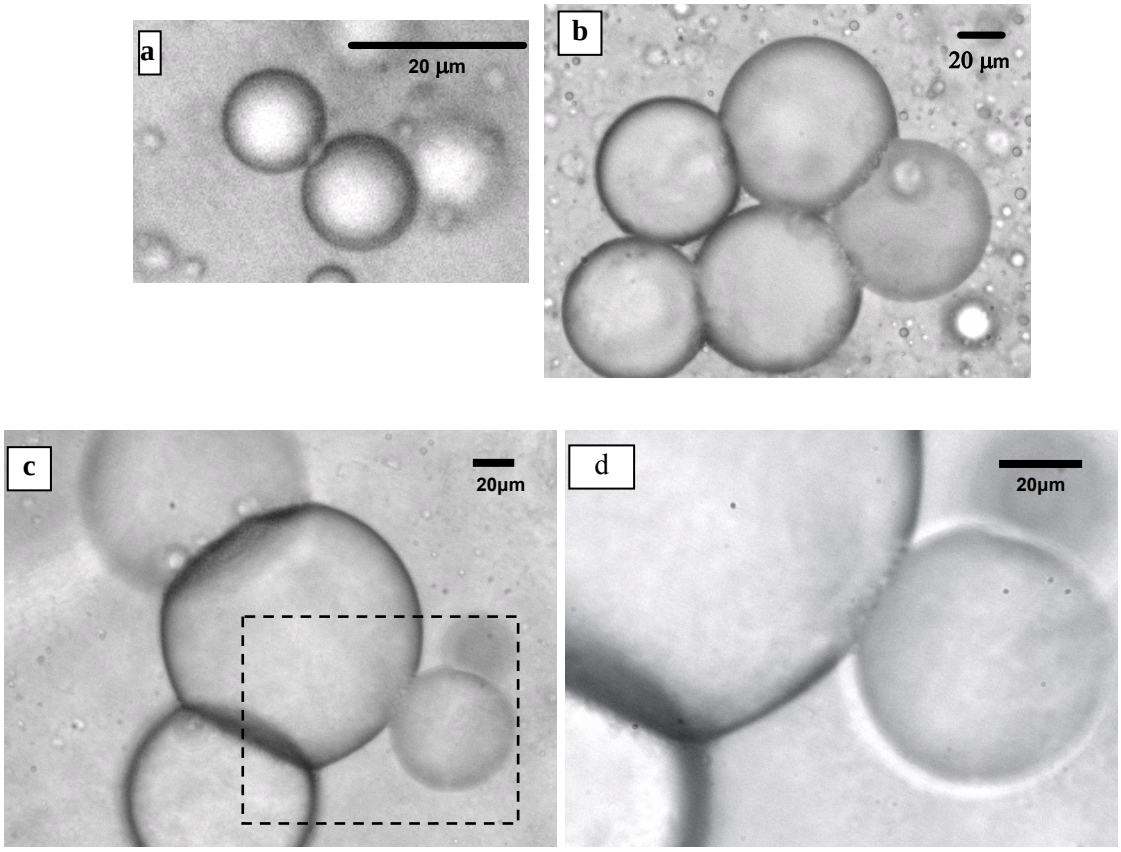

Figure 22. DCDMS coated particles on PIB drops: (a) two drops bridged by a single particle; (b) and (c) multidrop clusters. Note the pronounced flattening of the drops in the region where the particles bridge them. (d) The dotted rectangle in (c) imaged with a higher magnification objective. Individual bridging particles are visible.

3.4 SUMMARY AND CONCLUSIONS

Recent results on particle-stabilized oil/water systems show that partially-wetting particles can adsorb at two liquid/liquid interfaces simultaneously. We propose that such particles added to a blend of immiscible polymers can bridge across drops and glue them together, and that such gluing will significantly affect the rheological properties of the blends. This chapter demonstrates that:

- Fumed silica particles can cause PIB drops in PDMS to stick together.
- Blends of PIB, PDMS and fumed silicas show complex rheological properties, with gel-like behavior evident in the low-frequency dynamic moduli. This gel-like behavior has at least three causes: (1) particle-particle interactions in the bulk, (2) drop-drop hydrodynamic interactions, (3) particle-induced drop clustering.
- The rheological properties of such blends are dependent on mixing history.
- Spherical, monodisperse colloidal silica particles offer a more convenient model system than fumed silica to study bridging effects of particles in immiscible polymer blends.

4.0 RHEOLOGY OF POLYETHYLENEOXIDE/POLYISOBUTYLENE (PEO/PIB) BLENDS WITH PARTICLE-INDUCED DROP CLUSTERS[74]

In the previous chapter we attempted to examine the rheological consequences of bridging using droplet/matrix blends of PIB/PDMS/fumed silica system. The study showed evidence of particle bridging-induced drop clustering, and also suggested that such clusters give the droplet-matrix blend gel-like characteristics. However, there were two serious deficiencies inherent in the PIB/PDMS/fumed silica system: (a) bridging could not be proved by optical microscopy because the fumed silica particles were too small, and (b) the fumed silica particles substantially altered the bulk rheological properties of the continuous phase, and hence the rheological changes specifically attributable to bridging could not be isolated.

In this chapter, we revisit the issue using monodisperse spherical silica particles rather than fumed silicas. We prove by direct microscopy that bridging can indeed induce droplet clustering in droplet-matrix emulsions. Furthermore, such clustering causes significant qualitative changes in the rheological properties, and in particular, induces weak gel-like behavior in droplet-matrix blends.

4.1 EXPERIMENTAL

4.1.1 Particles

Monodisperse spherical silica particles of 2.7 μm diameter were purchased from Tokuyama Corporation. The native silica particles had silanol groups on their surface which were hydrophobically-modified as follows.[72] The particles were dried at 350 °C for 5 hours and then stored overnight in a closed flask under air. They were then degassed under vacuum at 60 °C for 2 hours, and then immediately reacted with a solution of octadecyltrimethylsilane (OTS) in anhydrous cyclohexane. The resulting particle-in-cyclohexane suspension was centrifuged, the supernatant liquid replaced with anhydrous cyclohexane, and particles were redispersed. The centrifugation-redispersion cycle was repeated once more with cyclohexane, three times with chloroform, and finally with ethanol. The ethanol was then evaporated and the particles dried in air at 110 °C for 30 minutes. These hydrophobically-modified particles will be called "OTS-silica" in this chapter.

4.1.2 Model fluids

Experiments were conducted using blends of polyethylene oxide (PEO) dispersed in polyisobutylene (PIB). Some properties of these fluids are listed in Table 1. Both fluids are nearly Newtonian under experimental conditions. The reason for changing to the PEO/PIB system rather than PIB/PDMS system of the previous chapter[65] is that the refractive index of the OTS-silica particles is close to that of PDMS, and hence silica particles at the PIB/PDMS interface are difficult to image. Thus, although particle-bridged drop clusters can be imaged in

the PIB/PDMS system, the particles themselves are often difficult to resolve (see Figure 22 in chapter 3[65]).

Table 1: Properties of model fluids

Polymer	MW g/mol	Density g/cm^3	Viscocity @ 25 °C Pa.s	Ea [§] J/mol	Interfacial tension mN/m
Polyethylene oxide (PEO)	400	1.124	60.4	38150	8.21
Polyisobutylene (PIB)	1200-1375	0.905	0.108	57510	

§ $\frac{d(\ln \eta)}{dT} = -\frac{E_a}{RT}$, where T (Kelvin) is temperature. E_a values were obtained by fitting viscosity data between 18 °C and 33 °C.

However, while the particles are more clearly visible with the PEO/PIB system, it has its own deficiencies as compared to the previous PIB/PDMS case, viz. (1) the relatively large density difference between the PEO and PIB can cause sedimentation of the PEO drops thus limiting the duration of experiments, and (2) only a low MW PEO of very low viscosity can be used, and hence only blends with a very low viscosity ratio (~ 10^{-3}) can be studied. Higher molecular weights PEO would permit viscosity matching, however, such experiments would require high temperatures since high MW PEOs crystallize with a melting point of 65 °C. Of course, such high temperature experiments are not entirely a disadvantage since they provide an opportunity for quenching the structure for *ex situ* imaging.

Addition of 0.2 wt% particles (the largest quantity studied in this chapter) caused no measurable change in the rheological properties of either of these fluids. This is not surprising; at 0.2 wt% (< 0.1 vol%), the particle-in-fluid systems constitute very dilute suspensions and rheological changes are not expected. This is extremely convenient when interpreting the rheology of particle-containing blends since all rheological changes induced by the particles can be unambiguously attributed to their effect on the droplet/matrix interface. This is in contrast to our previous research[65] using fumed silica particles in which the particles induced weak gel-like behavior when dispersed in the matrix phase even when no drops were present. In that research, it proved difficult to separate the "bulk" effect of particles from their interfacial effect.

Blends are designated Ex-y where x is the weight percent of drops (5, 10, 20), and y is the weight percent of particles (0 or 0.2). A suspension of 0.2% particles in the PIB, used as a control, is denoted E0-0.2 for consistency. Blends were prepared by adding PEO, then PIB followed by 0.2% OTS-coated silica particles into a petridish and mixing all of them together by hand with a spatula. The hand-mixed blends were then degassed to remove air bubbles. This blending procedure gave qualitatively consistent results in all cases, however, the rheological properties of the as-mixed samples (prior to any shearing) sometimes showed quantitative differences, presumably due to the inherently-irreproducible nature of hand-mixing.

4.1.3 Visualization

Blends were sheared in a home-built shear cell in which the sample is held between two glass plates in a parallel plate geometry. The cell uses an ARES rheometer as the motor drive to rotate the bottom plate, whereas the top plate does not rotate, but can be moved vertically to set the desired gap between the plates. All experiments in this chapter were conducted at a gap of 0.25

mm. During and after shearing, the morphology was visualized by an optical assembly consisting of a flexible light guide for illumination in a "transmitted-light" configuration, a standard microscope head (Olympus) with 4x, 20x and 40x objectives, and an area-scan digital camera (Sony). Most of the images in this chapter were taken with the 20x objective for which the depth of field is less than 10 μm, i.e. objects that are over 5 μm farther or nearer than the focal point appear significantly blurred. The microscope head is mounted on a movable stage which is driven by a micrometer screw so that different areas of the sample can be imaged. Most of the visualization was performed at a distance of 7.5 mm from the center; however, the shear cell is designed such that the sample can be visualized all the way from the center of rotation to the edge.

4.1.4 Rheology

Rheological experiments were conducted using an ARES 2000 rheometer using a cone-and-plate geometry (40 mm diameter, 1° cone). Sample temperature was maintained at 25 °C using a Peltier plate. Samples were subjected to the desired shear history (specified later) and then the complex moduli were measured between 100 rad/s and 0.01 rad/s at a strain of 20%. A limited number of experiments were conducted to confirm that samples do not undergo significant rheological changes over the timescale of a single frequency sweep.

4.1.5 Contact angle measurements

Glass slides were hydrophobized by immersing into 6.25 vol% OTS in cyclohexane solutions for 5 minutes, followed by washing with pure cyclohexane. A hydrophobically-modified slide was

immersed in a home-built windowed chamber containing PIB, and a drop of PEO dispensed over it and allowed to sink to the slide surface and wet it partially. This sessile drop was imaged using the Kruss Drop Shape Analysis System (DSA 100) and the contact angle found to be 169° +/- 2°, i.e. the hydrophobic glass slide (and presumably the hydrophobic silica particles) are preferentially-wetted by PIB.

4.2 RESULTS: DIRECT VISUALIZATION

The first goal was to verify that the OTS-silica particles can adsorb at the PEO/PIB interface, and that they can bridge drops together into non-coalescing clusters. Microscope observation of as-mixed samples readily revealed drops such as Figure 23 which establish that particles can adsorb at the PEO/PIB interface. It was also apparent that the particles protrude considerably out of the PEO drops, i.e. the OTS-silicas were preferentially-wetted by PIB. This was consistent with the contact angle measurement cited above, although the actual value of the contact angle may be somewhat different with the particles due to the different procedure of OTS treatment. Experiments on water/oil systems[34, 75, 76] confirm that such protruding particles are a necessary condition for bridging, i.e. such OTS-silica particles should be able to bridge across PEO drops.

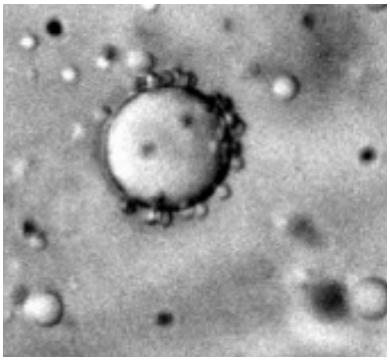

Figure 23. OTS-silica particles adsorb on surface of a PEO drop in PIB.

A few examples of particle-bridged drops were indeed evident (not shown) in the as-mixed blends. Generally these consisted of two or three drops bridged together, but in some samples large clusters were seen. A particularly striking example was evident in a E20-0.2 sample that had been left quiescent in a petridish for several weeks. Most of the PEO drops in this sample had sedimented due to their higher density, but there were several examples in this sample of long chains of drops bridged by particles (Figure 24). We believe that such long chains were formed due to weak flow as the as-mixed sample (which was initially non-uniformly distributed in the petridish) flowed under gravity in the petridish. In particular, we believe that flow induces collisions between the drops and the particles (causing particle adsorption onto drops), as well as collisions between particle-laden drops (causing bridging).

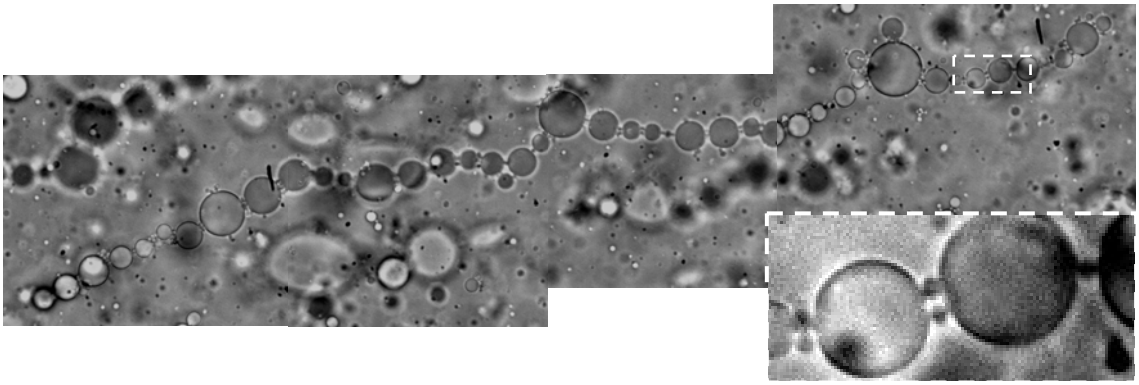

Figure 24. A long chain of PEO drops in PIB bridged via OTS-silica particles. Two other chains are also visible, albeit out of focus. This chain was too long to be captured in a single frame, and hence several images have been juxtaposed above. The dotted rectangle has been magnified in the inset to show bridging particles.

We therefore examined the effect of shear flow on the bridging-induced drop clustering by direct visualization. These experiments were conducted on samples with only 5 wt% PIB since at higher drop volume fractions, image quality was very poor due to intense scattering. In early shearing experiments at 3.3 s^{-1}, we made the following observations: (1) as-loaded samples showed small drops and only occasional drop clusters, although image quality was very poor, (2) shearing promoted drop clustering, and the size of the clusters and of the drops comprising the clusters depended on shear rate.

To study the effects of shearing and of shear rate, the following experiment was conducted. A E5-0.2 sample was first sheared at 3.3 s^{-1} for a half hour (Figure 25a). The morphology was not very clear in Figure 25a owing to the small drop size, however, careful examination suggests that some drop clusters may be present. Shearing was then continued at a lower rate of 0.3 s^{-1}. After only 200 strain units (~ 11 minutes) of shearing, bridged drop clusters were still visible but the drops had also coalesced to a substantial degree (Figure 25b). Upon continued shearing at 0.3 s^{-1}, coalescence continued and drop clusters bridged by multiple

particles were evident (Figure 25c) at 40 min shearing, but a new phenomenon was also manifested: large drops with several particles arranged in an approximately hexagonal lattice on the interface were visible (Figure 25c and d at 40 min shearing and Figure 25e at 70 minutes shearing). We refer to such drops as "golf ball" drops. The images yield a lattice spacing of about 11.5 μm, which is far larger than the particle diameter itself. The lattice spacing shows no apparent variation from one drop to another or with shearing time. Such an ordered lattice of interfacially-adsorbed particles is visible only on the surface of drops that are at least a few ten μm in diameter. Finally, we note that the lattice ordering does not appear to interfere with bridging, e.g. the largest drop in Figure 25c has a hexagonal packing of particles, and is also bridged to its neighbors.

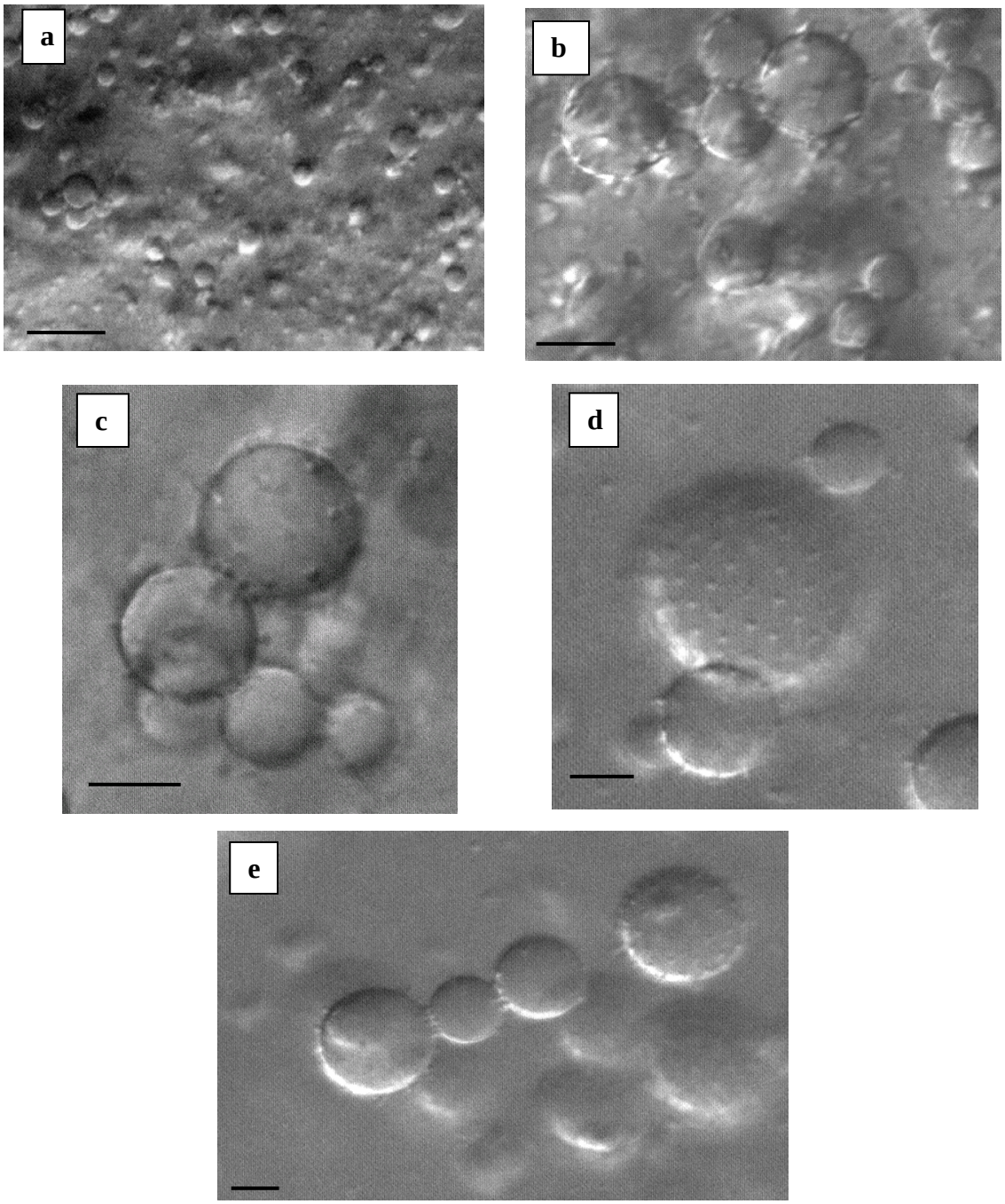

Figure 25. E5-0.2 after (a) shearing at 3.3 s^{-1} for half hour, followed by 0.3 s^{-1} for; (b) 10 minutes; (c) and (d) 40 minutes; (e) 70 minutes shows clusters of PEO bridged drops as well as golf ball drops. Note the ring of bridging particles in (d) and the multiple bridging particles connecting drops in (e). All scalebars are 20 μm in length.

Hexagonally-ordered monolayers of particles have been noted several times previously at oil-water interfaces,[14, 77-80] however, to our knowledge, this is the first example of particles ordering in a lattice at a polymer/polymer interface. In oil/water systems, lattice formation is believed to result from interparticle repulsion between interfacially-adsorbed particles.[77, 81] Interparticle attraction is also believed to play a role in lattice formation in some cases.[16, 80, 82] At least two different interparticle repulsive mechanisms have been proposed, (1) that some residual charges at the particle/oil interface gives the particles some net charge which causes a Coulombic repulsion mediated through the oil phase,[78, 81] and (2) interfacially-adsorbed particles have a net dipole moment and hence neighboring particles exhibit dipolar repulsion.[77] Both these repulsion mechanisms depend on at least one side of the particles (either the particle/water interface or the particle/oil interface) having net charge. The fact that particles order on a 2-D lattice at the PEO/PIB interface suggests that these particles also have some net charge: a somewhat surprising conclusion considering that the system is non-aqueous (except for any incidental water absorbed from the atmosphere into the PEO phase).

Finally, for completeness, we also examined the particle-free PEO/PIB blend i.e. E5-0 under the same shear conditions. The as-mixed E5-0 blend had extremely small drops. Upon shearing at 3.3 s^{-1} for 30 minutes the drops had coalesced, but were still very small (Figure 26a). The shear rate was then lowered to 0.3 s^{-1} and the sample was sheared for 40 minutes (Figure 26b), and then for a further 70 minutes (Figure 26c). Certainly the first 30 minutes of shearing induced some coalescence in the system, but with further shearing, there does not appear to be a significant change in drop size. At the present viscosity ratio, the critical capillary number for drop breakup is about 5.[83, 84] At this critical capillary number, calculations suggest that even mm-sized drops should be stable at a shear rate of 0.3 s^{-1}. Thus, the slow change in drop size is not

attributable to drop breakup competing with coalescence, but to slow coalescence alone. A similar conclusion of slow coalescence will be drawn from the rheological data in the following section. Thus, a comparison of Figure 25 and Figure 26 indicates that addition of particles promotes coalescence in the blend, and hence after a given shear history, drops are typically larger in the particle-containing system than in the particle-free system.

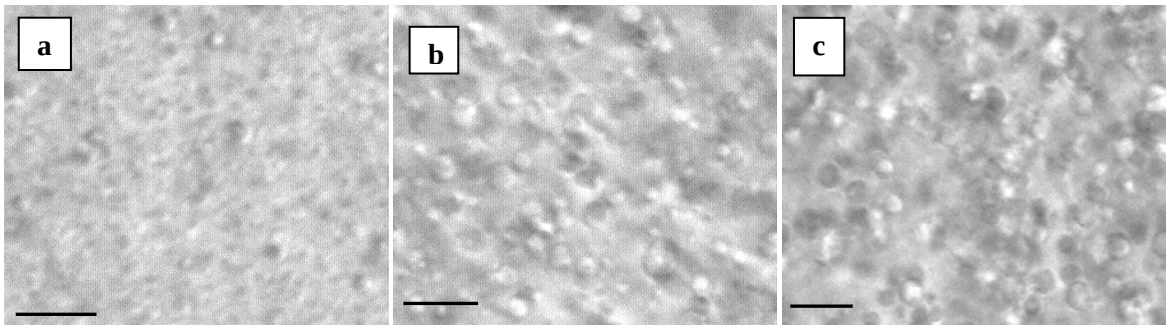

Figure 26. (a) E5-0 sheared at 3.3 s^{-1} 30 min, (b) shearing at 0.3 s^{-1} for 40 minutes and (c) continued shearing at 0.3 s^{-1} for further 70 minutes. All scalebars are 20 μm in length.

Stable *Pickering* emulsions require that the particles prevent coalescence, and indeed coalescence suppression is indicated by much previous research on particles in oil/water *Pickering* emulsions[2, 85, 86] and limited research on polymer/polymer blends with interfacially-active particles.[47, 48, 66, 87] However, particles are also known to sometimes promote coalescence, most notably, hydrophobic particles are well-known to be excellent defoaming agents because they promote coalescence of air bubbles,[88-90] and demulsification due to added particles has also been documented.[91, 92] Bacteria are also used as demulsifiers,[93, 94] and at least in some cases, the mechanism appears to be physical rather than biological. In particular, highly hydrophobic bacteria have also been shown to demulsify oil-in-water emulsions, whereas hydrophilic bacteria

demulsify water-in-oil emulsions.[94-96] Such particle-induced defoaming or demulsification is generally attributed to the "bridging-dewetting mechanism".[88-90] For spherical particles, this mechanism requires that the particles be preferentially-wetted by the dispersed phase. In contrast, in the present situation the particles promote coalescence even though they are preferentially-wetted by the continuous phase, and we have no explanation for this observation.

In summary, while the optical experiments are qualitative, the following conclusions can be drawn with confidence:

- OTS-silica particles can bridge across drops of a blend and glue the drops together into clusters.
- Shear flow is effective at inducing collisions between drops and particles as well as between different particle-laden drops, and hence shear flow induces drop clustering.
- At the concentration studied here (0.2 wt.%), particles do not inhibit coalescence. Indeed, in this particular case, they seem to promote coalescence i.e. upon decreasing the shear rate, drops grow much faster in a particle-containing blend as compared to a particle-free blend.
- When the drops are sufficiently large, particles can organize in a hexagonal lattice on the interface indicating significant repulsion between interfacially-adsorbed particles.

Finally we note that many of the images of Figure 25 give an impression that the clusters are composed of only two or three drops. This is however an artifact of the narrow depth of field (< 10 μm) of the optical system. During the actual experiment, we were able to examine clusters by refocusing at several depths. In that case, it becomes clear that the clusters extend in three dimensions and are larger than appear from single images. For example, all the drops in Figure

25c, and nearly all the drops in Figure 25e are actually glued to each other by bridging particles: a fact not apparent from these images taken at a single focal depth.

The rest of this chapter is devoted to investigating the rheological consequences of the above phenomena, with particular focus on bridging-induced drop clustering.

4.3 RESULTS: RHEOLOGY

It is reasonable to expect that the above morphological changes induced by the particles cause significant changes in the rheological properties. This chapter only discusses dynamic oscillatory properties in the linear viscoelastic region. In the first section below, we will demonstrate that particles do indeed induce significant changes in the linear viscoelastic properties and that these changes can be interpreted in terms of the above morphological changes. We then postulate that at a given particle loading, the main issue of interest, viz. particle bridging-induced clustering of drops and its rheological consequences, must depend principally on the stress applied and the drop volume fraction. Accordingly in the subsequent two sections below, we will consider the effect of these two parameters on the drop clustering process.

The visualization experiments of the previous section were restricted to blends with a relatively low fraction (5 wt%) of drops principally to ensure good image quality. However, as will be shown later in this chapter, at such a low drop fraction, the rheological changes associated with particle bridging-induced clustering occur very slowly, especially at low shear rates. Thus, blends with 5% drops are not convenient for rheological studies, and hence most rheological experiments were conducted on the E20-0.2 blend (i.e. 20% PEO drops) in which drop clustering occurs much faster.

A second difference between the rheological and the visualization experiments is that the rheological studies were performed on an AR2000 rheometer and hence under stress-controlled conditions. In contrast, the visualization studies, in which a strain-controlled ARES rheometer was used to drive the flow, were conducted under rate-controlled conditions. However, the stresses applied in this section have been chosen to match the rates in the previous section; in particular, for the E20-0.2 sample, the 200 Pa and 25 Pa stresses used below correspond respectively to rates of roughly 3.3 s^{-1} and 0.3 s^{-1} used in the previous section.

4.3.1 Qualitative discussion of Dynamic Oscillatory experiments

The primary goal of this section is to examine the dynamic oscillatory properties of the blends under conditions that mimic the flow visualization experiments, and to interpret specific rheological changes in terms of morphological changes already known from the previous section. Therefore, the E20-0 and E20-0.2 blends were subjected to shear histories similar to the previous section; after the desired shear history, the oscillatory moduli and complex viscosity were measured.

Consider first the particle-free E20-0 blend "as-loaded" in the rheometer without any additional shearing. The rheological properties of the matrix phase PIB are shown in Figure 27a. The properties of the drop phase PEO are not shown since its G′ is too small to be measured, and $|\eta^*|$ is too small (steady shear viscosity = 0.11 Pa.s) to be displayed in Figure 27a. From Figure 27a, it is immediately apparent that the E20-0 blend shows an additional relaxation process that is not present in the two components (PEO and PIB); this additional relaxation is manifested as a higher G′ than the components, and a higher $|\eta^*|$ than the components in the low frequency

region. This additional relaxation, henceforth called the "shape relaxation process", is known to be attributable to interfacial tension, and specifically to the deformation and relaxation of drops in the blend.[61, 63, 68] Dimensional analysis shows, and detailed theory confirms,[63, 68] that (1) the characteristic relaxation frequency is proportional to $\alpha/R\eta_m$ (where α is the interfacial tension and R is the drop size) and (2) the low frequency $|\eta^*|$, i.e. the terminal complex viscosity, is independent of the drop size or interfacial tension. Figure 27a shows that shearing at 200 Pa for 15 minutes, and then later shearing at 25 Pa for 30 min causes relatively little change in the linear viscoelastic properties, and in particular, there is only a small shift of the shape relaxation process to lower frequencies. This suggests a relatively small change in drop size, i.e. the PEO drops coalesce only slightly after reducing the shear stress from 200 Pa to 25 Pa. This is in accord with the optical microscopy result (Figure 26) that stepping down the shear rate from 3.3 s^{-1} to 0.3 s^{-1} caused only a small change in drop size.

Upon addition of particles (Figure 27b), several differences are apparent. First, the sample "as-loaded" in the rheometer, i.e. before applying any shear (except that experienced during loading) shows a qualitative change in behavior at low frequency: G′ shows a distinct plateau and $|\eta^*|$ shows a slight upturn at low frequencies. The low-frequency plateau modulus, G'_p, is quite small (< 0.05 Pa) and not quite reproducible in the as-loaded sample: independently-mixed samples upon loading (but prior to any shearing) show G'_p values ranging from 0.01 Pa to 0.05 Pa. In some cases, a clear plateau was not evident in the G′ of the as-loaded sample, instead the G′ *vs.* ω curve showed a decreasing slope at low frequencies. This variability of the as-loaded samples is likely attributable to the inherent irreproducibility of hand-mixing, yet, it is important to note that the low frequency plateau was always present; in no case did the as-loaded E20-0.2

sample show a "normal" decrease in G′ with frequency as did E20-0. Such a low-frequency plateau in G′ is indicative of gel-like behavior of the sample, i.e. addition of 0.2 wt% particles induces gelation of the droplet-matrix system. Such gel-like behavior is similar to that observed in our previous research on PIB/PDMS/fumed silica blends. However, the important simplification in the present system is that the particles by themselves did not effect any measurable changes in the rheological properties; the low frequency plateau modulus occurs only when particles and drops are both present. In light of the optical microscopy, we attribute the gelation to the particle-induced clustering of drops into a loose network structure. Network structures can deviate from linear viscoelasticity at small strains, and we conducted strain sweep experiments between 0.1% to 20% strain to test whether the oscillatory measurements are in the linear viscoelastic region. The oscillatory moduli were found to be independent of strain at high frequencies (e.g. 10 rad/s), whereas the moduli decreased somewhat with increasing strain at low frequencies (e.g. 0.1 rad/s). Thus we conclude that the oscillatory measurements are not in the linear viscoelastic region at 20% strain. In spite of this non-linearity, we have persisted with frequency sweep measurements at 20% strain because at smaller strains (which may be in the linear viscoelastic region), the data are highly noisy, making it impossible to measure the low-frequency moduli at all.

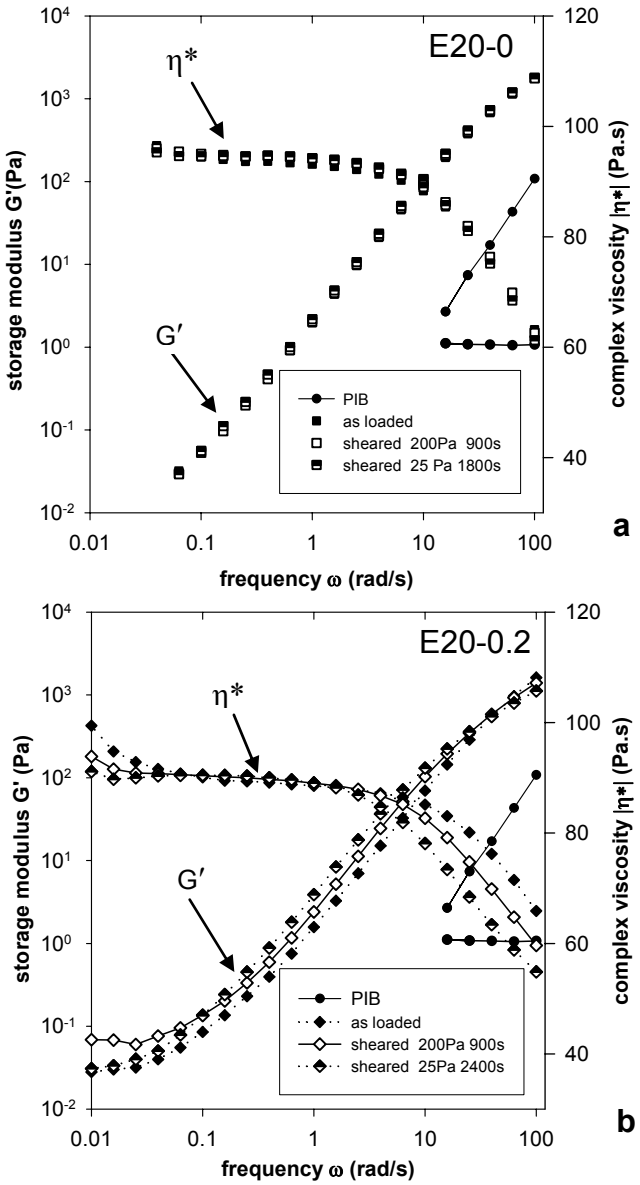

Figure 27. Storage modulus G'and the magnitude of the complex viscosity $|\eta^*|$ of (a) E20-0, and (b) E20-0.2, under conditions noted in the text.

Finally, it must be emphasized that in Figure 27b and in the following experiments, the G'_p of the E20-0.2 blend are of the order of 1 Pa or less, i.e. while the sample is technically a gel,

it has a low modulus, suggesting that only a small fraction of drops in the sample contribute to the cluster network.

The previous section on flow visualization showed that upon decreasing the shear rate from 3.3 s^{-1} to 0.3 s^{-1}, the clusters were comprised of much larger drops, i.e. substantial coalescence occurred. An analogous experiment was conducted rheologically: the as-loaded sample was sheared, first at 200 Pa for 15 min, and then at 25 Pa for 40 minutes. Dynamic oscillatory experiments reveal that each of these shearing steps causes the shape relaxation process to shift to lower frequencies (most clearly visible from the $|\eta^*|$ *vs.* ω data). As mentioned above, the characteristic frequency of the shape relaxation process scales inversely with the drop size, thus, this shift is indicative of coalescence; presumably, the mean drop size in the as-loaded sample was small, and it increased by flow-induced coalescence upon shearing at 200 Pa, and then increased further upon shearing at 25 Pa.

In summary, the linear viscoelastic properties are consistent with the flow visualization results. In particular, (1) the particle-containing E20-0.2 sample shows a low frequency plateau in G′, which may be attributed to a network of particle-bridged drops, (2) in the E20-0.2 sample, a step down in the shear stress causes a large shift in the interfacial relaxation process to lower frequency, which is consistent with the significant coalescence noted in the visualization experiments, and (3) the particle-free E20-0 sample shows only a slight shift in the interfacial relaxation process with decreasing stress, consistent with the slow coalescence noted in the previous section.

The chief interest of this chapter is bridging-induced drop clustering. Flow visualization suggests that there is relatively little drop clustering in the as-loaded sample. Significant number of bridging clusters become evident only after the sample has been sheared for an extended

period. It is therefore of immediate interest to examine the kinetics of clustering by examining the evolution of the plateau in G' as the sample is sheared. The bridging and clustering kinetics must depend on flow-induced collisions between particle-laden drops. Thus, we hypothesize that the clustering kinetics are principally dependent on the same parameters that affect drop collisions, viz. the stress (or shear rate) applied, and the volume fraction of drops. In the following two sections, we will examine these two variables systematically.

4.3.2 Effect of Stress on Oscillatory Properties and Plateau Modulus

E20-0.2 was subjected to the shear history of Figure 28a at four different stress levels: 25 Pa, 50 Pa, 200 Pa, and 800 Pa. A fresh sample was used at each stress level. In each case, shearing was interrupted periodically to measure the complex moduli of the sample. Below we will discuss in detail the evolution of the linear viscoelastic properties at two stress levels, 25 Pa and 200 Pa.

Figure 28b shows the evolution of G′ and $|\eta^*|$ upon shearing at 25 Pa for extended periods. Early during the shearing process – at least up to 4200 s – the G′ vs. ω data showed a trend of decreasing slope at low frequency, but a well-developed plateau in G′ was not evident, and an upturn in $|\eta^*|$ at low frequencies was also not evident. This indicates that the particle-bridged network structure is not yet well-developed at this short shearing time. Over the same period however, there was a significant shift in the shape relaxation process to lower frequencies, which is most clearly evident from the $|\eta^*|$ *vs.* ω data up to 4200 s. As mentioned above, a shift of the shape relaxation process to lower frequencies indicates growth in drop size: the as-loaded drops are small, and hence flow-induced coalescence upon shearing at 25 Pa causes an increase

in drop size. After longer shearing (18600 s), a plateau in G′ and an upturn in $|\eta^*|$ developed at low frequency, indicating that extended shearing induces particle bridging-induced drop clusters. Thus, at the 25 Pa stress, the two processes, coalescence and bridging-induced drop clustering, appear to proceed at significantly different rates, with coalescence occurring much faster. At even longer shearing times (37900 s), the sample shows a decrease in G′ at all frequencies, along with a decrease in the complex viscosity at all but the highest frequencies.

Figure 28c shows the evolution of the dynamic oscillatory properties when E20-0.2 is sheared at 200 Pa. At this higher stress level, the plateau in G′ at low frequency develops rapidly, and there does not appear to be a clear separation between coalescence (if any) and bridging. Upon shearing, the first changes apparent (up to about 9300 s) are a decrease in G′ over most of the frequency range (except the low-frequency plateau) and a decrease in the plateau in $|\eta^*|$ at intermediate frequencies. Both these features are directly associated with the interfacial relaxation process i.e. the rheology indicates that the interfacial relaxation process becomes weaker with extended shearing. Upon extended shearing (18900 s and beyond), these changes continue, furthermore, the low-frequency plateau value of G′ itself decreases. We will speculate on the possible causes for these rheological changes below. The results of shearing at an even higher shear stress of 800 Pa (not shown), are similar to those at 200 Pa, (1) the plateau in G′ appears at very short shearing times, (2) the high-frequency G′ and the intermediate-frequency plateau in $|\eta^*|$ reduce upon modest shearing indicating a weaker interfacial relaxation process.

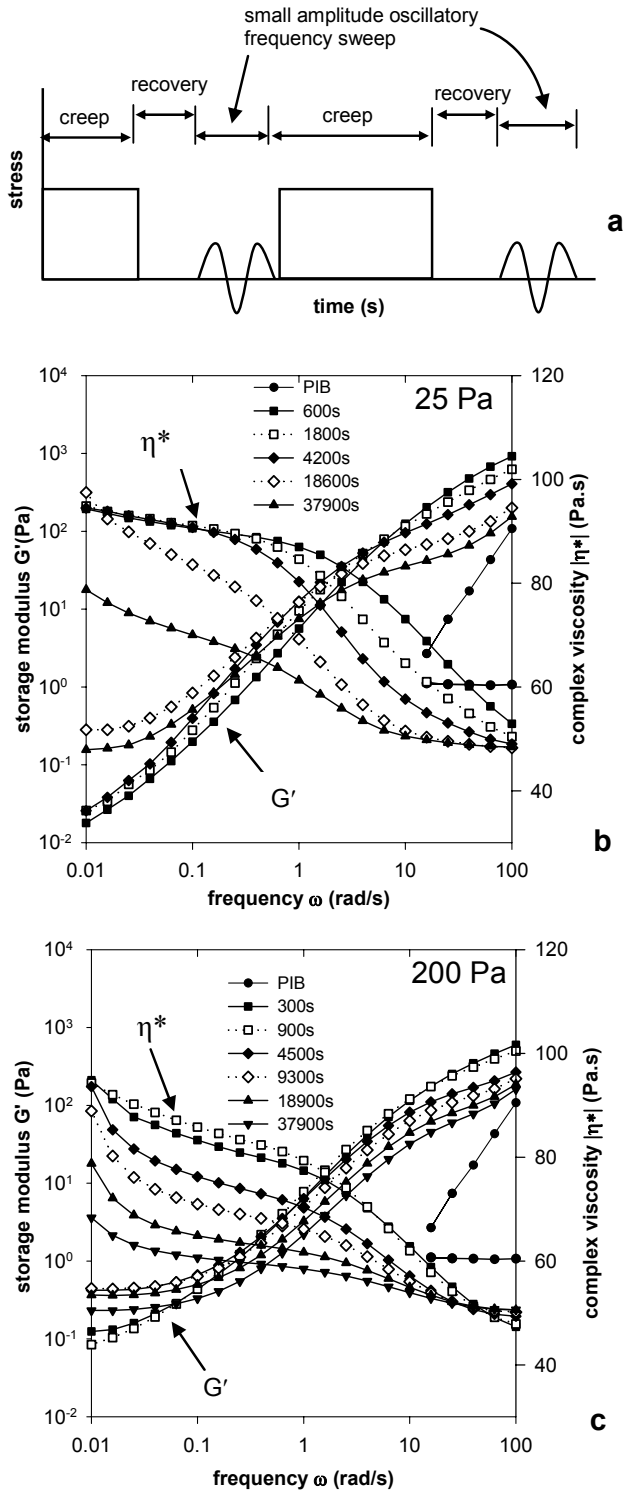

Figure 28. (a) Shear rate protocol for E20-0.2, and corresponding dynamic oscillatory results at (b) 25 Pa, and (c) 200 Pa. The legend refers to shearing time at that stress level.

The magnitude of the low-frequency storage modulus, G'_p can provide a convenient measure of the main issue of interest, viz. the particle bridging-induced clustering process. Figure 29 plots the magnitude of the plateau modulus as a function of time. If a clear plateau was not evident, G'_p has been arbitrarily assigned a value of 0.01 Pa; this is strictly for convenience of drawing the graph. It is clear that the plateau modulus develops much more slowly at low stress levels. The physical picture of cluster formation involves collisions between different particle-laden drops to give the adsorbed particles an opportunity to bridge. Since these collisions are induced by shear flow, clustering may, at its simplest, be modeled as a strain-controlled process, i.e. a plot of G'_p vs. strain would superpose the data at the different stresses. Such a plot (not shown) does not show good superposition, thus indicating that the clustering process is not strictly strain-controlled. However, such a plot does indicate that a strain of 4000 units is sufficient to show a well-developed low-frequency plateau in G' at all the stresses studied.

Several comments about these experiments are in order. Firstly, upon repeated runs of E20-0.2 at 200 Pa shearing the values of G'_p at short shearing times were not highly reproducible, whereas the values of G'_p upon extended shearing were reproducible. This indicates that the irreproducible hand-mixing affects the structure of the sample at short times, but extended shearing erases memory of the initial blending. It would be interesting to examine whether this remains true at other particle concentrations.

Secondly, in some experiments (including some in Figure 29), at very short shearing times (or strains), the low frequency plateau modulus *decreases* with short shearing before increasing again. It is not clear why this is so: it may be that in some cases, the flow experienced during loading creates a network which is not stable under flow; thus short shearing first disrupts the network, before extended shearing can induce bridging and form a network again.

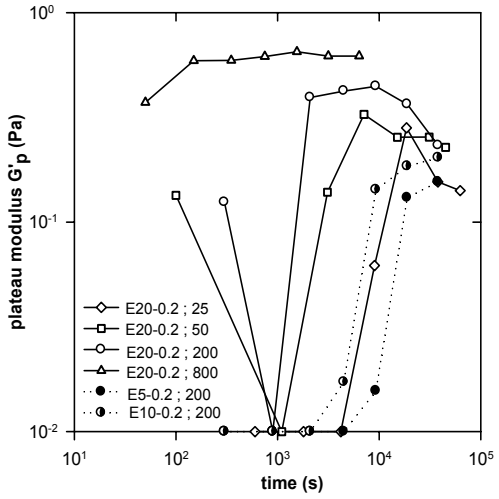

Figure 29. Development of G'_p with shearing time. The legend identifies the sample, followed by the stress (in Pa) applied. If a well-developed plateau was not evident, G'_p has been arbitrarily assigned a value if 0.01 Pa for convenience of drawing the graph.

Finally we speculate on two features of the time-evolution of the oscillatory properties upon shearing. The first feature is the decrease in the plateau in $|\eta^*|$ at intermediate frequencies; Figure 28c shows an excellent example, but all samples (including Figure 30 below) show this feature. Furthermore, with increasing stress, this decrease in plateau viscosity occurs rapidly, e.g. at 800 Pa (not shown), there was a significant drop in viscosity after only 6 minutes of shearing. This decrease in $|\eta^*|$ indicates a weakening of the interfacial relaxation process (coalescence alone would not decrease the $|\eta^*|$ plateau). The second feature is the downturn in G'_p at even longer shearing times for some samples in Figure 29.

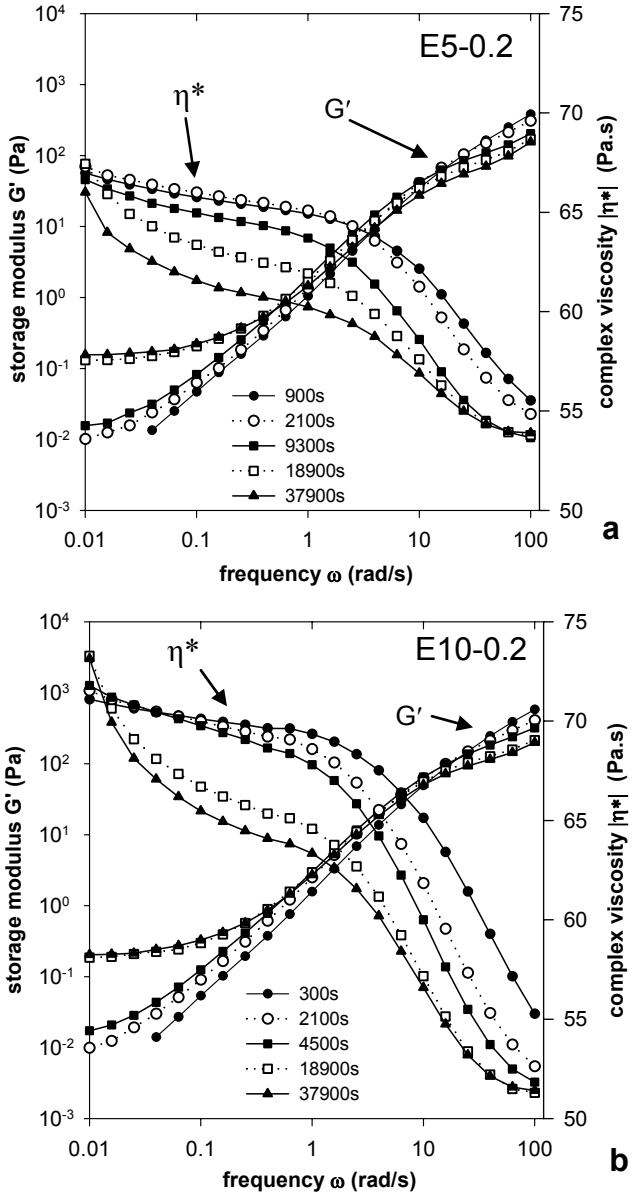

Figure 30. Dynamic oscillatory results of shearing at 200Pa for (a) E5-0.2 and (b) E10-0.2.

We speculate on two possible causes for these features. The first is that as shearing induces clustering, the clustered drops deform less in small-amplitude oscillatory flow than free drops. This could cause a weakening of the interfacial relaxation process. The second is that the denser PEO drops may sediment to some extent during the experiment, thus leaving fewer drops

in the matrix. Sedimentation would reduce the volume fraction of drops contributing to the shape relaxation process, as well as weaken the network of drop clusters. Flow visualization of E5-0.2 suggests that sedimentation can occur: after extended shearing at 0.3 s^{-1} (~ 25 Pa) for several hours, large patches of PEO were found deposited on the bottom of the cell, and the number of drops remaining in the bulk reduced visibly. However, we emphasize that we have no direct evidence that sedimentation occurs under conditions of our rheological experiments.

4.3.3 Effect of volume fraction of PEO drops on Oscillatory Properties and Plateau Modulus

As mentioned above, apart from the stress, the volume fraction of drops is likely to be an important parameter in the clustering process. The same shear history of Figure 28a was applied to E10-0.2 and E5-0.2, with 10% and 5% drops respectively. The stress was fixed at 200 Pa in these experiments. Figure 30 shows the results of these experiments. Qualitatively, the results are similar to Figure 28c (which is at the same stress of 200 Pa), and once again, extended shearing causes a plateau in G′ at low frequency. The corresponding data for evolution of G'_p with time have been added to Figure 29. It is clear that at lower drop volume fraction, the low-frequency plateau in G′ develops much more slowly, and the magnitude G'_p also reduces.

We also attempted to scale the kinetic effect of changing volume fraction by replotting the data of the three different drop volume fractions at 200 Pa (open, filled, and half-filled circles in Figure 29) in the form of G'_p *vs.* time$\times\phi_d$ (i.e. which assumes that the clustering rate is proportional to drop volume) as well as G'_p *vs.* time$\times\phi_d^2$ (which assumes that clustering rate

proportional to the square of drop volume, which may be more appropriate for modeling drop collisions). Neither gave satisfactory superposition of the data at the three volume fractions.

4.4 SUMMARY AND CONCLUSIONS

Interfacially-active particles can simultaneously adsorb at two liquid/liquid interfaces. When such particles are added to a droplet-matrix blend, they can bridge across drops and thus glue them together into non-coalescing drop clusters. The chief goal of this chapter was to examine the rheological consequences of such bridging-induced drop clustering in PEO-in-PIB blends containing hydrophobic silica particles. Optical microscopy reveals that the particles are indeed able to glue together drops, either into irregular clusters, or into chains, and that flow promotes drop clustering. At the concentration of particles studied (0.2 wt%), the particles do not suppress coalescence of drops; indeed coalescence appears to be promoted by particles. If the drops are sufficiently large, particles can order in a hexagonally-packed lattice on their interface.

The chief rheological consequence of bridging is the appearance of a low-frequency plateau in the G′, suggesting that drop clustering induces gel-like behavior in the blend. The actual value of the low-frequency modulus is only O(1 Pa) suggesting that only a small fraction of the drops in the blends participate in the network of drop clusters. We tracked the development of the low-frequency plateau in G′ (which can be regarded as an indicator of drop clustering) as the sample was sheared. These results show that the plateau develops more rapidly with increasing drop volume fraction and with increasing shear stress.

5.0 INTERFACIAL ACTIVITY OF PARTICLES AT PI/PDMS AND PI/PIB INTERFACES: ANALYSIS BASED ON GIRIFALCO-GOOD THEORY[97]

As discussed in chapter 3 and 4, the partial wettability of the particles is the key to their interfacial adsorption at fluid-fluid interfaces. This explanation of the interfacial activity of particles is well established in oil/water systems, but has also been invoked to explain interfacial activity of particles in polymeric systems.[65, 98] The partial wettability-based picture will become invalid for particles whose size is comparable to the radius of gyration of the two homopolymers, because in that case the particles can swell the polymer chains, and thus act somewhat like a solvent.[99] However, for the much larger particles considered in this chapter, partial wettability can provide a potentially simple explanation of particle adsorption at polymer/polymer interfaces.

In qualitative terms, a particle that is partially-wetted by two immiscible phases may be regarded as having a "chemical nature" that is intermediate between the two phases. The chemical differences between oil and water are large, which may explain why a large variety of particles adsorb at oil/water interfaces.[4, 85, 86] In comparison, the chemical differences between any two polymers – even highly immiscible ones – are quite modest, and hence a given particle type is less likely to have a "chemical nature" intermediate between two polymers. This qualitative argument (to be made quantitative later) suggests that particle adsorption at polymer/polymer interfaces will be much less common than at oil/water interfaces. Furthermore,

as the chemical nature of the two polymeric phases approaches each other (e.g. as the critical point for phase mixing is approached), particle adsorption is expected to become even less likely.

Contrary to this expectation, our early experiments on a model polymer blend of polyisoprene (PI) and polydimethylsiloxane (PDMS), showed that a wide variety of particle types adsorb readily at the PI/PDMS interface. Intrigued by this, we then tested a second pair of polymers, polyisoprene and polyisobutylene (PIB), which are chemically even more similar to each other (as gauged by the interfacial tension between them) and still found that most particles types adsorb at the interface. The goal of this chapter is to describe these observations, and interpret them in terms of the Girifalco-Good theory of the work of adhesion.

This chapter is organized as follows. We first show experimentally that particles readily adsorb at polymer/polymer interfaces. We then discuss the theory of interfacial adsorption, followed by experiments to determine the solid/polymer interfacial energy, and finally compare the theoretical predictions with our experimental observations.

5.1 MATERIALS AND METHODS

Table 2 lists the three polymers used in this research, along with some of their properties. These polymers were chosen for experimental convenience: they are molten at room temperature, thus allowing all experiments to be performed at room temperature. The surface tensions of the polymers were measured by the pendant drop method at room temperature and are listed in Table 2.

Table 2. Homopolymers and their properties.

Polymer	Supplier	MW (g/mol)	Viscosity (Pa.s)[a]	Density[b] (kg/m^3)	Surface tension (mN/m)
Polydimethylsiloxane (PDMS)	Rhodia	135,600	100	960	19.2
Polyisobutylene (PIB)	Soltex	2400	333	910	32.1
Polyisoprene (PI)	Kuraray America	29,000	131	910	35.9

[a] Terminal complex viscosity at 25°C measured with an ARES 2000 rheometer.

[b] Quoted by manufacturer.

Two blend pairs were made from these three polymers: PI/PDMS and PI/PIB. The interfacial tension between PI and PDMS was measured by the pendant drop method and found to be 2.73 mN/m. The interfacial tension between PI and PIB could not be measured by the pendant drop method because the very small density difference between them causes an unacceptable uncertainty in the result. Accordingly, the PI/PIB interfacial tension was measured by the deformed drop retraction method. Details of the method are available elsewhere,[44, 100] but briefly, droplet-matrix blends of 5% PI in PIB were sheared in a home-built shear apparatus so as to deform the drops into ellipsoidal shapes. Upon cessation of shear, the interfacial tension-driven recovery of the drops to spherical shapes was recorded by video microscopy. Interfacial tension can be obtained from the kinetics of the shape recovery.[44, 100] The PI/PIB interfacial tension was found to be 0.28 mN/m; this low value is indicative of the chemical similarity of the two polymers.

The various particles used in this research are listed in Table 3. Most of them are commercial materials and were made available by the manufacturers. The only exception is the monodisperse 2.7 μm diameter spherical silica particles, which were purchased from Tokuyama Corp. The as-received silica particles had hydrophilic surfaces, which were hydrophobically-modified by treating with dichlorodimethylsilane (DCDMS) as described previously.[65] The Scanning Electron Microscopy (SEM) images of the particles are shown in Figure 31.

Table 3. Test particles, suppliers and specific sizes

Particles	Shape, Average Size[a] (μm)	Supplier
PTFE	Irregular, 8	Dyneon
Silica[b]	Spherical, 2.7	Tokoyama Corp
Titanium dioxide	Irregular, 0.5	Sigma Aldrich
Iron oxyhydroxide	Elongated, 0.6 x 0.1	Elementis Pigments
Carbonyl iron	Spherical, 3	ISP Technology

[a] All sizes except silica are approximate

[b] Rendered hydropbobic by treating with dichlorodimethylsilane (DCDMS)

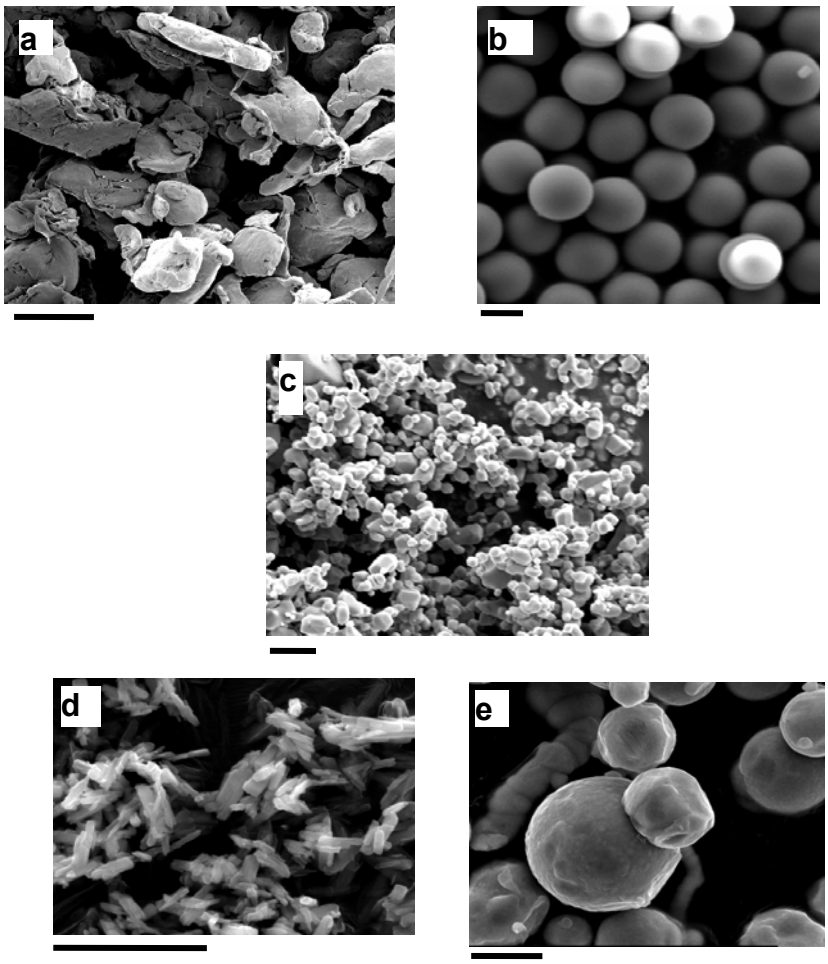

Figure 31. SEM images of the particles used in this research: (a) PTFE; (b) DCDMS-coated hydrophobic silica; (c) titanium dioxide; (d) iron oxyhydroxide; (e) carbonyl iron. The scalebar below (a) represents 10 μm, whereas all other scalebars represent 2 μm.

Interfacial activity of particles was tested by blending the particles into blends of the immiscible homopolymers and then examining the blends by optical microscopy. Blends were composed of 5 wt% PI, 0.1 wt% of particles, and the remainder PIB (or PDMS). Blends were prepared by pre-dispersing the appropriate amount of particles into the matrix phase (PIB or PDMS), and then blending in the PI phase as drops. All blending was performed in a petridish by hand with a spatula. The particle loading was kept to a low value of 0.1 wt% to minimize

visualization problems; higher loading causes intense scattering and/or opacity of the blends. Optical microscopy was conducted on a CKX-41 microscope equipped with 20x and 40x magnification objectives, and images were captured with a Basler 302f area scan camera.

5.2 RESULTS

5.2.1 Interfacial adsorption of particles

Initial tests of interfacial activity of particles were conducted with the PI/PDMS system. In some cases, e.g. PTFE particles added to PI/PDMS blends, interfacial adsorption was obvious even in the as-blended samples. In most cases however, most particles appeared to be located in the matrix phase in the as-blended samples. Interfacially adsorbed particles became evident (or much more obvious) after allowing samples to sit quiescently for 2-3 days. We believe that under quiescent conditions, the PI drops rise upwards due to their lower density whereas the denser particles settle downwards. This internal motion induces collisions between drops and particles, allowing particle adsorption. Figure 32 shows images of the various particle types adsorbed at the PI/PDMS interface. In all cases, interfacial adsorption of particles is unambiguously evident. Figure 32d is especially striking: the PI drop has a prominently non-spherical shape indicating that FeOOH particles jam the interface, and hence interfacial tension cannot force the drop to retract back to a spherical shape. This sample was a mixture of mostly spherical and some non-spherical drops, and such non-spherical drops have been noted previously in oil/water systems, even in an early paper on interfacial adsorption of particles a century ago.[4]

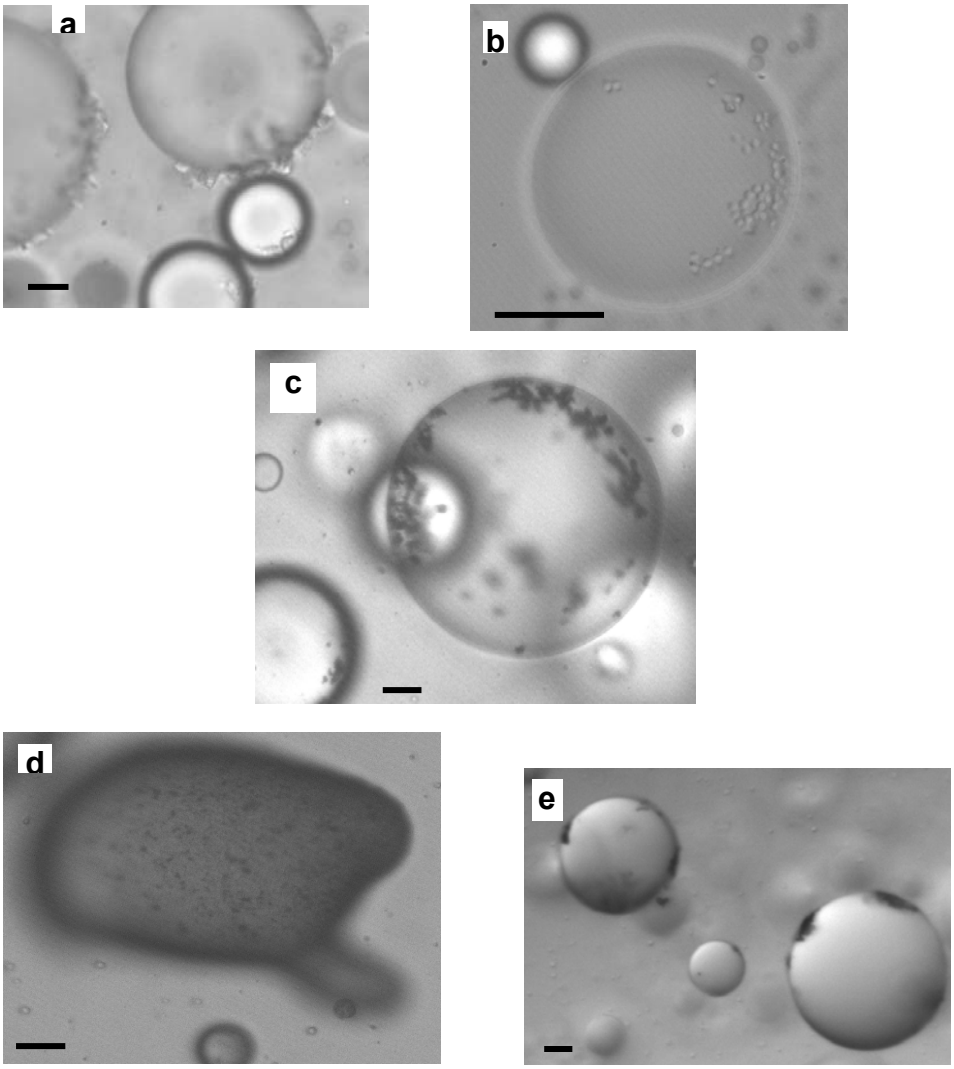

Figure 32. Optical microscopy images of various particles adsorbed at the PI/PDMS interface: (a) PTFE; (b) DCDMS-coated hydrophobic silica; (c) titanium dioxide; (d) iron oxyhydroxide; (e) carbonyl iron. In all cases, the drop phase is PI. Note that in (d) interfacial crowding of particles causes a strongly non-spherical drop shape. All scalebars are 20 μm.

Figure 33 shows images of PI/PIB blends with added particles. Once again, all five particle types adsorbed readily at the PI/PIB interface even though the two phases are much more miscible than the PI/PDMS system.

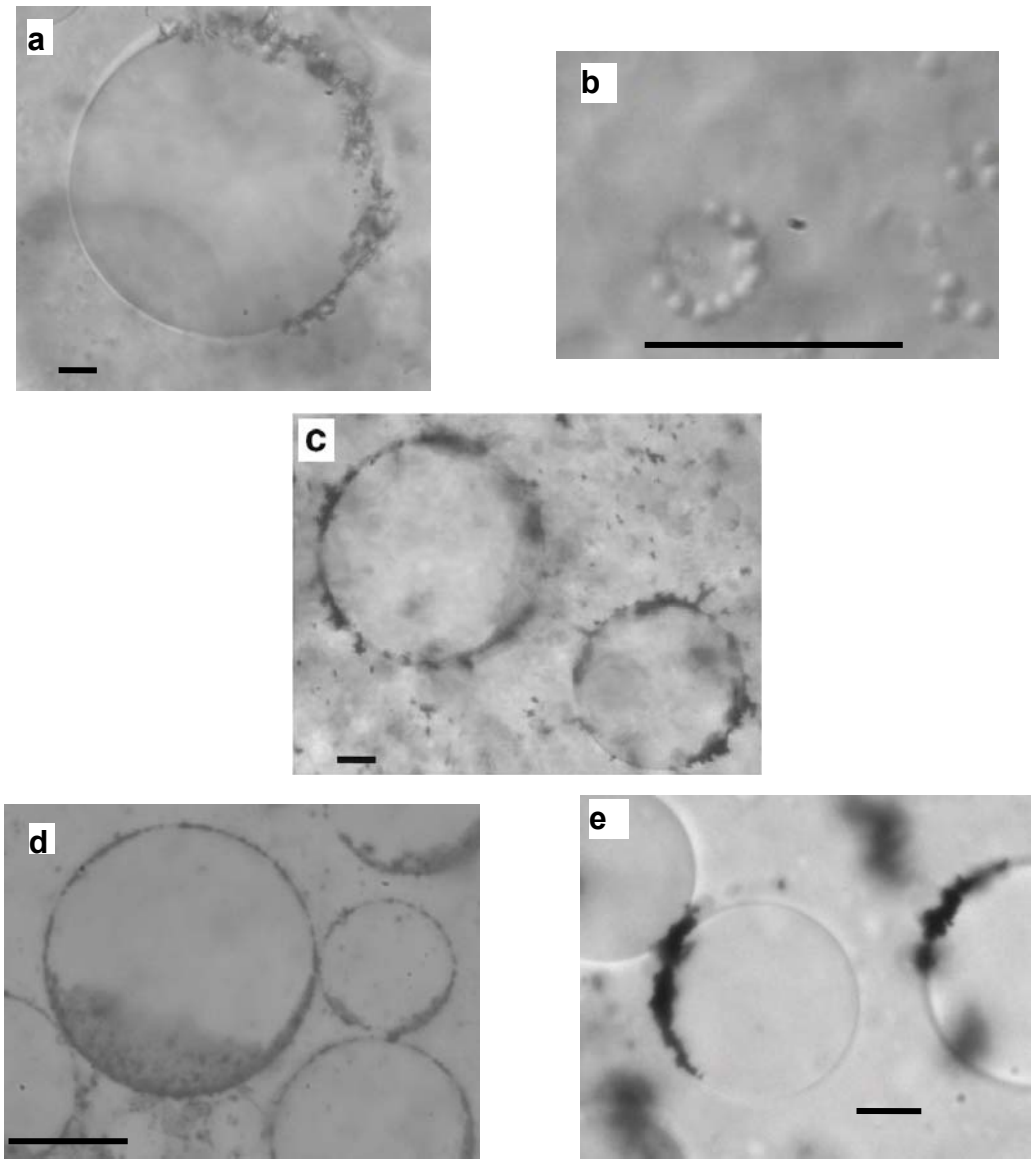

Figure 33. Optical microscopy images of various particles adsorbed at the PI/PIB interface: (a) PTFE; (b) DCDMS-coated hydrophobic silica; (c) titanium dioxide; (d) iron oxyhydroxide; (e) carbonyl iron. In all cases, the drop phase is PI. All scalebars are 20 μm.

We note that the images of Figure 33 have been chosen to show one or two large drops, whereas most drops in the blend were smaller. Furthermore, we reiterate that the low particle loading of 0.1% was chosen only to improve images; we have also conducted some experiments

with higher particle loadings which show numerous examples of tightly-covered drops. However, the image quality is usually far poorer. Finally, all the images presented here correspond to drops that were inside the bulk of the sample (and not resting against or wetting glass slides).

Thus to summarize the chief experimental result of this chapter, a wide variety of particles were found to adsorb readily at PI/PDMS and PI/PIB interfaces. We find the PI/PIB case to be especially remarkable because particles adsorb at the interface in spite of the chemical similarity of the phases. The goal of the rest of this chapter is to test whether a simple scheme for estimating interfacial and surface energies can predict the observed interfacial activity.

5.2.2 Young's equation

In the Introduction, we discussed the partial-wettability as the reason for interfacial activity of particles. Quantitatively, the condition for interfacial activity is that $0° < \theta_{12} < 180°$. The contact angle can be related to the interfacial energies as per Young's equation:

$$\cos\theta_{12} = \frac{\alpha_{2s} - \alpha_{1s}}{\alpha_{12}} \qquad [16]$$

where α_{1s}, α_{2s} and α_{12} are the interfacial energies of the phase1/solid, phase2/solid, and phase1/phase2 interfaces respectively. Thus, the condition for interfacial activity becomes $|\cos\theta_{12}| < 1$ i.e. $|\alpha_{2s} - \alpha_{1s}| < \alpha_{12}$. In contrast, if $|\cos\theta_{12}| > 1$ i.e. $|\alpha_{2s} - \alpha_{1s}| > \alpha_{12}$, the particle will be located entirely in the phase which fully wets the particles (phase 1 if $\alpha_{1s} < \alpha_{2s}$, and vice versa otherwise).

In the Introduction, we made a qualitative argument that interfacial activity at polymer/polymer interfaces is less likely than at oil/water interfaces; we can now make this

argument more quantitative. Immiscible polymers are much more chemically-similar to each other than oil and water. As the chemical nature of the two phases approaches each other, the denominator α_{12} is expected to approach zero faster than the numerator $|\alpha_{2s} - \alpha_{1s}|$.[101-103] Thus, with increasing similarity of the phases, $|\cos\theta_{12}| < 1$ is not likely.

5.2.3 Theory: Work of adhesion, solid surface tension, and critical surface tension

While Equation 16 is theoretically rigorous, it cannot immediately predict interfacial activity. Specifically, while the interfacial tension α_{12} between the two polymers can be measured experimentally (see Materials and Methods section), the solid/liquid interfacial tensions α_{1s} and α_{2s} cannot be determined by a direct experiment. We will therefore use well-established approaches to estimate the *interfacial* tensions between two phases from the *surface* tensions of the two phases. For immiscible phases a and b, the interfacial tension α_{ab} can be written as:

$$\alpha_{ab} = \alpha_a + \alpha_b - W_{ab}^{adh} \qquad [17]$$

where α_a and α_b are the surface tensions (against air) of the two phases, and W_{ab}^{adh} is the work of adhesion. A large body of literature has been devoted to correlating the work of adhesion with the surface energies of each of the two phases, their chemical nature, and polarity.[104-106] A commonly used equation for the work of adhesion is the Girifalco-Good equation:[104, 105]

$$W_{ab} = 2\phi\sqrt{\alpha_a \alpha_b} \qquad [18]$$

where ϕ is an empirical fitting parameter, often taken to be 1; $\phi = 1$ will be assumed in the remainder of this chapter. Thus:

$$\alpha_{ab} = \alpha_a + \alpha_b - 2\sqrt{\alpha_a \alpha_b} \qquad [19]$$

α_{1s} and α_{2s} required in Equation 16 can be obtained from Equation 19, if the three surface tensions α_1, α_2, and α_s are known. Substituting α_{1s} and α_{2s} from Equation 19 into Equation 16 yields:

$$\cos\theta_{12} = \frac{\alpha_2 - \alpha_1 - 2\sqrt{\alpha_2 \alpha_s} + \sqrt{\alpha_1 \alpha_s}}{\alpha_{12}} \qquad [20]$$

Solving this equation for α_s:

$$\alpha_s = \left(\frac{\alpha_2 - \alpha_1 - \alpha_{12}\cos\theta_{12}}{2\left(\sqrt{\alpha_2} - \sqrt{\alpha_1}\right)} \right)^2 \qquad [21]$$

Interfacial activity of the particle requires that $-1 < \cos\theta_{12} < 1$, i.e.

$$\left(\frac{\alpha_2 - \alpha_1 - \alpha_{12}}{2\left(\sqrt{\alpha_2} - \sqrt{\alpha_1}\right)} \right)^2 < \alpha_s < \left(\frac{\alpha_2 - \alpha_1 + \alpha_{12}}{2\left(\sqrt{\alpha_2} - \sqrt{\alpha_1}\right)} \right)^2 \qquad [22]$$

In summary, Equation 22 is the Girifalco-Good theory's prediction for the range of α_s values which permit interfacial activity of the particles at a phase1/phase2 interface. For the PI/PDMS case, we can substitute the surface tensions for α_{PI} and α_{PDMS} from Table 2, and $\alpha_{PI/PDMS}$= 2.73 mN/m noted in the "Materials and Methods" section, to obtain the condition for interfacial activity in the PI/PDMS system:

$$18.8 < \alpha_s (mN/m) < 36.4 \qquad [23]$$

A similar calculation for the PI/PIB system yields:

$$29.1 < \alpha_s (mN/m) < 39.2 \qquad [24]$$

It is of immediate interest to test whether the surface energies of the interfacially-active particles of Figure 32 and Figure 33 do indeed lie within these ranges, if so, Equation 22 would have predictive value.

How can α_s be measured experimentally? We use the Zisman's concept of critical surface tension.[105, 107, 108] Consider a liquid/air meniscus in contact with a solid surface. Applying Equation 16 to this situation:

$$\cos\theta_L = \frac{\alpha_s - \alpha_{sL}}{\alpha_L} \qquad [25]$$

where θ_L is the contact angle of the liquid/air interface at the solid surface. It has been observed that as the surface tension of the liquid decreases, θ_L approaches 0° ($\cos\theta_L$ approaches 1), i.e. the liquid has an increasing tendency to wet the surface.[105, 107, 108] The critical surface tension of the solid, α_{sc}, is defined as the highest surface tension of the liquid that can completely wet the surface, i.e. liquids with $\alpha_L < \alpha_{sc}$ fully wet the surface, whereas those with $\alpha_L > \alpha_{sc}$ partially-wet the surface. By definition, at the critical surface tension, $\cos\theta_L = 1$, and hence from Equation 25:

$$\alpha_{sc} = \alpha_s - \alpha_{sL} \qquad [26]$$

Applying Equation 16 to α_{sL} in Equation 25, it is easy to show that:

$$\alpha_s = \alpha_{sc} \qquad [27]$$

thus allowing the solid surface energy to be obtained experimentally. Fox and Zisman's procedure[107] for finding α_{sc} was devised for solids that were available in the form of a flat solid substrate. In this case, the contact angle of various test fluids on the solid substrate is measured, $\cos\theta_L$ is plotted as a function of α_L (the so-called Zisman plot) and then the data are extrapolated to $\cos\theta_L = 1$. However in the case of solid particles, this procedure cannot be applied since it is not possible to measure θ_L values directly. Hence *Marmur et al.*[72, 109] have developed an alternate method, called the float/sink test. In this test, the solid particles are scattered on the surface of a test liquid. If the particles sink, they are regarded as being fully wetted by the fluid, whereas if they float they are only partially wetted. This test is repeated using several test fluids spanning a

range of surface tensions; it is then easy to determine α_{sc} as the surface tension below which particles sink. This is the method we will follow in the next section to determine α_{sc}.

Finally, we note that Equation 18 is not the only means of correlating the work of adhesion to the surface tension. An alternate form is the harmonic equation:

$$W_{ab}^{adh} = \frac{4\alpha_a \alpha_b}{\alpha_a + \alpha_b} \qquad [28]$$

which has been shown to work well for interfaces between materials of low polarity such as polymer/polymer interfaces.[106, 110] The corresponding prediction for the interfacial tension is:

$$\alpha_{ab} = \alpha_a + \alpha_b - \frac{4\alpha_a \alpha_b}{\alpha_a + \alpha_b} \qquad [29]$$

Using Equation 29 in Equation 26 still predicts Equation 27, i.e. the idea that the solid surface energy is equal to its critical surface tension is not dependent on the Girifalco-Good equation for the work of adhesion.

5.2.4 Determination of critical surface tension

Float/sink experiments were conducted using the liquids listed in Table 4. Initial experiments using the eight fluids marked with a superscript "1" yielded approximate critical surface tensions for most of the particles used. Additional experiments were then conducted with the fluids marked "2" in order to establish the critical surface tensions more narrowly. In each case, approximately 10 ml of the liquid was placed in a vial. A small quantity of particles were placed on a weighing pan and spread with a spatula to disrupt any large aggregates. They were then transferred to the vial by inverting the pan on the mouth of the vial and tapping the pan gently. If particles floated, they were observed for at least 10 minutes. The values of critical

surface tension assigned to each particle type are listed in Table 4. Two values are quoted for each particle type: an upper bound (α_L at which particles float) and a lower bound (α_L at which particles sink). Some comments about each particle type are in order.

The critical surface tension of PTFE particles was found to be between 25-28.5 mN/m. This is significantly higher than the value of ~ 20 mN/m noted previously.[105] However, the manufacturing process for these particles involves thermal degradation, which may have raised their surface energy.

In the case of DCDMS-treated particles in nitrobenzene, most of the particles floated and only a small fraction sank. Hence the corresponding surface tension of 43.9 mN/m is regarded as the upper bound. In contrast, most of the TiO_2 particles sank in diiodomethane, and hence 50.8 mN/m is regarded as the lower bound for TiO_2.

The float/sink test gave ambiguous results for the iron particles; these particles floated in glycerol, but sank in water. This contradicts the idea implicit in the concept of critical surface tension that particles sink only when α_L is *reduced*. The critical surface energy for pure iron[111] of 46 mN/m suggests that they should have floated in ethylene glycol. In summary, we are unable to obtain a reliable value for α_s for the iron particles using the float/sink method.

Finally we note that gravitational effects are expected to be weak in the float/sink experiment. The relevant dimensionless quantity, $\frac{R^2 \Delta\rho g}{\alpha_L}$ (where R is particle size, $\Delta\rho$ is the density difference between the particle and liquid, and g is gravity) is on the order of 10^{-5} for iron particles, and much smaller for all the others. This small value indicates that gravitational forces are much weaker than interfacial forces.

Table 4. Results of float/sink tests.

Test liquid	Surface tension α_L (mN/m)	PTFE	DCDMS	TiO_2	FeOOH	Fe
Hexane[1]	18.4	Sink	Sink	Sink	Sink	Sink
Octane[1]	21.6	Sink	Sink	Sink	Sink	Sink
Cyclohexane[1]	25.0	Sink	Sink	Sink	Sink	Sink
Toluene[1]	28.5	Float				
1,2 dichloroethane[1]	33.3	Float	Sink	Sink	Sink	Sink
Benzaldehyde[2]	38.8		Sink			
Nitrobenzene[1]	43.9	Float	Float>Sink	Sink	Sink	Sink>Float
ethylene glycol[2]	46.5			Sink		Sink
Diiodomethane[1]	50.8	Float	Float	Sink>Float	Sink	Sink
Glycerol[2]	63.3			Float	Sink	Float
Water[1]	72.3	Float	Float	Float	Float	Sink>Float
Particle surface energy, α_s assigned		25-28.5	38.8-43.9	50.8-63.3	63.3-72.3	uncertain; 46 for pure iron
Limits as per Equation 22	PI/PDMS	$18.8 \pm 0.2/36.4 \pm 2.0$				
	PI/PIB	$29.1 \pm 3.0/39.2 \pm 4.0$				

5.2.5 Comparison with experiment

Equations 23 and 24 had noted the Girifalco-Good prediction of the range of surface energies within which particles are expected to be interfacially-active in the PI/PDMS and PI/PIB system. These same ranges are listed in the last two rows of Table 4. It is immediately apparent that the PTFE particles are the only ones whose surface energy lies unambiguously within the bounds predicted by Girifalco-Good theory. The surface energies of TiO_2 and FeOOH, and possibly Fe, are much larger than upper bounds, and hence these particles are predicted not to be interfacially-active. Experimentally however, Figure 32 and Figure 33 show interfacial activity of all particle types. Thus, we conclude that the Girifalco-Good theory with $\phi = 1$, combined with the Zisman concept of critical surface tension, is inadequate to predict the interfacial activity of the particles.

Some comments about errors are in order. All the interfacial and surface tensions measured by the pendant drop method are expected to be highly accurate, to be well within 5%.[112] The interfacial tension between PI and PIB measured by DDRM may have a more significant error (estimated to be about 15% based on repeated measurements). However, the range of α_s for interfacial activity (Equation 22) is not highly sensitive to α_{12} and even a 20% error in measuring α_{12} does not change the conclusion at the end of the previous paragraph.

We have also considered whether an alternative equation for the work of adhesion, the harmonic mean equation (Equation 28) can predict the observed interfacial activity. Following the same procedure as used to derive Equation 22, we derived the range of surface energies within which the harmonic mean equation predicts interfacial activity. These limits are $22.6 < \alpha_s (mN/m) < 31.5$ for interfacial activity at the PI/PDMS interface, and

$31.5 < \alpha_s (mN/m) < 36.5$ for PI/PIB interfaces. Once again, the experimentally-determined surface energies of most of the particles lie above these ranges, i.e. the harmonic mean equation cannot predict the interfacial activity.

Both Girifalco-Good equation and the harmonic mean equation are simplistic approaches for obtaining the interfacial tension from the surface tensions; however, these equations have the advantage of involving quantities that are readily accessible experimentally. The more sophisticated Fowkes theory of the work of adhesion may be able to make more accurate predictions of interfacial activity. A brief description of Fowkes theory is given in the next section.

5.3 FOWKES THEORY OF SURFACE TENSION

Fowkes theory of surface tension expresses surface tension (surface energy α) as the sum of components of surface tension, where each component arises from a specific intermolecular interactions. Mathematically, Fowkes expression for surface tension is expressed as:

$$\alpha = \alpha^d + \alpha^p \qquad [30]$$

Where α^d is the dispersive component of α, originating from van der Waals or London force interactions. α^p is the polar component, originating from dipole-dipole and hydrogen bonding interactions.

Substituting Equation 30 in Equation 19, we get

$$\alpha_{ab} = \alpha_a + \alpha_b - 2\sqrt{\alpha_a{}^d \alpha_b{}^d} - 2\sqrt{\alpha_a{}^p \alpha_b{}^p} \qquad [31]$$

Therefore for phase 1/phase 2 interfacial tension Equation 31 can be rewritten as:

$$\alpha_{12} = \alpha_1 + \alpha_2 - 2\sqrt{\alpha_1^{\,d}\alpha_2^{\,d}} - 2\sqrt{\alpha_1^{\,p}\alpha_2^{\,p}} \quad [32]$$

$$\alpha_1 = \alpha_1^{\,d} + \alpha_1^{\,p} \quad [33]$$

$$\alpha_2 = \alpha_2^{\,d} + \alpha_2^{\,p} \quad [34]$$

Since α_1, α_2 and α_{12} are experimentally determined quantities, α^p and α^d of phase 1 and phase 2 can be determined numerically by simultaneously solving Equation 32 and 33/34.

But to comment on the interfacial activity of particles, we need to calculate the contact angle $\cos\theta_{12}$. Therefore, rewriting Equation 20 in the form of Fowkes expression we get

$$\cos\theta_{12} = \frac{(\alpha_2^{\,d} + \alpha_2^{\,p}) - (\alpha_1^{\,d} + \alpha_1^{\,p}) - 2\sqrt{(\alpha_s^{\,d} + \alpha_s^{\,p})}(\sqrt{\alpha_2^{\,d} + \alpha_2^{\,p}} - \sqrt{\alpha_1^{\,d} + \alpha_1^{\,p}})}{\alpha_{12}} \quad [35]$$

To predict the interfacial activity of various particles, based on the value of $\cos\theta_{12}$ we need to know the values for α_s^d and α_s^p, however, it is not clear how this information required to apply this theory may be obtained experimentally.

5.4 SUMMARY AND CONCLUSIONS

The primary conclusion of this chapter is that a wide variety of particle types adsorb at the interface between immiscible homopolymers, even when the homopolymers are chemically quite similar to each other (as gauged by the low interfacial tension between them). Research on "interfacial composites" – polymer blends in which solid particles are adsorbed at the interface – is a newly-active area of research, and our results suggest that a wide variety of particles may be candidates for use in interfacial composites.

Secondarily, we have tested the value of Girifalco-Good theory as a means to predict the interfacial activity. The solid surface energy required by Girifalco-Good theory was assumed to be equal to the critical surface tension of the particles. The critical surface tension was then

found by float/sink tests with several test fluids. Our results suggest that the Girifalco Good theory is not able to predict interfacial activity of particles. While we still believe that partial wettability of particles by both phases is responsible for their interfacial adsorption, some more elaborate theoretical approach is necessary to capture the relevant surface energies.

6.0 EFFECT OF PARTICLES ON THE RHEOLOGY AND MORPHOLOGY OF POLYISOPRENE/POLYDIMETHYLSILOXANE (PI/PDMS) BLENDS

As discussed in the previous chapter, various kinds of particles readily adsorb at the interface between polyisoprene (PI) and polydimethylsiloxane (PDMS). A possibility emerging from the adsorption of particles at the polymer-polymer interface is their use as particulate compatibilizers in polymer blends. Compatibilizers are large molecule polymeric surfactants which due to their amphiphilic chemical nature are known to be interfacially active.[113] Depending on the chemical nature of two phases, a given compatibilizer can be interfacially active in one blend but might not be in another, thus making it system specific. In contrast to compatibilizers, non amphiphilic particles may be less specific i.e the same particle may adsorb at the interface between several polymer pairs, and thus may prove to be generic.

Typically, compatibilizers improve dispersion and promote blending of immiscible polymers by reducing the size of drops. This can be due to encouraging drop breakup[114] or stopping coalescence.[113] The phenomenon of coalescence suppression of drops is usually considered to be more important in achieving a small drop size.[113] Therefore, we hypothesize that similar to compatibilizers, the consequence of particle adsorption may be the suppression of coalescence of drops. If particles are able to suppress coalescence of drops, just the way compatibilizers do, we expect to see its rheological manifestation in both dynamic oscillatory

and steady shear experiments. We will use rheology as a microstructural tool to probe the effect of particle adsorption, specifically on the drop size of particle laden blends.

We propose to use the same particle types as in chapter 5 viz. polytetrafluoroethylene (PTFE), iron (Fe), iron oxyhydroxide (FeOOH), titanium dioxide (TiO_2), with the exception of spherical silica particles. In contrast to commercial availability of large quantities of PTFE, iron, iron oxyhydroxide and TiO_2 particles, spherical silica particles are available only in small batches. Therefore we have not used them in this research, where experiments with various particle loadings might be required to study the effect of interfacial particle adsorption. Furthermore, if complete coverage of drop surface is required for suppression of coalescence, the amount of spherical particles required will be larger than irregular particles like PTFE, iron oxyhydroxide and TiO_2.

6.1 EXPERIMENTAL

6.1.1 Model Fluids

Experiments were performed with polyisoprene (PI) and polydimethylsiloxane (PDMS). These polymers were chosen as they were molten at room temperature, thus allowing the experiments to be conducted at room temperature. The viscosities of PI and PDMS are reasonably well-matched so it is possible to study both PI-in-PDMS blends and the reverse blends.

Particle laden blends were prepared by hand mixing using a plastic spatula. Each sample contained 0.5 vol% of particles. A particle free blend consisting of 20% by weight of minority phase was first prepared. This was then poured on top of 0.5 vol% of particles, and then particles

and blend were mixed together. Particle containing blends are designated as Sx-y0.5, where x is the weight percent of PDMS, y is the particle type added. Thus the particle free blend will be referred to as S20-0. All samples were degassed under vacuum to remove the air bubbles before any rheology or visualization experiments were performed.

6.1.2 Rheology

Rheological experiments were conducted in stress controlled mode using an ARES 2000 rheometer with a cone-and-plate geometry (40 mm diameter, 1° cone). Sample temperature was maintained at 25 °C using a Peltier plate. Samples were subjected to the desired shear history (specified later) and then the complex moduli were measured between 100 rad/s and 0.1 rad/s at a strain of 20%.

6.1.3 Visualization

Samples were visualized in a home built shear cell (same as in chapter 4). They were sheared between two parallel glass plates where the bottom plate was able to rotate and was driven by a rheometer motor. The stationary top plate was fixed to an overhanging structure. The optical assembly consisted of a sliding arm with a microscope nose piece consisting of 4x, 20x and 40x objectives. This sliding arm was able to slide from the center to all the way to the edge of the sample.

6.2 RESULTS

6.2.1 Rheology and Morphology of particle laden blends

To test whether the adsorption of particles at the interface between PI and PDMS was able to suppress coalescence of drops, the blends were subjected to the shear history shown in Figure 34. The samples were sheared for 2000 strain units at each stress level. After each shearing step, the blend was allowed to recover after the cessation of flow. Then dynamic oscillatory frequency sweep was conducted to probe the morphology resulting from shearing of the blend. This procedure was repeated at successively lower stresses of 200 Pa, 100 Pa and 50 Pa.

In dynamic oscillatory experiments for blends, we expect to see the presence of a characteristic shoulder at low frequency in modulus (G') versus frequency (ω) data as shown in Figure 35a. Detailed theory and dimensional analysis suggest that the magnitude of this shoulder is $\frac{\alpha}{R}$, where α is the magnitude of the interfacial tension between two phases and R is the radius of drops.[46,61,63] The characteristic frequency at which the shoulder occurs is proportional to $\frac{\alpha}{R\eta_m}$ where η_m is the matrix viscosity. Thus the shift in the shoulder of G' to lower or higher frequencies at different stress levels can trace the change in drop size. Similarly the complex viscosity $\left|\eta^*\right|$ for the blend shows a shoulder and its shift can qualitatively trace the drop size evolution as shown in Figure 35b.

It is known that the drops in the blend retract back to their spherical shape after the cessation of flow due to the interfacial tension between the droplet and matrix. This retraction causes the elastic recovery (recoil) of the blend. Since the Newtonian polymers hardly show any

recoil behavior, the recoil of the blend can be attributed solely to the action of the interface.[59,115] Previous research on the recovery of polymer blends has shown that the recovery kinetics can be captured by an exponential function with a single retardation time (to be discussed later). Therefore, we expect to see qualitatively a graph of recovered strain versus time similar to Figure 35c. Dimensional analysis suggests that the leveling off value of recovered strain follows $\gamma_\infty \propto Ca \propto \frac{R\sigma}{\alpha}$, where Ca is the capillary number before the flow was stopped. Also the retardation time τ_2 for the drops to retract back to the spherical shape is $\tau_2 \propto \frac{R\eta_m}{\alpha}$.

These scalings lay the basis of judging the drop coalescence from the rheology of blends. A more detailed description of τ_2, γ_∞ and their morphological interpretation is presented in the next section.

Specifically, if the particles are able to suppress coalescence of drops: a) Oscillatory properties will be independent of the applied shear stress, b) Retardation time τ_2 will be independent of stress but γ_∞ will decrease proportionately with stress.

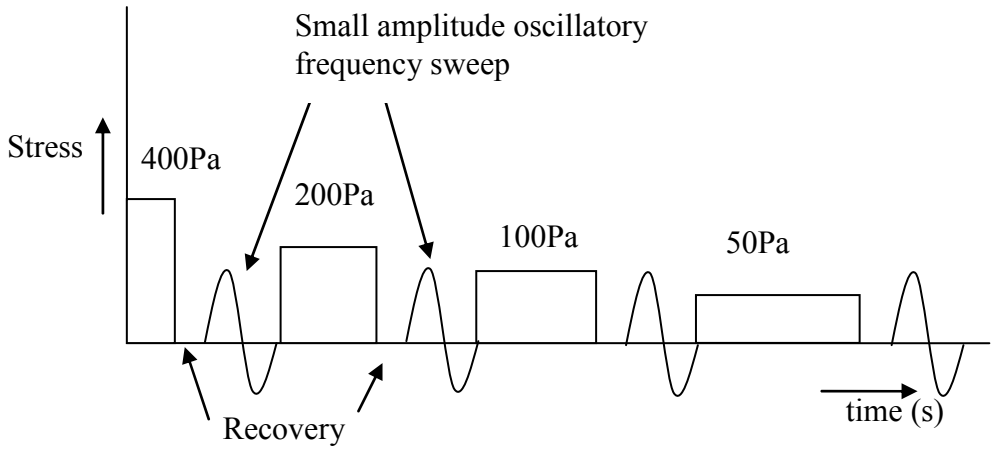

Figure 34. Shear history applied to the blends.

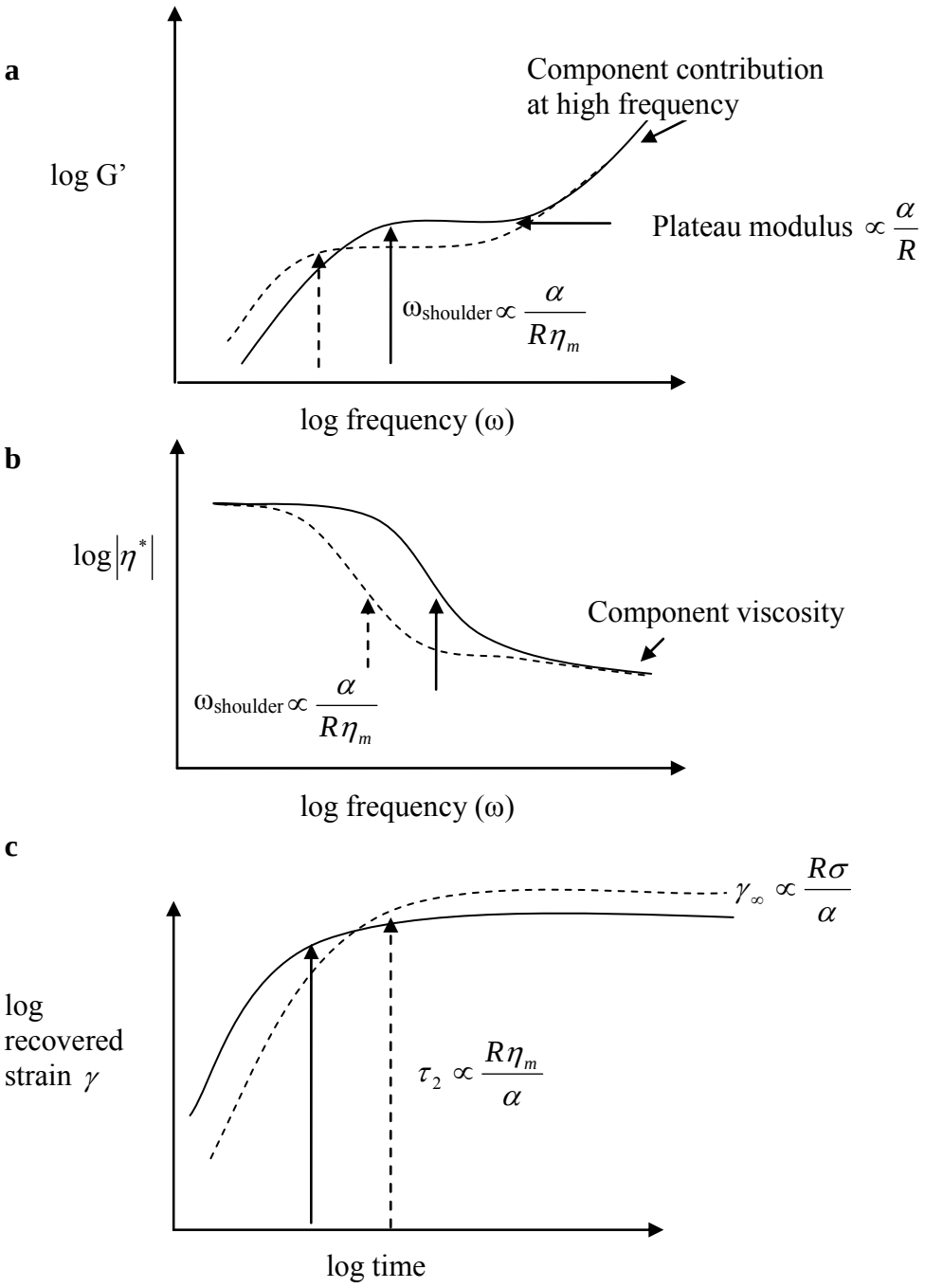

Figure 35. (a) Shift in G'shoulder to low frequency (solid line versus dotted) indicating increase in R. (b) Horizontal $|\eta^*|$ shift to left (dotted lines). (c) log(γ) versus log(time); keeping everything else constant, if R decreases, γ_∞ and τ_2 also decrease when the stress is decreased.

The results of rheological experiments are organized as follows: a) a qualitative discussion of dynamic oscillatory data for particle free and particle laden blends, and b) quantitative analysis of strain recovery data for both particle free and particle laden blends.

6.2.1.1 Dynamic Oscillatory behavior

We first present the dynamic oscillatory behavior of the blends S20-0 and particle containing blends S20-PTFE0.5, S20-Fe0.5, S20-FeOOH0.5, S20-$TiO_2$0.5 in Figure 36a and b. In each case G' graphs are shifted by a factor of 10 and $|\eta^*|$ graphs are shifted by 50 Pa.s with respect to each other. Only the first step after 400 Pa shearing and the last step after 50 Pa shearing are shown. The data for intermediate stresses lie between these two stress levels. The solid lines are for 400 Pa shearing and the dotted lines represent dynamic oscillatory response after 50 Pa shearing.

As shown in Figure 36a, G' of the blend resulting from volume average of component contribution was quite small, reflecting the near-Newtonian behavior of the components. Compared to this the G's and $|\eta^*|$ of S20-0 showed the presence of a characteristic shoulder at lower frequency which is attributed to the additional contribution of the interface coming from the deformation and relaxation of drops.

In Figure 36a, it is clear that for particle free blend S20-0, G' shoulder moved to a lower frequency as the stress was lowered from 400 Pa to 50 Pa. Also, the plateau in G' at intermediate frequencies is reduced. Similar behavior was true for $|\eta^*|$ curves too. These shifts are identified by the arrows in Figure 36a and b. As discussed above, the frequency at which the shoulder appears is inversely proportional to R. Therefore on stepping down the shear stress drops coalesced with each other leading to an increase in drop radius R.

Similar to S20-0 blend, the blends with all particle types i.e PTFE, Fe, FeOOH and TiO_2 showed qualitatively the same feature of shift in G' and $|\eta^*|$ shoulder to a lower frequency when the shear stress was lowered from 400 Pa to 50 Pa, indicating coalescence. Thus at first glance, none of the particles appear to prevent coalescence in the S20 blends.

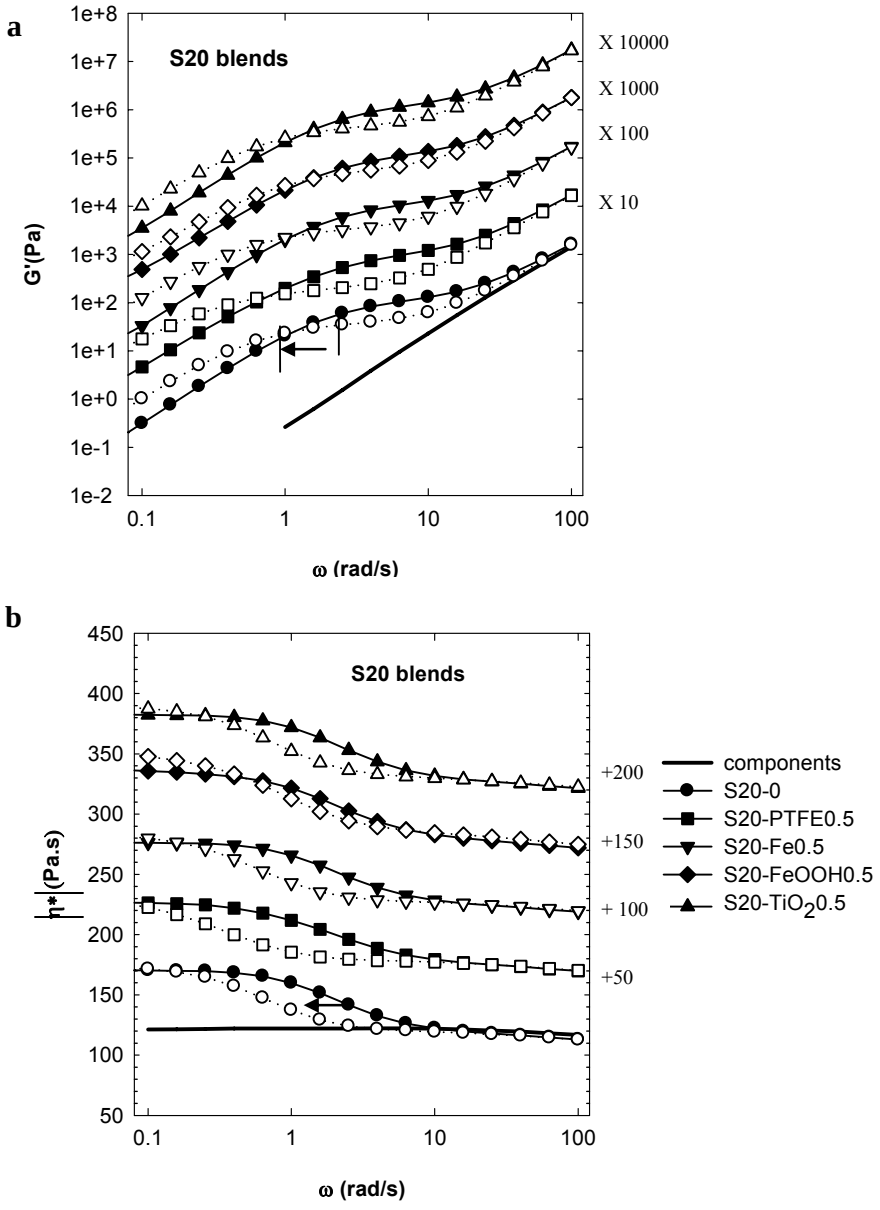

Figure 36. (a) G' vs. ω and (b) $|\eta^*|$ vs. ω for S20-0, S20-0.5PTFE, S20-0.5FeOOH, S20-0.5TiO_2.

We now consider the effect of particles in the inverted particle free system of PI drops in PDMS matrix which is referred to as S80-0 blend as shown in Figure 37a and b. Qualitatively, on stepping down of shear stress, all particle containing blends showed a shift in G' and $|\eta^*|$ shoulder to low frequency similar to S20 blends. $|\eta^*|$ also showed an upturn at low frequency after 50 Pa for S80-Fe0.5 and S80-$TiO_2$0.5.

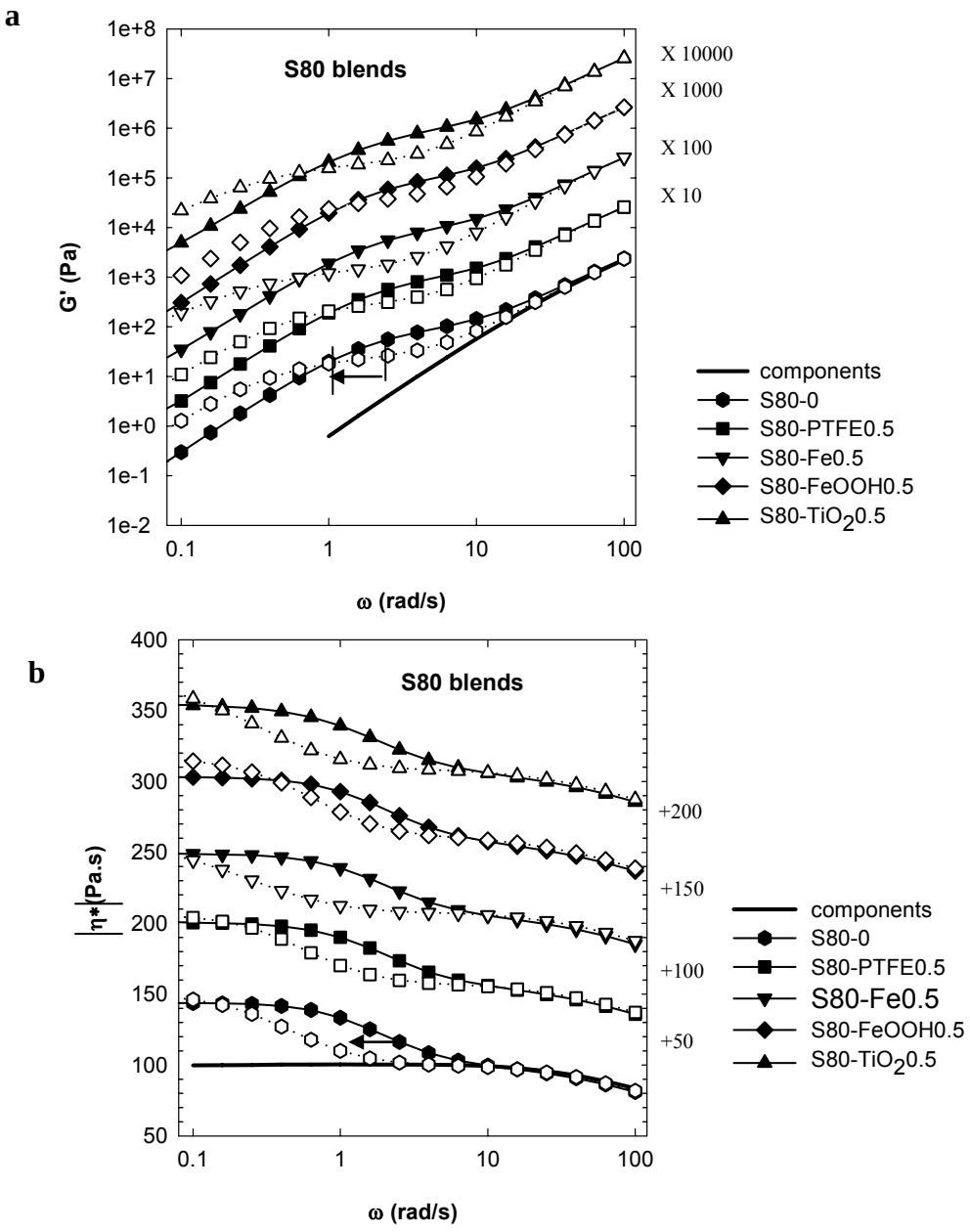

Figure 37. (a) and (b) Dynamic oscillatory behavior for S80-0, S80-0.5PTFE, S80-0.5Fe, S80-0.5FeOOH, S80-0.5 TiO_2.

As discussed above, qualitatively the oscillatory data show: All particle containing blends show decrease in plateau G' at intermediate frequency. Also there is a decrease in the frequency

at which the G' and $|\eta^*|$ shoulder appears. Therefore coalescence of drops is not suppressed. In the past, dynamic oscillatory data for immiscible polymer blends have been treated more quantitatively. Various authors have derived the size of the drops by fitting mathematical models to the data.[116,117-119] However, in our case, the fact that some blends show a non terminal behavior in G' and an upturn in $|\eta^*|$ at low frequency makes the shifts, especially in $|\eta^*|$, hard to evaluate quantitatively. Therefore, the change in drop size is traced by analyzing the recovery of blends after cessation of flow. The strain recovery of particle free and particle laden blends is discussed in the following section.

6.2.1.2 Strain recovery of blends

After the cessation of flow, the elastic recovery (recoil) of the blends was measured. As discussed before, the elastic recovery of the blend can be attributed solely to the retraction of the interface.[59,60] Thus, the recoil of the blend after the steady state shearing can give vital information about changes in morphology of the blend.

In the simplest description of strain recovery, the recovery kinetics follows a single exponential function:

$$\gamma = \gamma_\infty[1-\exp(-t/\tau_2)] \qquad [36]$$

where, γ_∞ is the ultimate recovered strain defined at t = ∞, and τ_2 is the retardation time for the drops to retract back to spherical shape.

The physical phenomenon of recovery involves the retraction of drops after cessation of flow. This makes it obvious to think that the recovered strain will primarily depend on the deformation of drop during flow, which depends on Ca, the ratio of viscous to interfacial stress. Indeed, Taylor's theory[57] predicts that at small Ca, the deformation (D_{Taylor}) is given by:

$$D_{Taylor} = Ca\frac{19p+16}{16(p+1)} \quad [37]$$

Thus both τ_2 and γ_∞ are a strong function of Ca and hence the deformation. The scaling relations explained before in section 6.3.1 show that the time scale for recovery τ_2 scales with the radius of the drop R ($\tau_2 \propto R$). The ultimate recovery follows $\gamma_\infty \propto Ca \propto \sigma R$, where σ is the shear stress applied before the cessation of flow. Therefore if the coalescence of the drops is suppressed i.e. R remains constant with stress then a) $\gamma_\infty \propto \sigma$ b) τ_2 independent of σ.

If the coalescence of drops is not suppressed then the following recovery behavior has already been observed experimentally for model polyisobutylene (PIB)/polydimethylsiloxane (PDMS) blends:

- γ_∞ independent of stress (σ), τ_2 inversely proportional to stress (σ)- implying Ca_{ss} (Ca at steady state) is constant: drop size grows by coalescence in the same proportion as the decrease in stress.[59]
- γ_∞ decreases weakly with σ ; $\tau_2 \propto \sigma^{-0.6}$ - implying that the drop size increases less than proportionately to the decrease in stress.[119]

Similar to PIB/PDMS model blends, particle free S20-0 (Figure 38a) blends showed a decrease in γ_∞ and an increase in time scale for recovery τ_2 when the stress was lowered. Qualitatively same trend for γ_∞ and τ_2 was shown by S20-Fe0.5 (Figure 38c), S20-FeOOH0.5 (Figure 38d) and S20-$TiO_2$0.5 (Figure 38e). However, S20-PTFE0.5 (Figure 38b) showed an opposite trend of γ_∞ increasing with the decrease in stress.

For the particle containing S80 blends two kinds of strain recovery versus time behavior were observed (a) γ_∞ decreased and τ_2 increased with stress for S80-0 (Figure 39a), S80-

PTFE0.5 (Figure 39b), S80-FeOOH0.5 (Figure 39d), S80-$TiO_2$0.5 (Figure 39e). (b) Both γ_∞ and τ_2 increased with stress S80-Fe0.5 (Figure 39c).

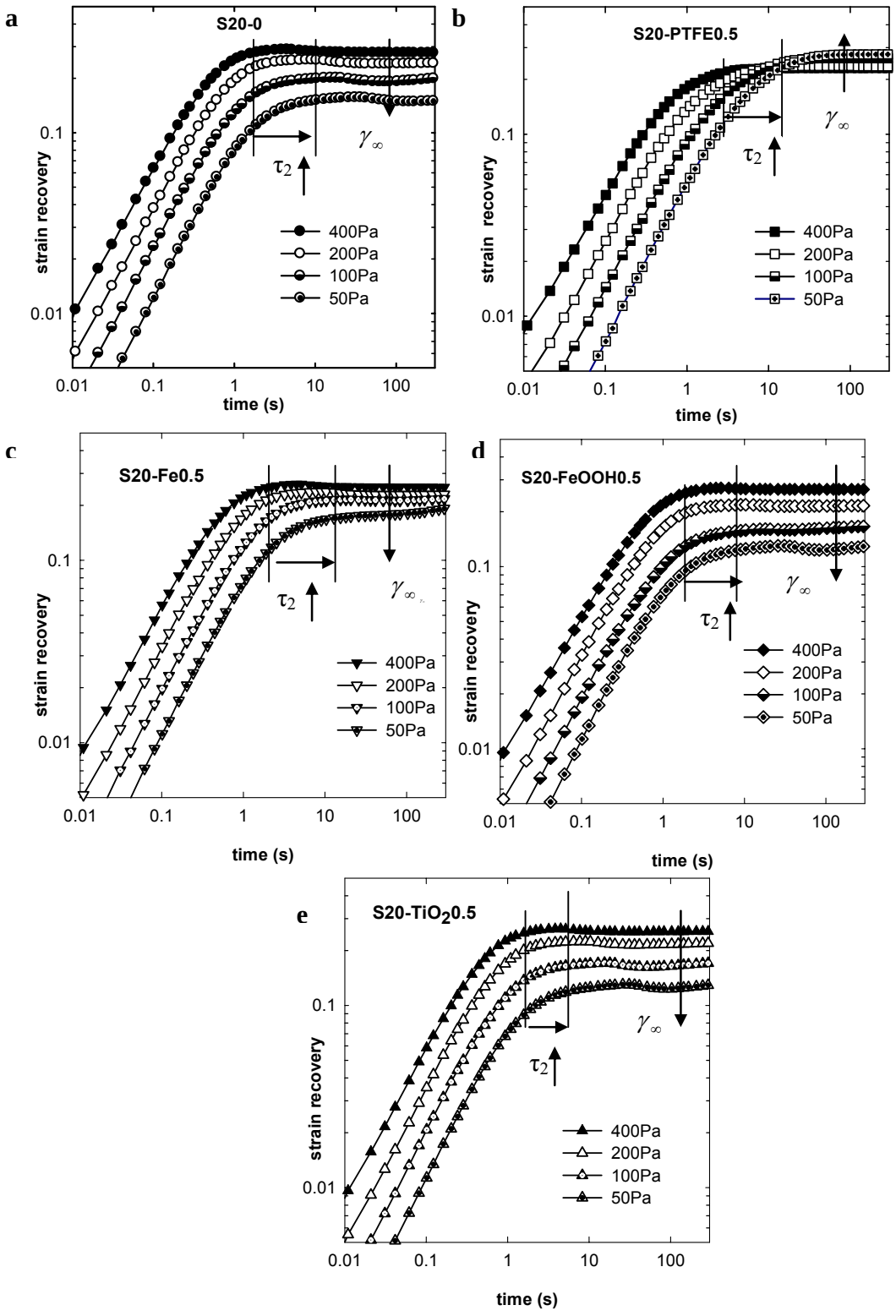

Figure 38. (a) Strain recovery (γ) versus time (s) for S20-0; (b) S20-PTFE0.5; (c) S20-Fe0.5; (d) S20-FeOOH0.5; (e) S20-$TiO_2$0.5.

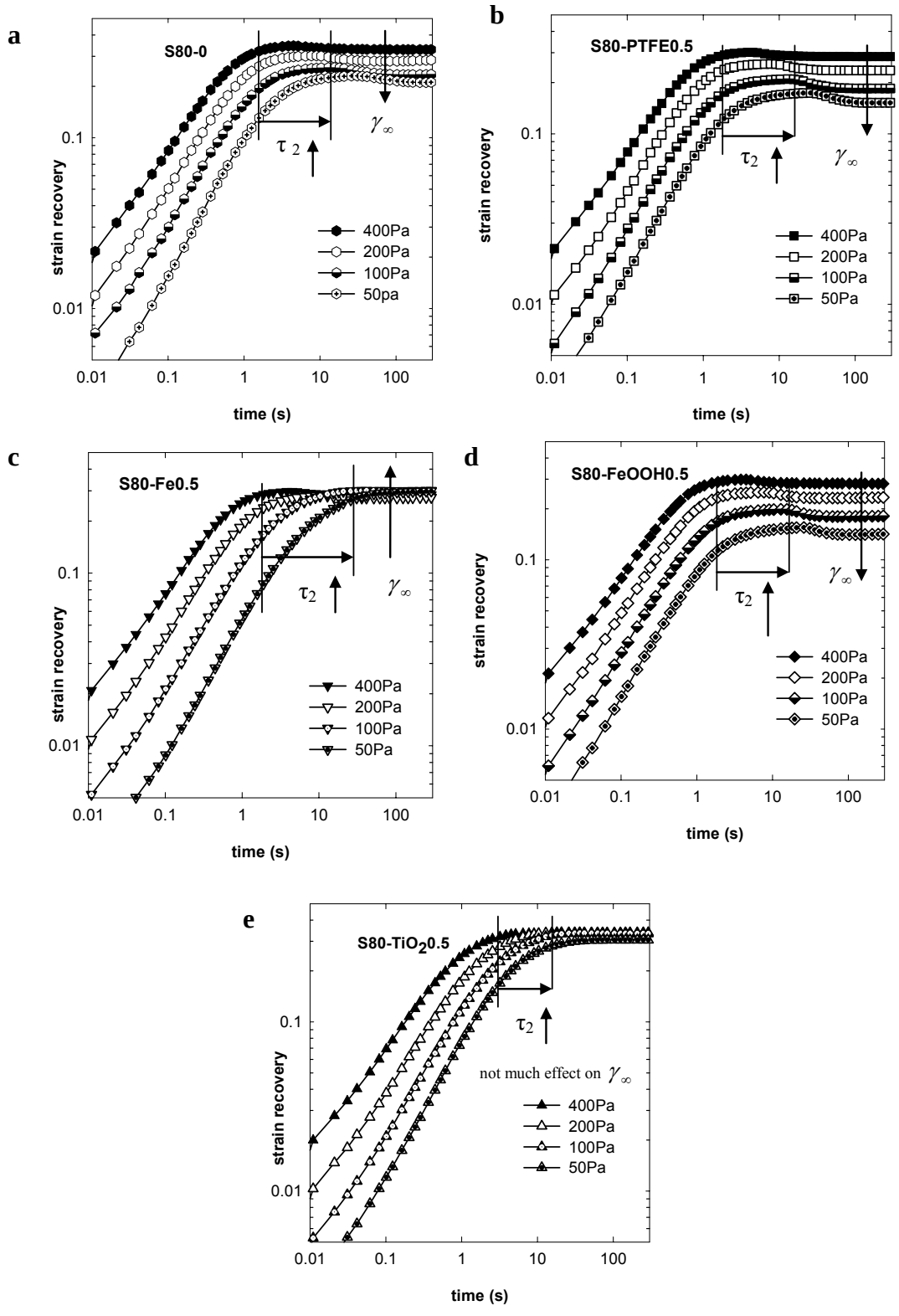

Figure 39. (a) Strain recovery (γ) versus time (s) for S80-0; (b) S80-PTFE0.5; (c) S80-Fe0.5; (d) S80-FeOOH0.5; (e) S80-$TiO_2$0.5.

The above trends of γ_∞ and τ_2 with decreasing stress are interpreted in terms of the morphological evolution of S20 and S80 blends, as discussed below.

Ultimate recovery (γ_∞): Quantitatively, S20-0 blend showed a decrease in γ_∞ with stress. Also, all particle types Fe, FeOOH and TiO_2 showed the same behavior as shown in Figure 40a. This suggests that the drops are able to coalesce with each other as the stress is lowered, but they are not able to increase in the same proportion as the decrease in stress. However, S20-PTFE0.5 blend showed a distinctly different behavior of increase in γ_∞ as the stress was lowered (Figure 40a), with γ_∞ values at low stress levels being much larger than all other S20 blends. This indicates that PTFE particles may be promoting coalescence of PDMS drops.

Similar to S20-0, S80-0 blends showed quantitatively a decrease in γ_∞ with stress. S80-PTFE0.5, S80-FeOOH0.5 also showed the same behavior as shown in Figure 40b. In contrast, S80-$TiO_2$0.5 blend showed a much higher γ_∞ than S80-0 blend, approximately independent of stress (Figure 40b). This is the case when increase in drop size fully "compensates" for the decrease in stress thus keeping Ca constant. S80-Fe0.5 blend showed an increase in γ_∞ as the stress was lowered which indicates that the drop size increases in a higher proportion than the decrease in stress, suggesting possible enhancement of coalescence (Figure 40b).

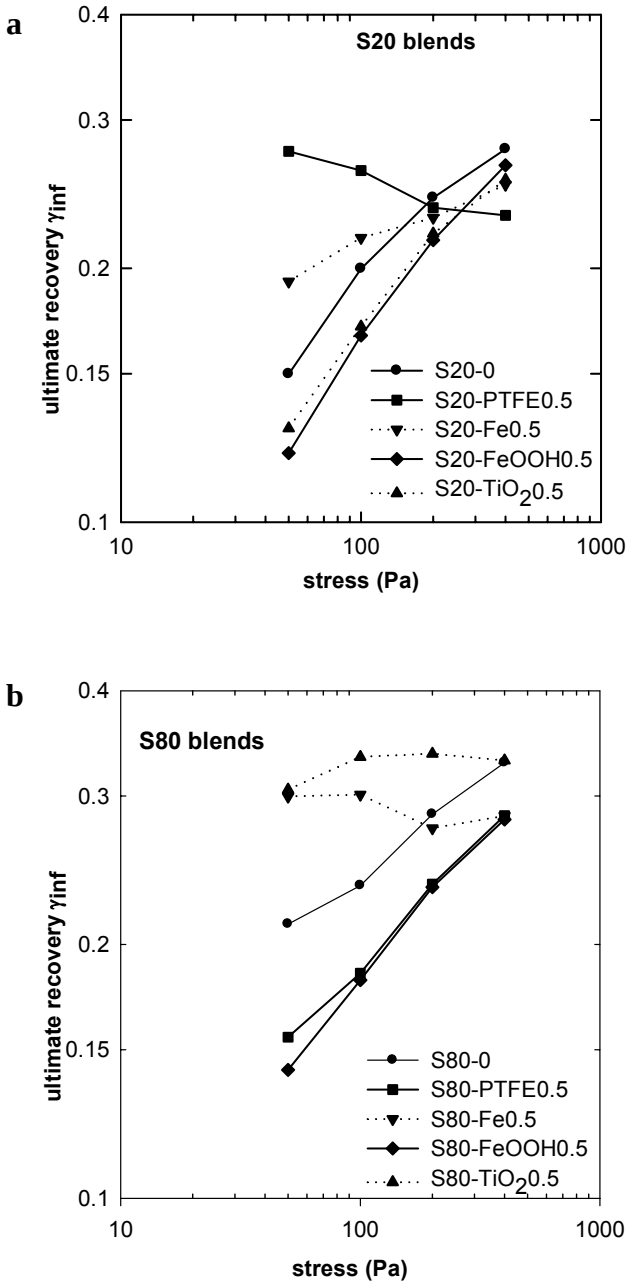

Figure 40. Variation of γ_{∞} with stress for (a) S20 blends and (b) S80 blends.

To further demonstrate that Fe and PTFE particles are possibly promoting coalescence in S20 and S80 blends respectively, the kinetics of recovery is presented. We have fitted the

recovered strain versus time data to a single exponential (Equation 30) by using both γ_∞ and τ_2 as the fitting parameters. The component contribution is subtracted from both S20 and S80 blends before the fitting, thus ensuring that the kinetics of recovery is governed solely by the retraction of the interface. Example of a typical fit to the exponential is shown in Figure 41. While the fit quality is not excellent for S20-PTFE0.5, the single exponential does capture some average retardation time. τ_2 versus stress data for both S20 and S80 blends are shown in Figure 42a and b.

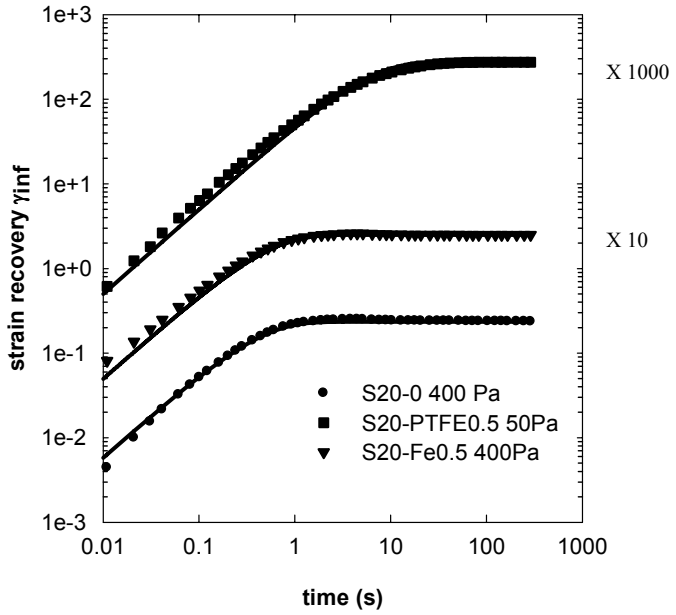

Figure 41. Good fit to single exponential for S20-0 and S20-Fe0.5 after 400 Pa and poor fit of S20-PTFEe0.5 after 50 Pa.

Kinetics of recovery: Figure 42a and b make the conclusions quantitative: three particle types (Fe, FeOOH and TiO_2) behave almost identically (quantitatively) to particle free S20-0 and show $\tau_2 \propto \sigma^{-0.6}$. S20-PTFE0.5 showed a much higher values for τ_2 than all other blends, especially at

50Pa stress level. This indicates that PTFE particles are causing the PDMS drops to coalesce much more rapidly with decreasing stress.

Similarly, PTFE, FeOOH behave identical to particle free S80 blends. S80-Fe0.5. S80-$TiO_2$0.5 blends show a larger τ_2 than all other blends, indicative of coalescence enhancement.

Finally, we comment on the fitting of the data to the single exponential- our fitting analysis shows that unlike particle free blends, the recovery kinetics of S20-PTFE0.5 blends does not fit perfectly to the exponential function with single retardation time at all stress levels. Similar behavior is shown by S80-Fe0.5 and S80-TiO_2 blends. We propose that this behavior of multiple retardation times might be attributable to the polydispersity of some of the particle laden blends.

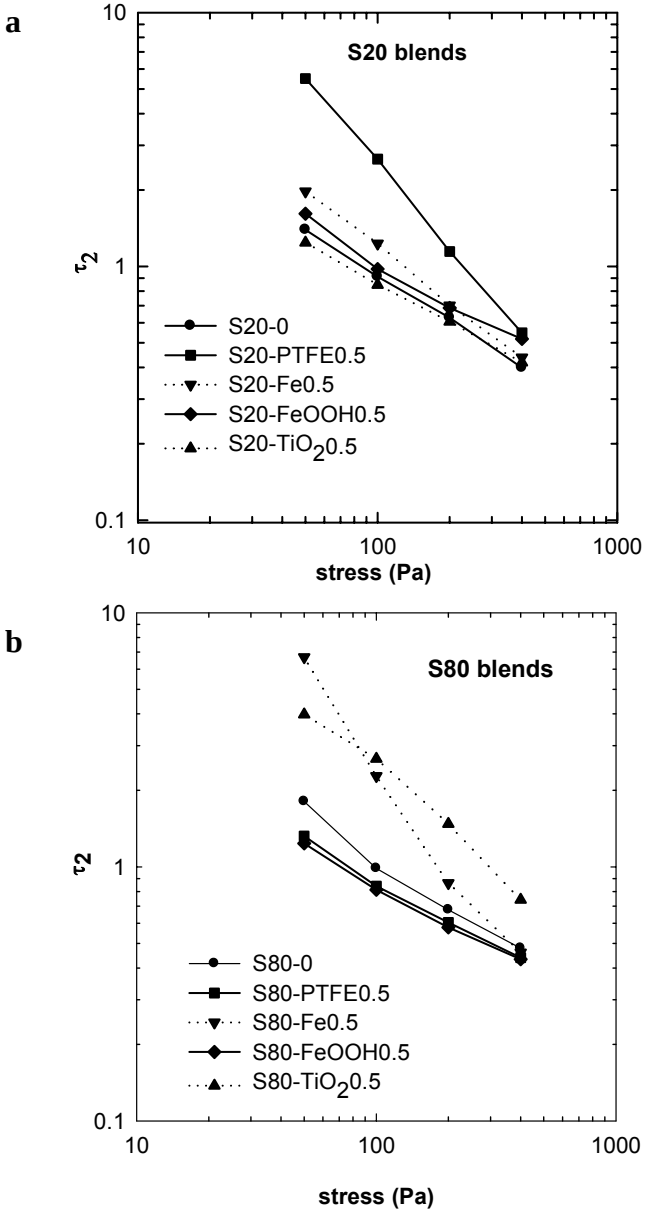

Figure 42. τ_2 versus stress: recovery kinetics for (a) S20 blends; (b) S80 blends.

Apart from the hypothesis of coalescence enhancement as the reason for a larger τ_2 for S20-PTFE0.5 and S80-Fe0.5 blends: irregular structures resulting from the jamming of interface

by particles can also lead to slow recovery kinetics. But such jamming can not explain a substantially larger γ_∞ for these particle types.

Thus from strain recovery data we infer that S20-PTFE0.5 sample shows a higher γ_∞ and τ_2 than S20-0 upon stepping down the stress, both indicating that addition of PTFE particles may be promoting coalescence in S20 blends. Here, other particle types Fe, FeOOH and TiO_2 do not seem to affect the coalescence of drops.

Similarly, S80-0.5Fe and S80-$TiO_2$0.5 samples show a higher γ_∞ and τ_2 than S80-0, both suggesting that addition of Fe particles may be promoting coalescence in S80 blends. The other particle types viz. PTFE and FeOOH do not seem to affect the coalescence of drops.

To summarize, our rheological results indicate that PTFE particles do not seem to have any effect on the coalescence of drops in S80 blends but are promoting coalescence in the S20 blend. Fe particles and TiO_2 may be promoting coalescence in S80 blends but have no effect in the inverted S20 blend. The remaining particles, FeOOH, do not affect the coalescence behavior.

To further substantiate the claim of coalescence promoting effect of Fe and PTFE in S20 and S80 blends respectively, we conducted flow visualization experiments in an optical shear cell.

6.2.2 Visualization

The blends were sheared between two parallel glass plates in a home built shear cell as described above. The aim of the visualization experiments was to directly test rheological indications that some particles promote coalescence. All the images were taken at a distance of 10 mm radially outwards from the center of the sample. All the samples were first sheared at a high shear rate of

2.7 s^{-1} for 2000 strain units and then the shear rate was lowered to 0.29 s^{-1} and the sample was given a total of 3000 strain units. The images obtained after shearing at a high shear rate were not very clear due to intense scattering caused by small drops.

The left column of Figure 43 presents micrographs of S20 blends after shearing at a high shear rate for 2000 strain units. The initial drop size is too small to quantify for S20-0 and S20-Fe0.5. However, S20-PTFE0.5 blends show a larger drop size after preshearing. Right column of Figure 43 shows micrographs after stepping down the shear rate. Coalescence occurs in all the blends, but is more prominent in S20-PTFE0.5 blends. This proves that PTFE particles promote the coalescence of PDMS drops in S20-PTFE0.5 blend. This is consistent with results of strain recovery experiments. In contrast, when Fe particles were added, there was coalescence of drops after 3000 strain units at low shear rates as shown in Figure 43f. But the drop size did not increase a lot. Moreover, the drop size remained more or less the same after 1000 strain units and 2000 strain units (not shown). This indicates a partial coalescence suppression of drop, although our rheological data do not suggest that coalescence is completely suppressed.

Similarly, Figure 44 (left column) shows the S80 blends after preshearing. Initial drop size was small, when sheared at high shear rate. After stepping down the shear rate, the drops coalesced in all cases. However, in the case of S80-Fe0.5, the drop size was observed to be larger in size than both S80-0 and S80-PTFE0.5. This indicates that to some extent Fe particles are promoting coalescence of drops. This observation is consistent with strain recovery data for S80-0.5Fe blend.

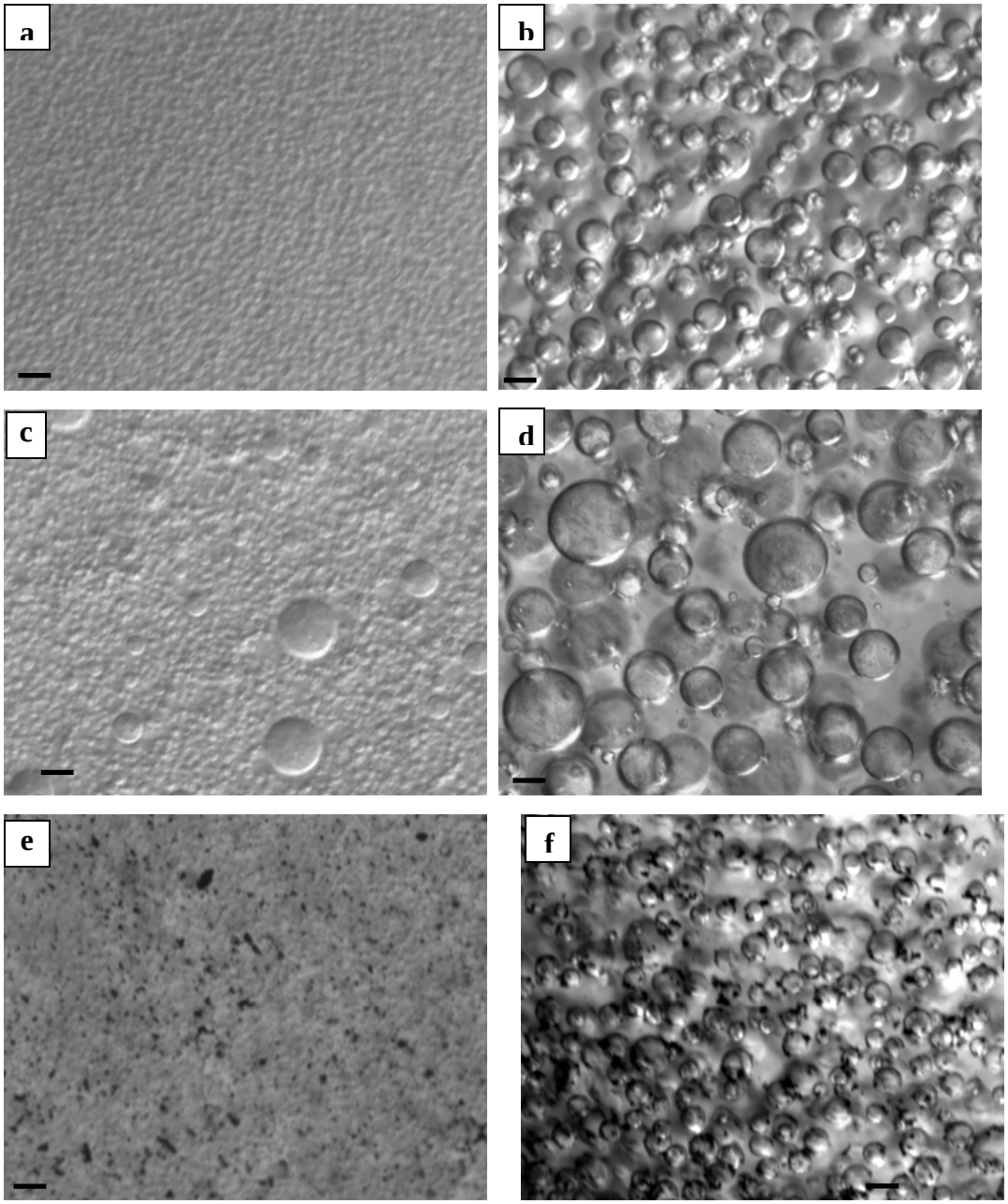

Figure 43. (a) and (b) S20-0; (c) and (d) S20-0.5PTFE; (e) and (f) S20-0.5Fe after preshearing and step down. All scalebars are 40 μm.

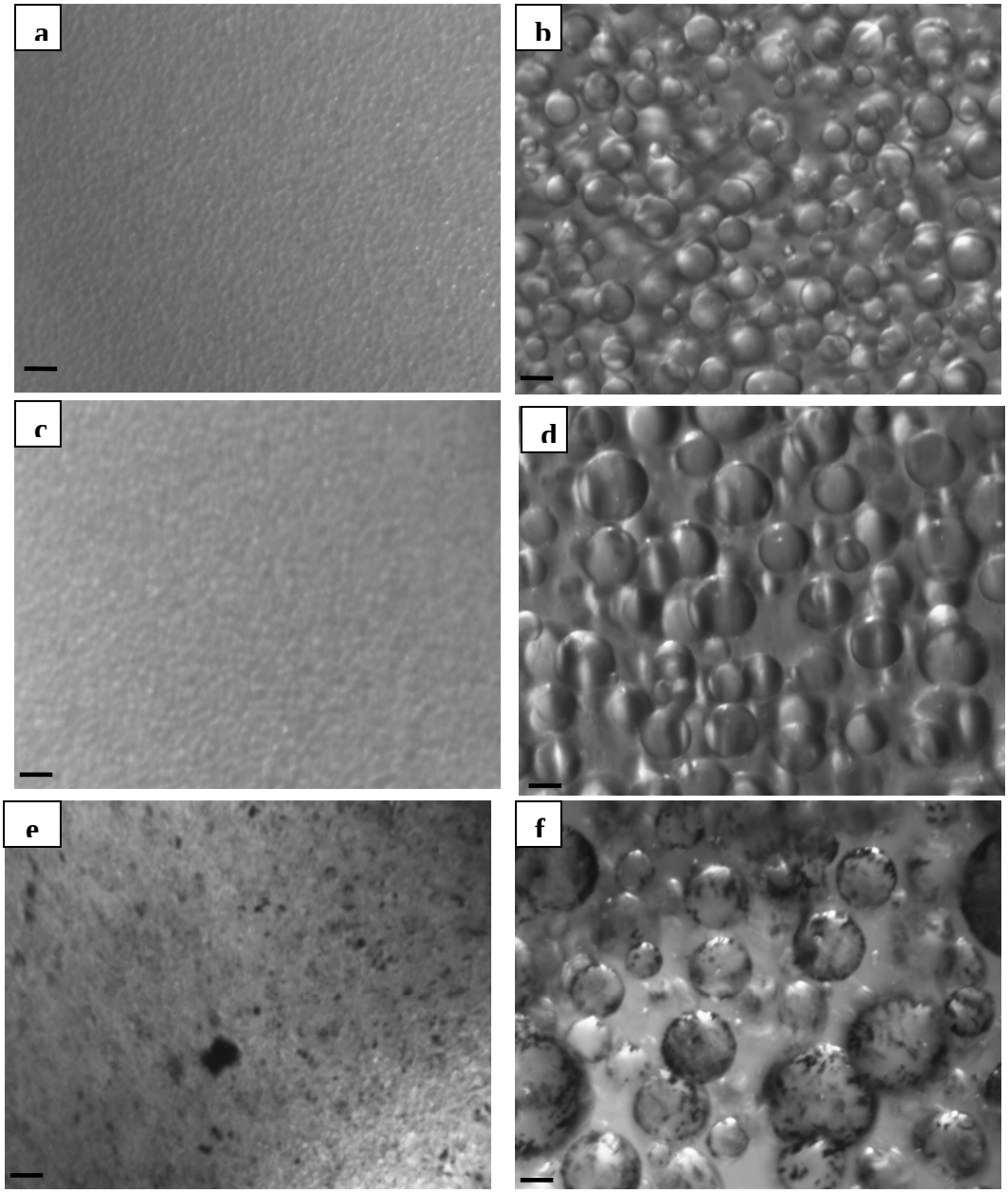

Figure 44. (a) and (b) S80-0; (c) and (d) S80-PTFE0.5; (e) and (f) S80-Fe0.5 after preshearing and step down. All scalebars are 40μm

The presence of different size drops which might be the reason for multiple retardation times in S20-PTFE0.5 and S80-Fe0.5 is evident in Figure 43d and Figure 44f respectively.

6.3 DISCUSSSION

The rheology and the visualization experiment results for all the particle laden blends are summarized in Table 5.

Table 5. Effect of particles on the drop size in S20 and S80 blends.

Blend	Coalescence behavior or effect on drop size
S20-PTFE0.5	Coalescence enhancement
S20-Fe0.5	May be suppression of coalescence
S20-FeOOH0.5	No effect
S20-$TiO_2$0.5	No effect
S80-PTFE0.5	No effect
S80-Fe0.5	Coalescence enhancement to some extent
S80-FeOOH0.5	No effect
S80-$TiO_2$0.5	No effect

The rheological data and the microscopic images both confirm that PTFE and Fe particles are promoting the coalescence drops in S20 and S80 blends respectively. A possible mechanism for PTFE particles promoting coalescence can be analogous to the bridging dewetting mechanism by hydrophobic particles for destabilization of aqueous foams. Here the particle are preferentially wetting towards the dispersed phase (i.e air). The particle bridging dewetting mechanism consists of following steps:

- A hydrophobic particle already adsorbed at an air-water interface comes in contact with another air water interface (Figure 45a).

- The particle forms an unstable bridge between two air-water interfaces (Figure 45b).
- If the particle is sufficiently hydrophobic, the water completely dewets the particle which makes two three phase contact lines coincide with each other (Figure 45c).This ultimately leads to perforation in the lamellar film and finally the foam collapses (Figure 45d).

This process is opposite of the stabilization mechanism of "bridging" where the particle is hydrophilic (preferentially wetting towards water), and is able to bridge two air-water interfaces together as shown in Figure 46a through d.

We think that a mechanism analogous to foam destabilization by particle dewetting can be responsible for coalescence promotion action of PTFE and Fe particles. Thus, we hypothesize that PTFE particles are preferentially wetted by PDMS, whereas Fe particles by PI.

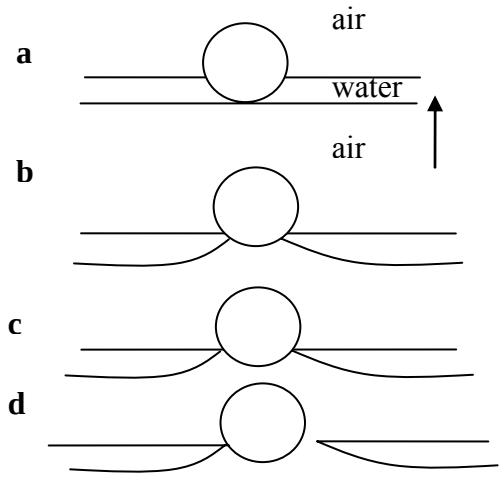

Figure 45. (a) Hydrophobic particle adsorbed at air-water interface, entering into another approaching air-water interface. (b) Particle bridging two air-water interfaces. (c) As the film thins hydrophobic particle is dewetted by water. (d) The particle detaches itself from the interface perforating the water film.

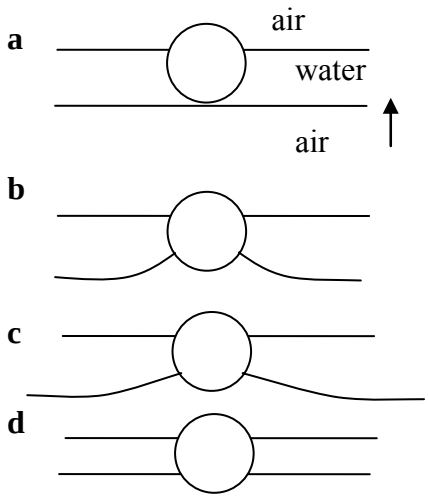

Figure 46. (a) Hydrophilic particle adsorbed at air-water interface with another air-water interface approaching from below. (b) The water film continues to thin. (c) The interface starts to flatten. (d) The hydrophilic particle bridges two air water interfaces.

6.4 LIMITATIONS OF THE EXPERIMENTS

The concentration of particles is chosen to be small to facilitate visualization experiments. Our experiments with 5 vol% of particles have shown to be very difficult to be observed optically. Also at 5 vol% particles the dynamic oscillatory data do not show a qualitative trend. Therefore, we believe that increasing the concentration of particles may be able to suppress coalescence, but at the same time it will not be experimentally convenient.

We have interpreted both qualitatively and quantitatively strain recovery and retardation time as indicators of drop coalescence. However, as mentioned above, some of the particle laden blends do not exhibit a single exponential recovery behavior. Thus, it is not clear how increase in retardation time can be interpreted only as the increase in drop coalescence.

6.5 CONCLUSIONS

To conclude, our rheological results suggest that at 0.5 vol% loading, particles used in this study (PTFE, Fe, FeOOH and TiO_2) are not able to act as compatibilizers i.e suppressing coalescence of drops in both S20 and S80 blends. This is supported qualitatively by our dynamic oscillatory data, where we report the shift in G' and $|\eta^*|$ shoulder to lower frequency in all cases. Quantitatively, strain recovery data support the idea that particles cannot suppress coalescence in S20 and S80 blends. Rheological data indicate that PTFE particles enhance coalescence of drops in S20 blends, whereas all other particle types have no effect. Microscopy studies support the enhancement of coalescence effect of PTFE particles in S20 blends. Moreover, rheologically Fe particles are shown to promote coalescence of PI drops to some extent in S80 blends, and all other particle types have no effect on the drop size. This is also confirmed by our *in situ* microscopic studies.

Our rheological experiments with 5 vol% loading of particles do not show qualitatively a clear trend of decrease/increase in strain recovery with stress for all particle types. Further, the recovery versus time data for some particle types, does not show leveling off behavior indicating a very slow recovery kinetics.

Finally, the observation that coalescence is enhanced by addition of certain particle types is consistent with the promotion of drop coalescence by hydrophobic OTS coated silica particles in polyethyleneoxide (PEO)/polyisobutylene (PIB) blends as discussed in chapter 4.

7.0 POLYMER FOAMS STABILIZED BY PARTICLES ADSORBED AT THE AIR/POLYMER INTERFACE[120]

So far we have discussed the adsorption of particles at fluid-fluid interfaces, such as polymer blends. We now shift gears from polymer-polymer interfaces to air/polymer interfaces, such as polymer foams. Polymer foams are commonly used for insulation, cushioning, or for reducing material usage, and hence the weight and cost of plastic parts. This chapter is restricted to closed-cell foams which are manufactured by generating gas bubbles in a liquid matrix (either a molten polymer or reacting monomers), and then solidifying the matrix so as to trap the gas bubbles.[121, 122] During the foaming process, the cell walls separating adjacent bubbles can rupture, causing cell coalescence, and eventually foam collapse. Stabilizing the polymer foam requires that the polymer matrix be solidified by vitrification (e.g. polystyrene foams), crosslinking (e.g. polyurethane foams), or crystallization (e.g. polyethylene foams); we are unaware of any polymer foams that remain stable for extended periods if the polymer matrix remains a liquid.

The situation is quite different in aqueous systems: common experience suggests a stable foam can be realized even from a fully-liquid system comprised of water and liquid surfactant. In this case, the surfactant adsorbs at the air/water interface causing effects such as Marangoni stresses, interfacial dilational elasticity, etc. which stabilize the foam. There have also been several recent examples of aqueous foams stabilized by partially-hydrophobic particles.[36, 39-41, 90, 123, 124] Such particles adsorb at the air/water interface and form a rigid shell ("armored

bubbles"[125]) that protects bubbles against coalescence. These effects are all interfacial in nature, i.e. unlike polymer foams, aqueous foams are stabilized by interfacial mechanisms. This immediately raises the question: is it possible to stabilize a polymeric foam by an interfacial mechanism? Here we will show that interfacially-adsorbed particles can indeed stabilize foams of polymers that cannot be foamed otherwise.

7.1 EXPERIMENTAL

7.1.1 Particle adsorption at air/polymer interfaces

A particle that is partially-wetted by a liquid can adsorb at the air/liquid interface. Interfacial adsorption of a large number of such particles can cause a monolayer to develop at the air/liquid interface, and the significant mechanical robustness of such a monolayer is then responsible for foam stabilization.[36, 39-41, 90, 123, 124] We have used polytetrafluoroethylene (PTFE) particles (Dyneon TE 9205; see Figure 47a) as foam stabilizing agents. The surface energy of the particles was measured by a "float-sink" test,[126] and estimated to be 25-28.5 mN/m. Two polymers were chosen for experiments (see Table 6 for details): polyisobutylene (PIB) which has a higher surface tension than the surface energy of the PTFE particles, and polydimethylsiloxane (PDMS) which has a lower surface tension than the surface energy of the PTFE particles.

Table 6. Homopolymers and their properties.

Polymer	Supplier	MW (kg/mol)	Viscosity (Pa.s)	Density (kg/m^3)	Surface tension mN/m
Polydimethylsiloxane (PDMS)	Rhodia	136	100 at 25°C	960	19.2
Polyisobutylene (PIB)	Soltex	2.4	333 at 25°C	910	32.1
Polystyrene (PS)	Eastman Chemical	1.3	170 at 85°C	1050	40.7[106]

A common rule of thumb is that solid particles will adsorb at an air/liquid interface if the surface energy (i.e. surface tension) of the liquid exceeds that of the solid particles.[127] Accordingly, we expect that the PTFE particles will adsorb at the air/PIB interface, but not at the air/PDMS interface.

To test these expectations, 5 wt% PTFE particles were dispersed into the two polymers by hand with a spatula, and the dispersions were degassed in vacuum. Visual observation of the degassed samples reveals a significant difference between the two samples. As expected, the PTFE-in-PDMS dispersion had a mirror-smooth surface typical of a liquid (Figure 47b) indicating that the PTFE particles were not adsorbed at the air/PDMS interface. In contrast, the surface of the PTFE-in-PIB dispersion (Figure 47c) appeared to have a "matte" texture because it was covered with adsorbed PTFE particles. We emphasize that the density of PTFE far exceeds that of *both* PIB as well of PDMS. Thus, the fact that particles are present at the air/PIB interface

but not at the air/PDMS interface cannot be attributed to buoyancy forces, and must be attributed to the differences in wettability: PDMS wets the particles fully, whereas PIB does not.

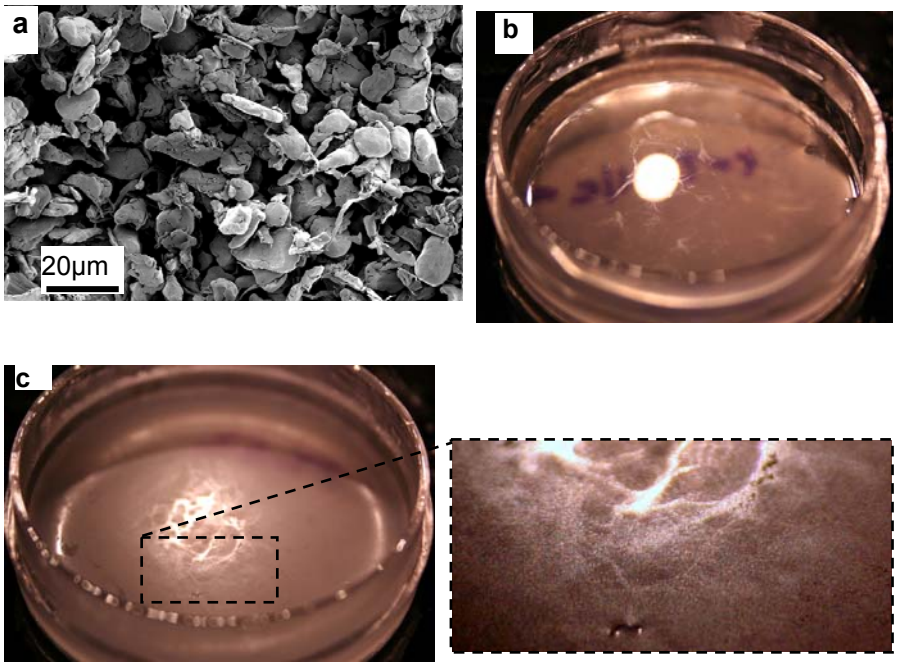

Figure 47. (a) SEM image of PTFE particles. (b) 5 wt% PTFE in PDMS dispersion shows a smooth surface. The white spot at the center of the petridish is the light source reflected from the air/PDMS surface. (c) 5 wt% PTFE in PIB dispersion shows a matte surface due to an adsorbed layer of particles. The matte texture is clearer in the inset.

7.1.2 Stable foams from liquid polymers

Based on the above results of particle adsorption, we hypothesized that the particles can stabilize a PIB foam, but not a PDMS foam. To foam the two polymers, a chemical blowing agent azobisformamide (ADC/L-C2 supplied by Lianda Corp.) was used. This blowing agent is available in the form of a powder of ~ 3 μm particles, and upon heating to approximately 200 °C, decomposes to release nitrogen. 0.2 wt% of the blowing agent was dispersed into the two

PTFE/polymer dispersions, and the resulting mixtures were charged to glass vials. The vials were suspended in an oil bath preheated to 180 °C, a temperature at which decomposition rate of the blowing agent is negligible. The temperature of the oil bath was then raised to 195 °C over 8 - 10 minutes to induce decomposition of the foaming agent.

In the case of the PTFE/PDMS dispersions, gas bubbles were observed to rise to the surface and burst, and hence – as expected – a stable foam was not realized. Figure 48a shows that not a single bubble survives at the end of the foaming process. In contrast, in the case of the PTFE/PIB dispersions, while the bubbles still rose to the top, they did not burst, but instead accumulated to form a stable foam (Figure 48b). We believe that as the gas bubbles rise upwards, PTFE particles adsorb on the surface of the bubbles. We hypothesize that early in the process, these adsorbed particles do not prevent coalescence, however, as coalescence proceeds, the interfacial concentration of particles grows sufficiently large that coalescence of bubbles is suppressed altogether. Upon cooling the PTFE/PIB foams to room temperature, contraction of the gas trapped in the bubbles caused the foams to shrink. Nevertheless, the foams did not collapse even after several months.

We have also repeated the above procedure with a dispersion of the blowing agent in PIB in the absence of PTFE particles. In this case, the gas bubbles escaped from the vial and stable foams were not realized.

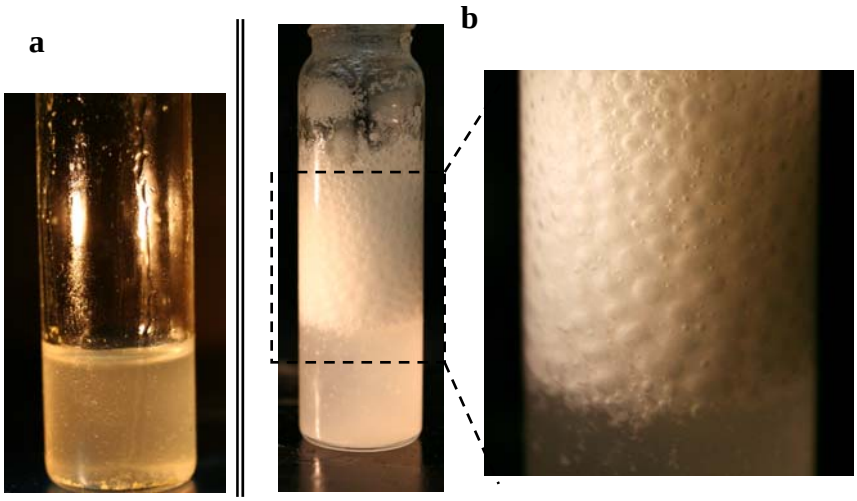

Figure 48. (a) PFTE/PIB dispersion after decomposition of blowing agent. No foam survives. (b) Stable foam of PTFE/PIB dispersion formed after decomposition of blowing agent. Note that (b) was taken after cooling to room temperature. Such cooling causes shrinkage (see text) and hence the foam volume in this image is less than that at the end of the foaming process.

7.2 PARTICLE-SCALE IMAGING: PARTICLE-STABILIZED FOAMS

Since the PIB and the PDMS are both liquid at room temperature, it is not possible to undertake a detailed characterization of the foams. In particular, it is not possible to conduct scanning electron microscopy (SEM) of the foams on the scale of single particles so as to directly examine the stabilizing monolayer. To enable SEM imaging, it is essential to realize particle-stabilized foams from a polymer that is solid at room temperature. We have selected polystyrene (PS) for these experiments: the surface tension of PS is ~ 40.7 mN/m at 20 °C,[106] and hence the rule of thumb cited in Section 7.1.1 suggests that PTFE particles should adsorb at the air/PS interface.

In order to maintain the experimental procedures as similar to the previous experiments as possible, a PS with a low molecular weight (see Table 6 for details) was selected. Due to its

low T_g (35 °C), this PS became a viscous liquid even at modest temperatures, and hence samples could be prepared by a procedure very similar to that used in the previous section: PTFE particles (either 0% or 5 wt%) and the blowing agent (0.2 wt%) were dispersed into the PS by hand-blending with a spatula at 75 °C, and cooled to room temperature. Chunks of the PS dispersions were placed in a vial and heated to 195 °C to decompose the foaming agent. The PS samples without PTFE did not give stable foams; the gas bubbles generated by decomposition of the blowing agent rose and escaped from the top surface of the sample. In contrast, a stable foam was realized from the PTFE/PS samples, furthermore, the foam did not collapse when the sample was maintained at 195 °C (i.e. with PS staying molten) for 5 minutes. In summary, the PTFE/PS system behaved similar to the PTFE/PIB system, but with the advantage that upon cooling to room temperature, a solid foam was obtained. Unfortunately, the solid foam was fragile and we were unable to recover it intact from the vial.

In order to facilitate recovery of the PTFE/PS foam, the foaming experiment was repeated with the inside of the vial covered in aluminum foil. Upon foaming and then cooling, the cylindrical sample of foam, still wrapped in aluminum foil, was successfully recovered from the vial, fractured, and examined under SEM. Figure 49a shows several bubbles embedded in the matrix. Higher magnification reveals that different bubbles have a wide range of particle coverages; for example, one of the bubbles in Figure 49b is heavily covered with particles, whereas the other is only sparsely covered. Figure 49c shows the particle-scale image of the inside of a foam bubble: it is clear that a portion of each particle is embedded in the PS phase, and the remainder emerges into the gas bubble. This strongly suggests that particle adsorption is indeed attributable to the partial wettability of the particles towards the polymer. The SEM

images also suggest that some PTFE particles are not adsorbed on the interface, but still remain in the bulk PS; we will comment on this at the end of this chapter.

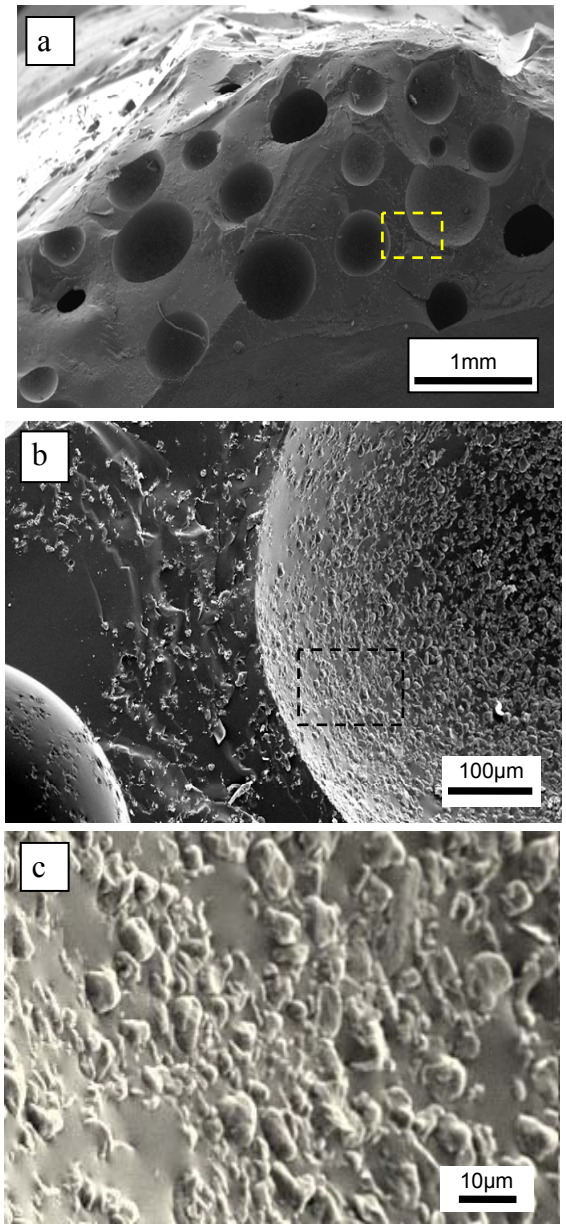

Figure 49. (a) SEM images of PS foams. The dotted rectangle from (a) is magnified in (b) The dotted black rectangle of (b) is magnified in (c).

7.3 DISCUSSION AND IMPLICATIONS

To summarize, the chief experimental observations are:

- None of the three polymers, PIB, PDMS, or PS could be foamed in the absence of added PTFE particles.
- Addition of PTFE particles led to PIB and PS foams. These foams were stable for extended periods even when the PIB or PS were maintained in the liquid state.
- Addition of PTFE particles did not lead to PDMS foams. This observation strongly supports the idea that the foam stabilization mechanism is interfacial in nature; if the particles do not adsorb at the air/polymer interface (as is the case with PDMS), they do not enhance foam stability.
- Particle-scale images of the PTFE/PS foams reveal foam bubbles coated with PTFE particles. There is a wide variation in particle coverage from one bubble to another.

The principal result of this chapter is that an otherwise non-foamable polymer may be foamed by addition of partially-wettable particles. Specifically, the partially-wettable particles can adsorb at the air/polymer interface and confer long-term stability on a polymer foam even when the polymer itself remains molten. This is of much relevance to preventing cell coalescence and foam collapse in practical foaming operations. For example, it is well-recognized that for successful foaming, a polymer must have sufficient melt elasticity. Some polymers, most notably linear polypropylene, have poor melt strength, and hence are difficult to foam due to severe cell coalescence during foaming.[122, 128-131] Accordingly, researchers have investigated the use of branched additives to modify the bulk rheology, e.g. increase the melt strength, and hence improve foamability.[129, 130, 132] This chapter shows that it is possible to use particulate additives for interfacial modification (rather than bulk rheology modification) to

achieve a similar effect. Furthermore, a possible advantage of this approach is that a low-surface energy additive such as PTFE is non-specific and may be an effective foam stabilizer in a wide variety of polymers. Our results are also relevant to specific polymer processing operations, e.g. rotational molding, in which the processed part must be maintained under melt conditions for extended periods. Incorporating foaming into such processes is challenging since foams can collapse if kept under molten conditions for extended periods.[133-135] In such situations as well, particulate additives offer a convenient method of improving the stability of the foam.

In the experiments described here, relatively large particles were used, and only at a modest particle loading of 5 wt%. Practical application of particles as foam stabilizers would likely involve smaller particles since (at a fixed weight loading) smaller particles are likely to have larger interfacial effects. We are presently examining the effect of particle size on foam properties. Furthermore, the SEM images of the PTFE/PS foams suggest that the bubble volume fraction is not very large, i.e. the foams have a relatively high mean density. Experiments in our laboratory are presently addressing this by increasing the concentration of the blowing agent.

Finally we note that while the focus of this chapter has been on the interfacial effects of added particles, it is well-recognized that particles can also affect the bulk rheology, especially if they can associate into a percolating network that can cause a yield stress. Such a yield stress would certainly contribute to bubble stability. In the present case, the overall particle loading is only 5 wt% (roughly 2.5 vol%), and hence at first glance, bulk rheological changes are not expected. Indeed in the three cases studied here, addition of 5 wt% PTFE particles caused no significant change in the rheology (as measured by a rotational rheometer). Nevertheless, the *overall* particle loading may underestimate the bulk rheological effect due to added particles. Specifically, in the two stable foam cases (PTFE/PIB and PTFE/PS) considered above, it is

possible that in the top part of the vial where the foam accumulates, the *local* particle concentration in the polymer films separating adjacent bubbles is larger than 5 wt %, and bulk rheological effects may be significant. Such bulk rheological changes may be responsible for the fact that the PTFE/PS foam was stable even though some bubbles appear to be only sparsely-covered with particles (Figure 49b). Thus, even if bulk effects are not the primary cause of foam stability, they may still be useful as an additional method to improve foam stability. Indeed there are reports[136-138] on foamed polymer nanocomposites showing that particles such as clay reduce cell sizes in polymer foams. These articles did not note interfacial adsorption of particles, and it may be the bulk rheological effect of added particles that causes foam stabilization.

8.0 FUTURE DIRECTIONS

8.1 DIRECT VERIFICATION OF THE BRIDGING-DEWETTING HYPOTHESIS

As discussed in chapter 6, we have been able to demonstrate both rheologically and microscopically that polytetrafluoroethylene (PTFE) particles are able to promote coalescence of drops in the case of polydimethylsiloxane (PDMS)-in-polyisoprene (PI) blends, and iron (Fe) particles are able to promote coalescence in the reverse system. We have also proposed that particle bridging dewetting is the mechanism for the coalescence promotion. To test the mechanism of bridging dewetting, we propose to verify whether Fe particles are preferentially wetted by PI and PTFE particles by PDMS. An alternative to using optical microscopy can be to use Scanning Electron Microscopy (SEM) to study the particle adsorption at the interface. But since both the polymers PI and PDMS are molten at room temperature, a conventional SEM of particle laden PI/PDMS blends is not possible. Due to this limitation, we recommend using a "crosslinkable" polymer blend system, where the dispersed phase can first be crosslinked and then retrieved after particle adsorption. The particle laden crosslinked dispersed phase can then be studied under the SEM. We propose to use a system which can be crosslinked (cured) under an ultraviolet (UV) radiation to minimize the possibility of contamination. The PI used in our previous research is not observed to be crosslinkable under UV radiation, therefore we have used a chemically different PI. However, the current UV curable PI may not have the same wettability

as the one used in chapters 6. Thus, our final goal is to crosslink the same PI which we have used in our previous rheological and microscopy experiments.

Some preliminary results with UV curable PI are presented below in section 8.2.2. The experimental results in this section demonstrate that particle adsorption can be studied using SEM. Nevertheless, further improvements in the blend system and experimental protocol will be required.

8.2 UV CURABLE POLYISOPRENE/POLYDIMETHYLSILOXANE (PI/PDMS) BLENDS

To verify whether a mechanism analogous to bridging dewetting is responsible for the coalescence promotion effect of Fe and PTFE particles by SEM, we propose to perform the following experiment as shown in Figure 50. For bridging dewetting mechanism to be active, we expect to observe Fe and PTFE particles either inside the PI and PDMS drops or adsorbed on the interior surface of the drops as shown in Figure 50. PI/PDMS cases (i.e. when the drops are crosslinked) can then be examined by SEM.

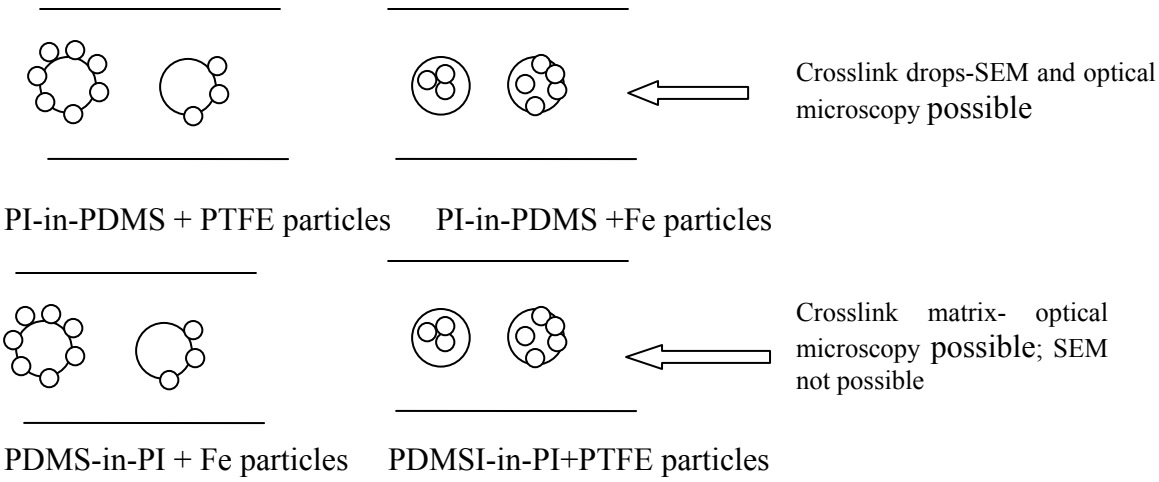

Figure 50. Schematic of experiments proposed to verify the bridging dewetting mechanism of PTFE and Fe particles.

The materials and experimental procedure followed to perform above experiments are described below.

8.2.1 Materials

UV crosslinkable PI was used, supplied by Septon Rubber Company with a trade name of UC 105. We have designated it as UVPI in the sections below. Benzophenone was used as a photo initiator.

8.2.2 Sample preparation

A blend of UVPI and 2 wt% benzophenone (photo initiator) was first prepared. The appropriate amount of benzophenone (BP) was dissolved in methylene chloride and was then added to UVPI to homogeneously disperse BP in UVPI. After this the methylene chloride was evaporated.

Similar to chapter 6, blends with 20 wt% of UVPI and PDMS were first prepared and then poured on top of 0.5 vol% Fe particles. The blend was prepared by hand mixing using a plastic spatula. After degassing the blend, it was sandwiched between two Mylar sheets separated by a spacer of 0.5 mm. The sandwiched blend was sheared very slowly in the rheometer. After slow shearing for 3 hours, the sandwiched blend was recovered from the rheometer without disturbing the morphology. The Mylar sandwiched blend was then cured under UV for 1 hour to allow the crosslinking of UVPI drops. After removal of the top Mylar sheet, the blend with crosslinked UVPI drops on the bottom Mylar sheet was held vertical in a beaker and the sample was collected at the bottom. An optical image of Fe particle containing UVPI-in-PDMS blend is shown in Figure 51a.

A small amount of blend was then placed on a filter paper and hexane was dripped on the paper to wash away the PDMS, leaving behind spherical, particle-laden crosslinked drops on the filter paper. The SEM micrograph of such crosslinked UVPI drops is shown below in Figure 51b. As shown in Figure 51c and d, the spherical UVPI drops have a smooth surface and do not have many particles. However, the optical micrographs show the presence of numerous particles in the middle of drops. This indicates that although some particles are adsorbed towards the inside surface of the drop, the majority of the particles are inside the drops. However, as mentioned before, the crosslinkable UVPI might have a different wettability than the PI which we have used in our rheology and microscopy experiments.

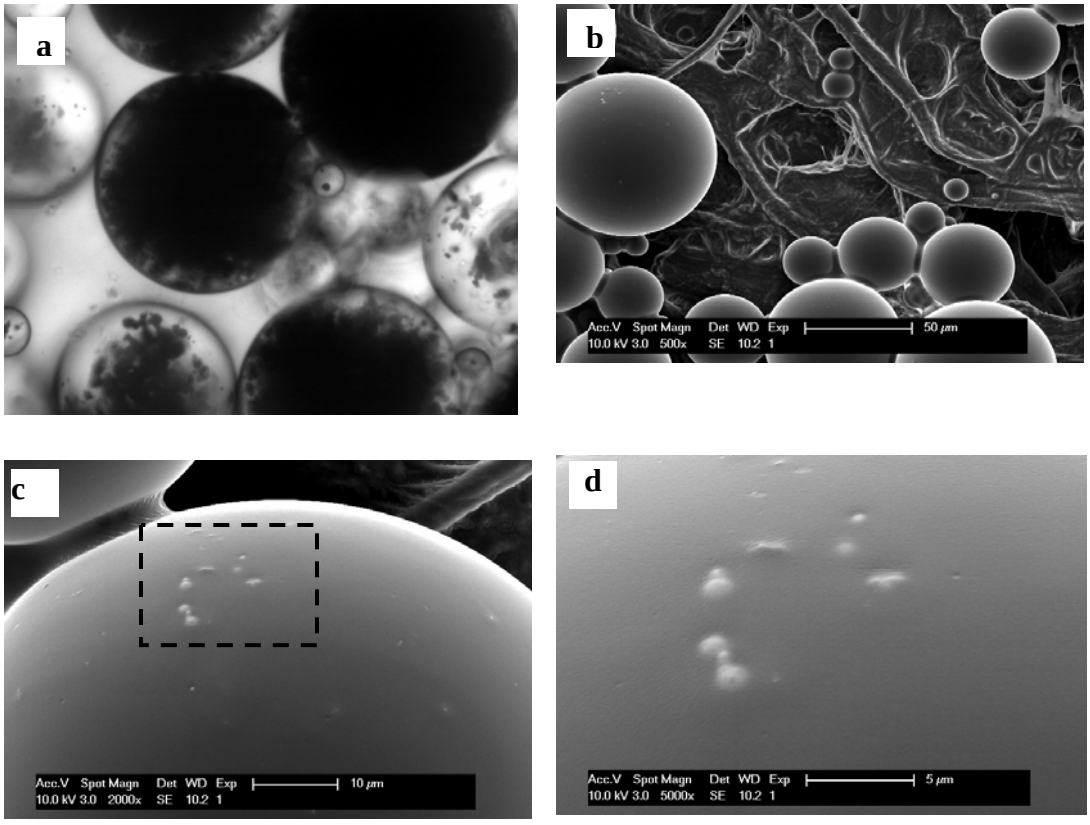

Figure 51. (a) Optical image of Fe particles. (b) SEM micrograph of Fe containing UVPI-in-PDMS blends. (c) Fe particles adsorbed on the inside surface of the drops. (d) High magnification SEM image of Fe particles.

Similar to Fe particles containing UVPI-in-PDMS blends, PTFE particles containing UVPI-in-PDMS blends were prepared and the crosslinked UVPI drops were recovered. An SEM image of these drops is shown below in Figure 52a and b. As shown in Figure 52b, PTFE particles are preferentially wetting towards PDMS.

It should be noted that an SEM image of PTFE particle laden PDMS-in-UVPI is not possible as PDMS drops are molten at room temperature. Therefore, a blend of PDMS drops in UVPI containing PTFE particles was prepared and sandwiched between two Mylar sheets with a 0.5 mm spacer. This sandwiched blend sample was then sheared very slowly for 3 hours in the rheometer, to facilitate the adsorption of PTFE particles at the interface. The sample was then

cured under UV radiation for 1 hour. The thin film of the blend was then recovered and observed under a microscope at a magnification of 60x. As shown in image below (Figure 52c), PTFE particles are clearly visible inside the PDMS drops. The optical images together with the SEM micrographs support the hypothesis that due to the preferential wettability of PTFE particles towards PDMS, the particles prefer to go inside the drops in the case of PTFE laden PDMS-in-UVPI blends. Therefore PTFE particles can promote coalescence of PDMS drops by bridging dewetting, analogous to hydrophobic particles destabilizing aqueous foam. Once again we reiterate that the chemical differences between PI and UVPI make these results strictly valid only for UVPI/PDMS blends.

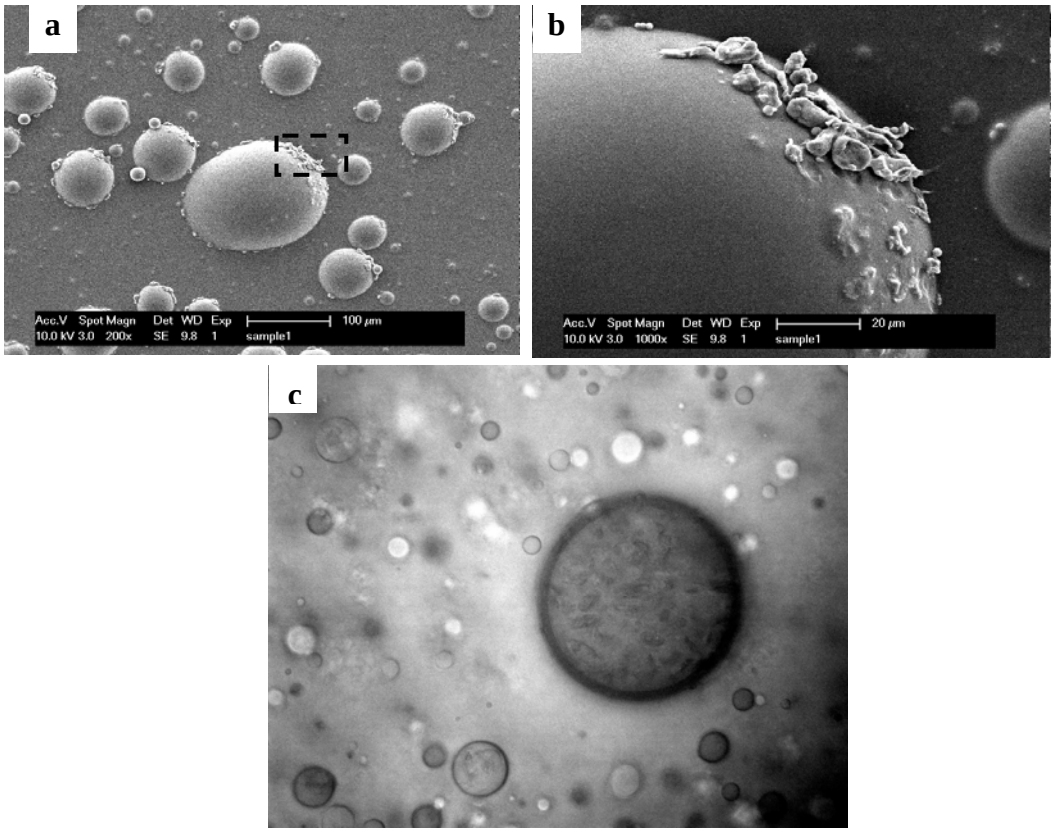

Figure 52. (a) SEM micrographs showing PTFE containing UVPI/PDMS blend. (b) PTFE particles preferentially wetted by PDMS. (c) PTFE particles inside the PDMS drops in PDMS-in-UVPI blends**.**

8.3 FOAMS STABILIZED BY FIBERS

We have already demonstrated in chapter 7 that polymer polystyrene (PS) and polyisobutylene (PIB) foams can be stabilized by PTFE particles. Similar to PTFE particles, low surface energy fibers such as polypropylene may be used to stabilize foams. In contrast to PTFE particles, fibers can entangle with each other forming a closely knit mesh, which may result in the formation of a rigid shell around the air bubbles. This may impart stability to the foam even when the loading of fibers is low. Moreover, even in the absence of the interfacial activity of the fibers at the air/polymer interface, the entanglements of the fibers in the bulk polymer may be strong enough to increase the viscosity of the polymer manifold, thus enhancing the stability of the foams.

8.4 CARBON NANOTUBES AT FLUID-FLUID INTERFACE

Carbon nanotubes (CNs) are reported to be excellent conductors and can have current densities much higher than metals like silver and copper. If these carbon nanotubes were able to adsorb at fluid-fluid interface in an emulsion and consequently form a drop network via bridging, then a conductive pathway may be formed through the emulsion. We also believe that this drop bridging via carbon naotubes will reduce their percolation threshold. A system to test the interfacial adsorption of CNs can be polyethyleneoxide/polyisobutylene (PEO/PIB) emulsion. As discussed in chapter 4, PEO/PIB emulsions are polymeric analogs of low viscosity oil/water emulsions. Since high molecular weight PEO is a crystalline solid at room temperature, this system offers an advantage of performing the experiments at high temperature when the system is molten, and then rapidly freezing the morphology. In context of particle laden blends, the

morphology can be studied by recovering solid particle laden PEO drops and observing it under the Scanning Electron Microscope. We suggest using carbon nanotubes in the PEO/PIB blends to see if they at all are able to reach at the interface and cause bridging. We do not suggest any rheological studies but instead seek to demonstrate by Scanning Electron Microscopy that carbon nanotubes can adsorb on PEO drops at all, and to see if a shell like structure is formed around the PEO drops similar to the studies reported by *Panhuis et al.*[139] in oil/water systems.

8.5 POLYISOPRENE/POLYDIMETHYLSILOXANE (PI/PDMS) BLENDS WITH IRON PARTICLES

The dispersion of iron particles (used in our previous research, refer to chapter 5 and 6) dispersed in a low dielectric fluid such as PDMS is expected to be conductive due to the presence of iron particles.

We have already observed the interfacial adsorption of iron particles in PI/PDMS blends. We think that if these PI drops are tightly covered by iron particles, this blend will have a higher conductivity than the particle suspension. This will be due to an overall increase in the hydrodynamic volume of the dispersed iron particles, from their adsorption at the PI/PDMS interface. The micrographs of a dispersion of iron particles in PDMS is shown below in Figure 53a. The image on the right shows a blend of 2 wt% PI drops, 4 wt% iron particles and PDMS. Iron particles are shown to adsorb at the interface (Figure 53b). PI drops appear completely black due to the tight coverage of the surface by iron particles after shearing for one day (Figure 53c).

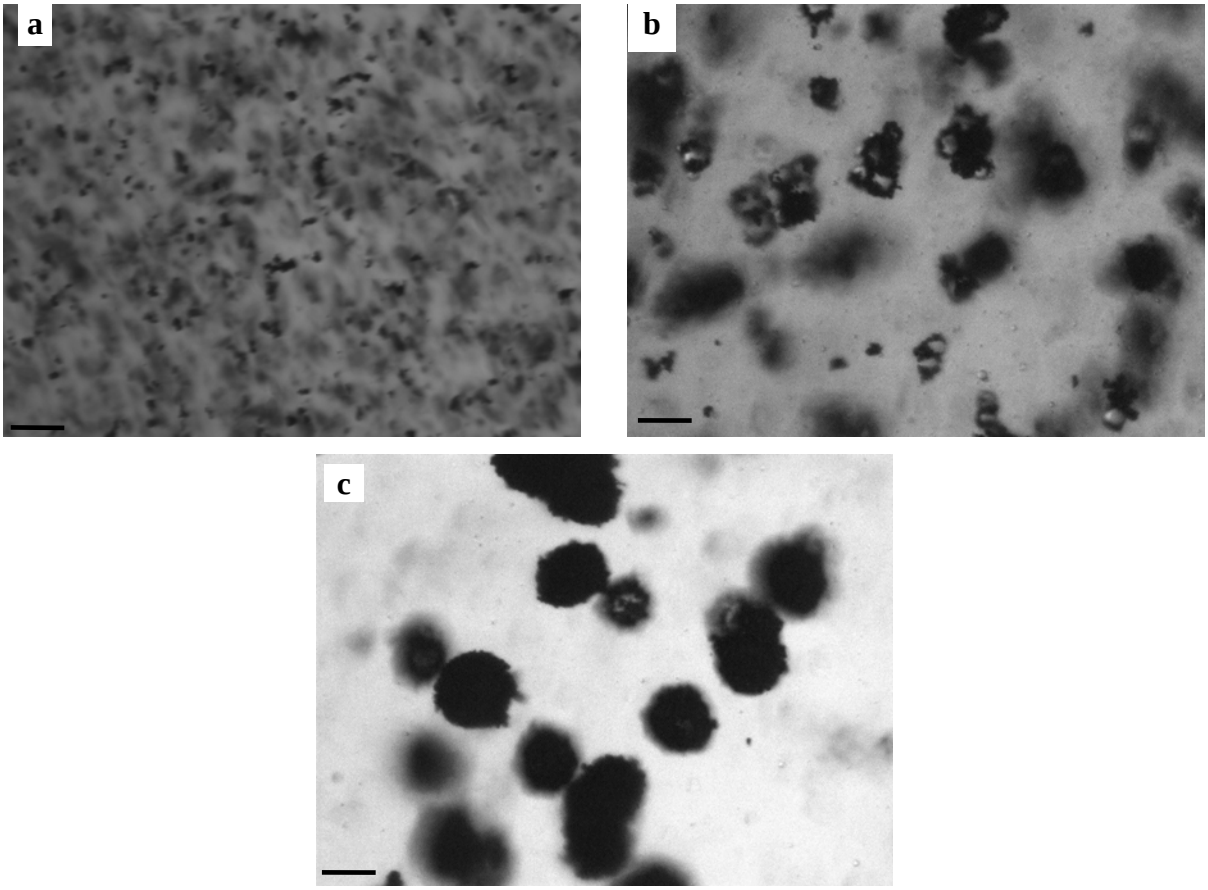

Figure 53. (a) PDMS containing 4 wt% of Fe particles. (b) PI-in-PDMS blends containing Fe particles after 2hrs of shearing and (c) after 1 day of shearing. All scalebars are 40 μm.

Furthermore, if these particles covered drops are made to align among themselves under the influence of an external electric field, we expect to see a further enhancement of conductivity.

BIBLIOGRAPHY

1. Ramsden, W., Separation of solids in the surface layers of solutions and suspensions (Observations on surface membranes, bubbles, emulsions and mechaniical coagulation).- Preliminary Account. *Proc. Roy. Soc.Lond.Ser.A* **1903,** 72, 156.

2. Tambe, D. E.; Sharma, M. M., The Effect of Colloidal Particles on Fluid-Fluid Interfacial Properties and Emulsion Stability. *Advances in Colloid and Interface Science* **1994,** 52, 1-63.

3. Binks, B. P., Particles as surfactants - similarities and differences. *Current Opinion in Colloid & Interface Science* **2002,** 7, (1-2), 21-41.

4. Pickering, S. U., Emulsions. *J. Chem. Soc* **1907,** 91, 2001.

5. Ashby, N. P.; Binks, B. P., Pickering emulsions stabilised by Laponite clay particles. *Physical Chemistry Chemical Physics* **2000,** 2, (24), 5640-5646.

6. Fujii, S.; Okada, M.; Furuzono, T., Hydroxyapatite nanoparticles as stimulus-responsive particulate emulsifiers and building block for porous materials. *Journal of Colloid and Interface Science* **2007,** 315, (1), 287-296.

7. Stiller, S.; Gers-Barlag, H.; Lergenmueller, M.; Pflucker, F.; Schulz, J.; Wittern, K. P.; Daniels, R., Investigation of the stability in emulsions stabilized with different surface modified titanium dioxides. *Colloids and Surfaces a-Physicochemical and Engineering Aspects* **2004,** 232, (2-3), 261-267.

8. Yang, F.; Liu, S. Y.; Xu, J.; Lan, Q.; Wei, F.; Sun, D. J., Pickering emulsions stabilized solely by layered double hydroxides particles: The effect of salt on emulsion formation and stability. *Journal of Colloid and Interface Science* **2006,** 302, (1), 159-169.

9. Wang, W. X.; Zhou, Z.; Nandakumar, K.; Xu, Z. H.; Masliyah, J. H., Effect of charged colloidal particles on adsorption of surfactants at oil-water interface. *Journal of Colloid and Interface Science* **2004,** 274, (2), 625-630.

10. Shen, S. L.; Wu, W.; Guo, K.; Meng, H.; Chen, J. F., A novel process to synthesize magnetic hollow silica microspheres. *Colloids and Surfaces a-Physicochemical and Engineering Aspects* **2007,** 311, (1-3), 99-105.

11. Melle, S.; Lask, M.; Fuller, G. G., Pickering emulsions with controllable stability. *Langmuir* **2005,** 21, (6), 2158-2162.

12. Binks, B. P.; Clint, J. H.; Mackenzie, G.; Simcock, C.; Whitby, C. P., Naturally occurring spore particles at planar fluid interfaces and in emulsions. *Langmuir* **2005,** 21, (18), 8161-8167.

13. Andresen, M.; Stenius, P., Water-in-oil emulsions stabilized by hydrophobized microfibrillated cellulose. *Journal of Dispersion Science and Technology* **2007,** 28, (6), 837-844.

14. Horozov, T. S.; Aveyard, R.; Clint, J. H.; Binks, B. P., Order-disorder transition in monolayers of modified monodisperse silica particles at the octane-water interface. *Langmuir* **2003,** 19, (7), 2822-2829.

15. Pieranski, P., Two Dimensional Interfacial Colloidal Crystals. *Physical Review Letters* **1980,** 45, (7), 569-572.

16. Horozov, T. S.; Aveyard, R.; Binks, B. P.; Clint, J. H., Structure and stability of silica particle monolayers at horizontal and vertical octane-water interfaces. *Langmuir* **2005,** 21, (16), 7405-7412.

17. Kralchevsky, P. A.; Paunov, V. N.; Ivanov, I. B.; Nagayama, K., Capillary Meniscus Interaction between Colloidal Particles Attached to a Liquid-Fluid Interface. *Journal of Colloid and Interface Science* **1992,** 151, (1), 79-94.

18. M.G Nikolaides, A. R. B., M.F Hsu, A.D. Dinsmore, M.P Brenner, C.Gay & D.A Weitz, Electric Field induced capillary attraction between like charged particles at liquid interfaces. *letters to nature* **2002,** 420, 299-301.

19. Aveyard, R.; Clint, J. H.; Nees, D.; Quirke, N., Structure and collapse of particle monolayers under lateral pressure at the octane/aqueous surfactant solution interface. *Langmuir* **2000,** 16, (23), 8820-8828.

20. Xu, H.; Lask, M.; Kirkwood, J.; Fuller, G., Particle bridging between oil and water interfaces. *Langmuir* **2007,** 23, (9), 4837-4841.

21. Stancik, E. J.; Widenbrant, M. J. O.; Laschitsch, A. T.; Vermant, J.; Fuller, G. G., Structure and dynamics of particle monolayers at a liquid-liquid interface subjected to extensional flow. *Langmuir* **2002,** 18, (11), 4372-4375.

22. Finkle, P.; Draper, H. D.; Hildebrand, J. H., The theory of emulsification. *Journnal of American Chemical Society* **1923,** 45, 2780-2788.

23. Binks, B. P.; Lumsdon, S. O., Influence of particle wettability on the type and stability of surfactant-free emulsions. *Langmuir* **2000,** 16, (23), 8622-8631.

24. Binks, B. P.; Whitby, C. P., Silica particle-stabilized emulsions of silicone oil and water: Aspects of emulsification. *Langmuir* **2004,** 20, (4), 1130-1137.

25. Arditty, S.; Whitby, C. P.; Binks, B. P.; Schmitt, V.; Leal-Calderon, F., Some general features of limited coalescence in solid-stabilized emulsions. *European Physical Journal E* **2003,** 11, (3), 273-281.

26. Bechhold, H.; Dede, L.; Reiner, L., Dreiphasige Emulsionen. *Kolloid, Zeit* **1921,** 28, (6).

27. Binks, B. P.; Lumsdon, S. O., Pickering emulsions stabilized by monodisperse latex particles: Effects of particle size. *Langmuir* **2001,** 17, (15), 4540-4547.

28. Binks, B. P.; Lumsdon, S. O., Effects of oil type and aqueous phase composition on oil-water mixtures containing particles of intermediate hydrophobicity. *Physical Chemistry Chemical Physics* **2000,** 2, (13), 2959-2967.

29. Stancik, E. J.; Kouhkan, M.; Fuller, G. G., Coalescence of particle-laden fluid interfaces. *Langmuir* **2004,** 20, (1), 90-94.

30. Stancik, E. J.; Fuller, G. G., Connect the drops: Using solids as adhesives for liquids. *Langmuir* **2004,** 20, (12), 4805-4808.

31. Ashby, N. P.; Binks, B. P.; Paunov, V. N., Bridging interaction between a water drop stabilised by solid particles and a planar oil/water interface. *Chemical Communications* **2004**, (4), 436-437.

32. Horozov, T. S.; Aveyard, R.; Clint, J. H.; Neumann, B., Particle zips: Vertical emulsion films with particle monolayers at their surfaces. *Langmuir* **2005,** 21, (6), 2330-2341.

33. Vignati, E.; Piazza, R.; Lockhart, T. P., Pickering emulsions: Interfacial tension, colloidal layer morphology, and trapped-particle motion. *Langmuir* **2003,** 19, (17), 6650-6656.

34. Horozov, T. S.; Binks, B. P., Particle-stabilized emulsions: A bilayer or a bridging monolayer? *Angewandte Chemie-International Edition* **2006,** 45, (5), 773-776.

35. Ian D. Morrison, S. R., *Colloidal dispersions , suspensions, emulsions and Foams*. Wiley Interscience: 2002.

36. Fujii, S.; Iddon, P. D.; Ryan, A. J.; Armes, S. P., Aqueous particulate foams stabilized solely with polymer latex particles. *Langmuir* **2006,** 22, (18), 7512-7520.

37. Gonzenbach, U. T.; Studart, A. R.; Tervoort, E.; Gauckler, L. J., Stabilization of foams with inorganic colloidal particles. *Langmuir* **2006,** 22, (26), 10983-10988.

38. Subramaniam, A. B.; Abkarian, M.; Mahadevan, L.; Stone, H. A., Mechanics of interfacial composite materials. *Langmuir* **2006,** 22, (24), 10204-10208.

39. Binks, B. P.; Horozov, T. S., Aqueous foams stabilized solely by silica nanoparticles. *Angewandte Chemie-International Edition* **2005,** 44, (24), 3722-3725.

40. Alargova, R. G.; Warhadpande, D. S.; Paunov, V. N.; Velev, O. D., Foam superstabilization by polymer microrods. *Langmuir* **2004,** 20, (24), 10371-10374.

41. Dickinson, E.; Ettelaie, R.; Kostakis, T.; Murray, B. S., Factors controlling the formation and stability of air bubbles stabilized by partially hydrophobic silica nanoparticles. *Langmuir* **2004,** 20, (20), 8517-8525.

42. Ray, S. S.; Okamoto, M., Polymer/layered silicate nanocomposites: a review from preparation to processing. *Progress in Polymer Science* **2003,** 28, (11), 1539-1641.

43. Ray, S. S.; Pouliot, S.; Bousmina, M.; Utracki, L. A., Role of organically modified layered silicate as an active interfacial modifier in immiscible polystyrene/polypropylene blends. *Polymer* **2004,** 45, (25), 8403-8413.

44. Xing, P. X.; Bousmina, M.; Rodrigue, D.; Kamal, M. R., Critical experimental comparison between five techniques for the determination of interfacial tension in polymer blends: Model system of polystyrene/polyamide-6. *Macromolecules* **2000,** 33, (21), 8020-8034.

45. Hong, J. S.; Kim, Y. K.; Ahn, K. H.; Lee, S. J.; Kim, C., Interfacial tension reduction in PBT/PE/clay nanocomposite. *Rheologica Acta* **2007,** 46, (4), 469-478.

46. Palierne, J. F., Linear Rheology of viscoleastic emulsions with interfacial tension. *Rheologica Acta* **1991,** 29, 204-214.

47. Hong, J. S.; Namkung, H.; Ahn, K. H.; Lee, S. J.; Kim, C., The role of organically modified layered silicate in the breakup and coalescence of droplets in PBT/PE blends. *Polymer* **2006,** 47, (11), 3967-3975.

48. Si, M.; Araki, T.; Ade, H.; Kilcoyne, A. L. D.; Fisher, R.; Sokolov, J. C.; Rafailovich, M. H., Compatibilizing bulk polymer blends by using organoclays. *Macromolecules* **2006,** 39, (14), 4793-4801.

49. Sumita, M.; Sakata, K.; Hayakawa, Y.; Asai, S.; Miyasaka, K.; Tanemura, M., Double Percolation Effect on the Electrical-Conductivity of Conductive Particles Filled Polymer Blends. *Colloid and Polymer Science* **1992,** 270, (2), 134-139.

50. Gubbels, F.; Jerome, R.; Teyssie, P.; Vanlathem, E.; Deltour, R.; Calderone, A.; Parente, V.; Bredas, J. L., Selective Localization of Carbon-Black in Immiscible Polymer Blends - a Useful Tool to Design Electrical Conductive Composites. *Macromolecules* **1994,** 27, (7), 1972-1974.

51. Gubbels, F.; Jerome, R.; Vanlathem, E.; Deltour, R.; Blacher, S.; Brouers, F., Kinetic and thermodynamic control of the selective localization of carbon black at the interface of immiscible polymer blends. *Chemistry of Materials* **1998,** 10, (5), 1227-1235.

52. Soares, B. G.; Gubbels, F.; Jerome, R.; Teyssie, P.; Vanlathem, E.; Deltour, R., Electrical-Conductivity in Carbon Black-Loaded Polystyrene-Polyisoprene Blends - Selective Localization of Carbon-Black at the Interface. *Polymer Bulletin* **1995,** 35, (1-2), 223-228.

53. Calberg, C.; Blacher, S.; Gubbels, F.; Brouers, F.; Deltour, R.; Jerome, R., Electrical and dielectric properties of carbon black filled co-continuous two-phase polymer blends. *Journal of Physics D-Applied Physics* **1999,** 32, (13), 1517-1525.

54. Evgeni, Z.; Roza, T.; Narkis, M.; Arnon, S., Particulate multi-phase polymeric nanocomposites. *Polymer Composites* **2006,** 27, (4), 425-430.

55. Charles L. Tucker III, P. M., Microstructural Evolution In Polymer Blends. *Annu Rev. Fluid Mechanics* **2002,** 34, 177-210.

56. Rallison, J. M., The deformation of small viscous drops and bubbles in shear flow. *Annual Review of Fluid Mechanics* **1984,** 16, 45-66.

57. Taylor, G. I., The formation of emuslions in definable fields of flow *Proc. Roy. Soc. Lond. Ser. A* **1934,** 146, 501-23.

58. Choi, S. J.; Scowalter, W. R., *Phys. Fluids* **1975,** 18, 420.

59. Vinckier, I.; Moldenaers, P.; Mewis, J., Elastic recovery of immiscible blends - 1. Analysis after steady state shear flow. *Rheologica Acta* **1999,** 38, (1), 65-72.

60. Vinckier, I.; Mewis, J.; Moldenaers, P., Stress relaxation as a microstructural probe for immiscible polymer blends. *Rheologica Acta* **1997,** 36, (5), 513-523.

61. Graebling, D.; Muller, R.; Palierne, J. F., Linear Viscoelastic Behavior of Some Incompatible Polymer Blends in the Melt - Interpretation of Data with a Model of Emulsion of Viscoelastic Liquids. *Macromolecules* **1993,** 26, (2), 320-329.

62. Macosko, C. W., *Rheology Principles, Measurements, and Applications*. Wiley-VCH, INc: 1994.

63. Oldroyd, J. G., The elastic and viscous properties of emulsions and suspensions. *Proc. Roy. Soc.Lond.Ser.A* **1953,** 218, 122-32.

64. Vinckier, I.; Moldenaers, P.; Terracciano, A. M.; Grizzuti, N., Droplet size evolution during coalescence in semiconcentrated model blends. *AIChE Journal* **1998,** 44, (4), 951-958.

65. Thareja, P.; Velankar, S., Particle-induced bridging in immiscible polymer blends. *Rheologica Acta* **2007,** 46, (3), 405-412.

66. Vermant, J.; Cioccolo, G.; Nair, K. G.; Moldenaers, P., Coalescence suppression in model immiscible polymer blends by nano-sized colloidal particles. *Rheologica Acta* **2004,** 43, (5), 529-538.

67. Maric, M.; Macosko, C. W., Improving polymer blend dispersions in mini-mixers. *Polymer Engineering and Science* **2001,** 41, (1), 118-130.

68. Palierne, J. F., Linear rheology of viscoelastic emulsions with interfacial tension. *Rheologica Acta* **1990,** 29, 204-214.

69. Vinckier, I.; Mewis, J.; Moldenaers, P., Relationship between rheology and morphology of model blends in steady shear flow. *Journal of Rheology* **1996,** 40, (4), 613-632.

70. Moldenaers, P., Personal communication. In 2005.

71. Van Helden, A. K.; Jansen, J. W.; Vrij, A., Preparation and characterization of spherical monodisperse silica dispersions in nonaqueous solvents. *Journal of Colloid and Interface Science* **1981,** 81, (2), 354-68.

72. Brandriss, S.; Margel, S., Synthesis and Characterization of Self-Assembled Hydrophobic Monolayer Coatings on Silica Colloids. *Langmuir* **1993,** 9, (5), 1232-1240.

73. Van Blaaderen, A.; Vrij, A., Synthesis and Characterization of Colloidal Dispersions of Fluorescent, Monodisperse Silica Spheres. *Langmuir* **1992,** 8, (12), 2921-2931.

74. Thareja, P.; Velankar, S., Rheology of immiscible blends with particle-induced drop clusters. *Rheologica Acta* **2008,** 47, (2), 189-200.

75. Boode, K.; Walstra, P.; Degrootmostert, A. E. A., Partial Coalescence in Oil-in-Water Emulsions .2. Influence of the Properties of the Fat. *Colloids and Surfaces A-Physicochemical and Engineering Aspects* **1993,** 81, 139-151.

76. Boode, K.; Walstra, P., Partial Coalescence in Oil-in-Water Emulsions .1. Nature of the Aggregation. *Colloids and Surfaces A-Physicochemical and Engineering Aspects* **1993,** 81, 121-137.

77. Pieranski, P., Two-dimensional interfacial colloidal crystals. *Physical Review Letters* **1980,** 45, (7), 569-572.

78. Aveyard, R.; Clint, J. H.; Nees, D.; Paunov, V. N., Compression and structure of monolayers of charged latex particles at air/water and octane/water interfaces. *Langmuir* **2000,** 16, (4), 1969-1979.

79. Stancik, E. J.; Gavranovic, G. T.; Widenbrant, M. J. O.; Laschitsch, A. T.; Vermant, J.; Fuller, G. G., Structure and dynamics of particle monolayers at a liquid-liquid interface subjected to shear flow. *Faraday Discussions* **2003,** 123, 145-156.

80. Nikolaides, M. G.; Bausch, A. R.; Hsu, M. F.; Dinsmore, A. D.; Brenner, M. P.; Weitz, D. A., Electric-field-induced capillary attraction between like-charged particles at liquid interfaces. *Nature* **2002,** 420, (6913), 299-301.

81. Aveyard, R.; Binks, B. P.; Clint, J. H.; Fletcher, P. D. I.; Horozov, T. S.; Neumann, B.; Paunov, V. N.; Annesley, J.; Botchway, S. W.; Nees, D.; Parker, A. W.; Ward, A. D.; Burgess, A. N., Measurement of long-range repulsive forces between charged particles at an oil-water interface. *Physical Review Letters* **2002,** 88, (24).

82. Kralchevsky, P. A.; Denkov, N. D.; Danov, K. D., Particles with an undulated contact line at a fluid interface: Interaction between capillary quadrupoles and rheology of particulate monolayers. *Langmuir* **2001,** 17, (24), 7694-7705.

83. de Bruijn, R. A. Deformation and breakup of drops in simple shear flows. Ph.D., Eindhoven University of Technology, The Netherlands, Eindhoven, 1989.

84. Grace, H. P., Dispersion phenomena in high viscosity immiscible fluid systems and application of static mixers as dispersion devices in such systems. *Chem. Eng. Commun.* **1982,** 14, 225-77.

85. Binks, B. P., Particles as surfactants - similarities and differences. *Current Opinion in Colloid and Interface Science* **2002,** 7, (1-2), 21-41.

86. Tambe, D. E.; Sharma, M. M., Factors Controlling the Stability of Colloid-Stabilized Emulsions .1. An Experimental Investigation. *Journal of Colloid and Interface Science* **1993,** 157, (1), 244-253.

87. Gelfer, M. Y.; Burger, C.; Chu, B.; Hsiao, B. S.; Drozdov, A. D.; Si, M.; Rafailovich, M.; Sauer, B. B.; Gilman, J. R. W., Relationships between structure and rheology in model nanocomposites of ethylene-vinyl-based copolymers and organoclays. *Macromolecules* **2005,** 38, (9), 3765-3775.

88. Garrett, P. R., Mode of action of antifoams. In *Defoaming*, Garrett, P. R., Ed. Marcel Dekker: New York, 1993.

89. Denkov, N. D.; Marinova, K. G., Antifoam effects of solid particles, oil drops, and oil-solid compounds in aqueous foams. In *Colloidal particles at liquid interfaces*, Binks, B. P.; Horozov, T. S., Eds. Cambridge University Press: Cambridge, 2006.

90. Pugh, R. J., Foaming in chemical surfactant free aqueous dispersions of anatase (Titanium dioxide) particles. *Langmuir* **2007,** 23, (15), 7972-7980.

91. Mizrahi, J.; Barnea, E., Effects of solid additives on the formation and separation of emulsions. *British Chemical Engineering* **1970,** 15, (4), 497-503.

92. Dickinson, E., Food emulsions####. In *Colloidal particles at liquid interfaces*, Binks, B. P.; Horozov, T. S., Eds. Cambridge University Press: Cambridge, 2006.

93. Van Hamme, J. D.; Singh, A.; Ward, O. P., Recent advances in petroleum microbiology. *Microbiology and Molecular Biology Reviews* **2003,** 67, (4), 503-+.

94. Kosaric, N.; Cairns, W. L.; Gray, N. C. C., Microbial deemulsifiers. In *Biosurfactants and biotechnology*, Kosaric, N.; Cairns, W. L.; Gray, N. C. C., Eds. 1987; Vol. 25, pp 247-321.

95. Gray, N. C. C.; Stewart, A. L.; Cairns, W. L.; Kosaric, N., Bacteria-induced de-emulsification of oil-in-water petroleum emulsions. *Biotechnology Letters* **1984,** 6, (7), 419-24.

96. Stewart, A. L.; Gray, N. C. C.; Cairns, W. L.; Kosaric, N., Bacteria-induced de-emulsification of water-in-oil petroleum emulsions. *Biotechnology Letters* **1983,** 5, (11), 725-30.

97. Thareja, P.; Velankar, S., Interfacial activity of particles at PI/PDMS and PI/PIB interfaces: Analysis based on Girifalco Good theory. *Colloid and Polymer Science* **2008**, In Press.

98. Chung, H.; Ohno, K.; Fukuda, T.; Composto, R. J., Self-regulated structures in nanocomposites by directed nanoparticle assembly. *Nano Letters* **2005,** 5, (10), 1878-1882.

99. Ginzburg, V. V., Influence of nanoparticles on miscibility of polymer blends. A simple theory. *Macromolecules* **2005,** 38, (6), 2362-2367.

100. Luciani, A.; Champagne, M. F.; Utracki, L. A., Interfacial tension coefficient from the retraction of ellipsoidal drops. *Journal of Polymer Science: Part B: Polymer Physics* **1997**, 1393-1403.

101. Cahn, J. W., Critical point wetting. *Journal of Chemical Physics* **1977,** 66, (8), 3667-3672.

102. Bertrand, E.; Bonn, D.; Kellay, H.; Binks, B. P.; Meunier, J., Fluctuation effects on wetting films. *Europhysics Letters* **2001,** 55, (6), 827-833.

103. Budkowski, A., Interfacial phenomena in thin films: Phase coexistence and segregation. In *Interfaces/Crystallization/Viscoelasticity*, Budkowski, A.; Hamley, I. W.; T. Koike, T., Eds. Springer: Berlin, 1999; pp 1-112.

104. Adamson, A. W.; Gast, A. P., *Physical Chemistry of Surfaces*. 6th ed.; Wiley: New York, 1997.

105. Ross, S.; Morrison, I. D., *Colloidal systems and interfaces*. Wiley: New York, 1988.

106. Wu, S., *Polymer Interface and Adhesion*. Marcel Dekker, Inc: 1982.

107. Fox, H. W.; Zisman, W. A., The spreading of liquids on low-energy surfaces. I. Polytetrafluoroethylene. *Journal of Colloid Science* **1950,** 5, 514-31.

108. Zisman, W. A., Relation of equilibrium contact angle to liquid and solid compositions. *Advances in Chemistry Series* **1964,** 43, 1-51.

109. Marmur, A. C., W; Zografi, G.J, *J.Coll Int Sci* **1986,** 113, (114).

110. Wu, S., Interfacial and surface tensions of polymers. *Journal of Macromolecular Science, Reviews in Macromolecular Chemistry* **1974,** 10, (1), 1-73.

111. Arkles, B., Tailoring surfaces with silanes. *Chemtech* **1977,** 7, 766-767.

112. Lin, S. Y.; Chen, L. J.; Xyu, J. W.; Wang, W. J., An Examination on the Accuracy of Interfacial-Tension Measurement from Pendant Drop Profiles. *Langmuir* **1995,** 11, (10), 4159-4166.

113. Sundararaj, U.; Macosko, C. W., Drop Breakup and Coalescence in Polymer Blends - the Effects of Concentration and Compatibilization. *Macromolecules* **1995,** 28, (8), 2647-2657.

114. Velankar, S.; Van Puyvelde, P.; Mewis, J.; Moldenaers, P., Effect of compatibilization on the breakup of polymeric drops in shear flow. *Journal of Rheology* **2001,** 45, (4), 1007-1019.

115. Gramespacher, H.; Meissner, J., Reversal of Recovery Direction During Creep Recovery of Polymer Blends. *Journal of Rheology* **1995,** 39, (1), 151-160.

116. Lee, H. M.; Park, O. O., Rheology and Dynamics of Immiscible Polymer Blends. *Journal of Rheology* **1994,** 38, (5), 1405-1425.

117. Vinckier, I.; Moldenaers, P.; Mewis, J., Relationship between rheology and morphology of model blends in steady shear flow. *Journal of Rheology* **1996,** 40, (4), 613-631.

118. Martin, J. D., The effect of surface active block copolymers on two phase flow. *PhD Thesis* **2007**.

119. Martin, J. D.; Velankar, S. S., Effects of compatibilizer on immiscible polymer blends near phase inversion. *Journal of Rheology* **2007,** 51, (4), 669-692.

120. Thareja, P.; Ising, B. P.; Kingston, S. J.; Velankar, S., Polymer foams stabilized by particles adsorbed at air/polymer interface. *Macromolecular Rapid Communications* **2008**, In Press.

121. Lee, S. T.; Ramesh, N. S., *Polymeric Foams: Mechanisms and Materials*. CRC: Boca Raton, 2004.

122. Mills, N., *Polymer foams handbook*. 1st ed.; Elsevier: Amsterdam, 2007.

123. Gonzenbach, U. T.; Studart, A. R.; Tervoort, E.; Gauckler, L. J., Ultrastable particle-stabilized foams. *Angewandte Chemie-International Edition* **2006,** 45, (21), 3526-3530.

124. Cohen-Addad, S.; Krzan, M.; Hohler, R.; Herzhaft, B., Rigidity percolation in particle-laden foams. *Physical Review Letters* **2007,** 99, (16), 168001.

125. Subramaniam, A. B.; Mejean, C.; Abkarian, M.; Stone, H. A., Microstructure, morphology, and lifetime of armored bubbles exposed to surfactants. *Langmuir* **2006,** 22, (14), 5986-5990.

126. Marmur, A.; Chen, W.; Zografi, G., Characterization of particle wettability by the measurement of floatability. *Journal of Colloid and Interface Science* **1986,** 113, (1), 114-20.

127. de Gennes, P. G.; Brochard-Wyart, F.; Quere, D., *Capillarity and Wetting Phenomena: Drops, Bubbles, Pearls, Waves*. Springer: New York, 2003.

128. Pop-Iliev, R.; Liu, F. Y.; Liu, G. B.; Park, C. B., Rotational foam molding of polypropylene with control of melt strength. *Advances in Polymer Technology* **2003,** 22, (4), 280-296.

129. Naguib, H. E.; Park, C. B., Strategies for achieving ultra low-density polypropylene foams. *Polymer Engineering and Science* **2002,** 42, (7), 1481-1492.

130. Spitael, P.; Macosko, C. W., Strain hardening in polypropylenes and its role in extrusion foaming. *Polymer Engineering and Science* **2004,** 44, (11), 2090-2100.

131. Burt, J. G., The elements of expansion of thermoplastics. Part II. *Journal of Cellular Plastics* **1978,** 14, (6), 341-5.

132. Yamaguchi, M.; Suzuki, K., Rheological properties and foam processability for blends of linear and crosslinked polyethylenes. *Journal of Polymer Science Part B-Polymer Physics* **2001,** 39, (18), 2159-2167.

133. Crawford, R. J.; Throne, J. L., *Rotational Molding Technology*. William Andrew Publishing/Plastics Design Library: 2002; p 425.

134. Pop-Iliev, R.; Xu, D. L.; Park, C. B., Manufacturability of fine-celled cellular structures in rotational foam molding. *Journal of Cellular Plastics* **2004,** 40, (1), 13-25.

135. Pop-Iliev, R.; Park, C. B., Melt compounding based rotational foam molding technology for manufacture of polypropylene foams. *Journal of Reinforced Plastics and Composites* **2002,** 21, (2), 101-120.

136. Widya, T.; Macosko, C. W., Nanoclay-modified rigid polyurethane foam. *Journal of Macromolecular Science-Physics* **2005,** B44, (6), 897-908.

137. Han, X. M.; Zeng, C. C.; Lee, L. J.; Koelling, K. W.; Tomasko, D. L., Extrusion of polystyrene nanocomposite foams with supercritical CO2. *Polymer Engineering and Science* **2003,** 43, (6), 1261-1275.

138. Lee, L. J.; Zeng, C. C.; Cao, X.; Han, X. M.; Shen, J.; Xu, G. J., Polymer nanocomposite foams. *Composites Science and Technology* **2005,** 65, (15-16), 2344-2363.

139. Panhuis, M. I. H.; Paunov, V. N., Assembling carbon nanotubosomes using an emulsion-inversion technique. *Chemical Communications* **2005**, (13), 1726-1728.